To the Graduate Council:

I am submitting herewith a thesis written by M. Keith Booker entitled "Mathematical Analysis of the Elevated-Temperature Creep Behavior of Type 304 Stainless Steel." I recommend that it be accepted in partial fulfillment of the requirements for the degree of Master of Science, with a major in Metallurgical Engineering.

Carl J. McHargue, Major Professor

We have read this thesis
and recommend its acceptance:

Accepted for the Council:

Vice Chancellor
Graduate Studies and Research

Thesis
77
.B665
copy

MATHEMATICAL ANALYSIS OF THE ELEVATED-TEMPERATURE CREEP BEHAVIOR OF TYPE 304 STAINLESS STEEL

A Thesis

Presented for the

Master of Science

Degree

The University of Tennessee, Knoxville

M. Keith Booker

June 1977

1323975

To Barbra

ABSTRACT

Austenitic stainless steels have gained worldwide importance as elevated-temperature structural materials. Often, they are used in service situations where creep effects become important. This investigation represents an effort to characterize the creep behavior of type 304 austenitic stainless steel.

Using data gathered from various international sources, generalized regression techniques were used to develop analytical representations for various aspects of the creep behavior of type 304 stainless steel. These aspects include rupture life, minimum creep rate, time and strain to the onset of tertiary creep, creep-rupture ductility, and creep strain-time behavior.

All models developed included analytical predictions of heat-to-heat variations in behavior as reflected by the ultimate tensile strength of a given heat of material. Such expressions yield a quantitative representation of the creep behavior of this material for design use.

TABLE OF CONTENTS

CHAPTER		PAGE
INTRODUCTION		1
I.	DESCRIPTION OF DATA USED	4
II.	ANALYSIS OF RUPTURE LIFE AND MINIMUM CREEP RATE DATA	14
	Review of Previous Techniques	14
	Techniques of Regression Analysis	16
	Techniques of Model Selection	21
	Identification of Candidate Models	24
	Evaluation of Candidate Models	37
	Effects of Ultimate Tensile Strength	53
	Prediction of Mean, Maximum, and Minimum Behavior	60
	Strain Rate Effects	82
III.	ANALYSIS OF CREEP DUCTILITY DATA	85
	Interpretation of Ductility Predictions	109
	Trends in Behavior	115
IV.	ANALYSIS OF CREEP STRAIN-TIME BEHAVIOR	118
	Methods for Development of Creep Equations	120
	Choice of Strain-Time Equation Form	121
	The Exponential Creep Equation	125
	The Rational Polynomial Creep Equation	128
	Fits to Experimental Curves	132
	Stress and Temperature Dependence of Equation Parameters	133
	Predictions of Creep Behavior	139

PAGE

Variable Load and Relaxation Behavior 148

Isochronous Stress-Strain Curves. 151

Analytical Limitations. 157

Advantages. 159

V. EXTRAPOLATION OF RESULTS. 163

Possible Effects of Changes in Deformation Mechanism. . . 167

VI. DISCUSSION OF RESULTS 175

Regression Analysis of Creep and Rupture Data 175

Relationship Between Ultimate Tensile Strength and Creep Properties 179

Predicted Trends in Ductility Data. 184

Comparison with ASME Code Case 1592 Allowable Stress Levels 186

VII. CONCLUSIONS 189

REFERENCES 193

VITA 206

LIST OF TABLES

TABLE		PAGE
I.	Summary of Rupture Life Data Used.	7
II.	Summary of Chemical Analysis of 20 Heats of Type 304 Stainless Steel in ORNL Testing Program	8
III.	Summary of Minimum Creep Rate Data Used.	9
IV.	Compositions and Product Forms of Materials Investigated in Ductility Analysis.	11
V.	Heat Treatments and Specimen Gage Lengths of Materials Studied in Ductility Analysis.	12
VI.	Summary of Ductility Data Used	13
VII.	Summary of Creep Data Used	13
VIII.	Terms Used in Choosing Candidate Models Through SELECT . .	26
IX.	Ten Leading Three Nonconstant Term Models as Identified by SELECT for Each Data Set.	30
X.	List of Candidate Models Used to Describe Rupture Life and Minimum Creep Rate Data.	34
XI.	Best Fit Values of the Coefficients in the Candidate Models for Rupture Life.	38
XII.	Best Fit Values of the Coefficients in the Candidate Models for Minimum Creep Rate.	41
XIII.	Values of the Coefficients of Determination from the Candidate Models for Rupture Life.	43
XIV.	Values of the Coefficients of Determination from the Candidate Models for Minimum Creep Rate.	44
XV.	Values of the Root Mean Square Error Obtained by Predicting the Long Time Rupture Life Data from Fits to the Short Time Data	45
XVI.	Values of the Root Mean Square Error Obtained by Predicting the Low Rate Minimum Creep Rate Data from Fits to the High Rate Data	46

PAGE

XVII. Values of the Pooled Root Mean Square Error from Fits to the Rupture Life Data and from Predictions of Long Time Data from Fits to Short Time Data (Long Time: $t_r > 2000$) 48

XVIII. Values of the Pooled Root Mean Square Error from Fits to the Minimum Creep Rate Data and from Predictions of Low Rate Data from Fits to High Rate Data (High Rate: $\dot{\epsilon}_m > 0.001\%/hr$) 49

XIX. Comparison of Results Obtained Using Models With and Without Ultimate Tensile Strength Terms. 54

XX. Best Fit Values of Coefficients in Equations Describing Ultimate Tensile Strength as a Function of Temperature . 72

XXI. Comparison Between Lower Central Tolerance Limits on Ultimate Tensile Strength for the ORNL Data With Current Limits 73

XXII. Relationship Between Minimum Creep Rate and Rupture Life . 89

XXIII. Relationship Between Minimum Creep Rate and Average Creep Rate to Tertiary Creep 90

XXIV. Results of Correlation Between Average Creep Rate to Tertiary Creep and Rupture Life. 91

XXV. Relationship Between Minimum Creep Rate and Average Creep Rate to Rupture. 93

XXVI. Relationship Between Average Creep Rate to Rupture and Rupture Life 94

XXVII. Results of Correlation Between Time to Tertiary Creep and Rupture Life 95

XXVIII. Best Fit Values of the Coefficients in the Candidate Models for Time to Tertiary Creep. 99

XXIX. Best Fit Values of the Coefficients in the Candidate Models for Average Creep Rate to Tertiary Creep. 100

XXX. Relationship Between Average Strain Rate to Rupture and Rupture Life 110

XXXI. Some Common Creep Strain-Time Relations. 122

PAGE

XXXII. Stress Values Corresponding to Maximum Values of the Parameter C. 160

XXXIII. Comparison Between Estimated Time-Dependent Allowable Stress Levels Calculated from the Current Results and Those Given in ASME Code Case 1592 188

LIST OF FIGURES

FIGURE		PAGE
1.	Schematic Illustration of the Various Quantities Used to Characterize the Creep Behavior of Type 304 Stainless Steel	5
2.	Variation in the Coefficient of Determination, R^2, With Number of Nonconstant Terms in Regression Models for the ORNL Rupture Life Data	28
3.	Variation in the Standard Error of Estimate, SEE, With Number of Nonconstant Terms in Regression Models for the ORNL Rupture Life Data	29
4.	Comparison of Experimental Time to Rupture and Minimum Creep Rate With Predicted Results from Models With and Without Ultimate Tensile Strength for 20 Heats of Type 304 Stainless Steel	56
5.	Comparison of Experimental Time to Rupture as a Function of Elevated-Temperature Ultimate Tensile Strength (U) With Values Predicted from Rupture Model With U for Different Heats of Type 304 Stainless; Tests Were at 593°C (1100°F) and 241 MPa (35 ksi)	57
6.	Comparison of Experimental Time to Rupture as a Function of Elevated-Temperature Ultimate Tensile Strength (U) With Values Predicted from Rupture Model With U for Different Heats of Type 304 Stainless; Tests Were at 593°C (1100°F) and 207 MPa (30 ksi)	58
7.	Comparison of Experimental Time to Rupture as a Function of Elevated-Temperature Ultimate Tensile Strength (U) With Values Predicted from Rupture Model With U for Different Heats of Type 304 Stainless; Tests Were at 649°C (1200°F) and 172 MPa (25 ksi)	59
8.	Comparison of Experimental Time to Rupture With Values Computed from Models With and Without Elevated Temperature Ultimate Temperature Strength (U) for 25-mm (1-in.) Plate of Reannealed Heat 9T2796 of Type 304 Stainless Steel	61
9.	Comparison of Experimental Time to Rupture With Values Computed from Models With and Without Elevated-Temperature Ultimate Tensile Strength (U) for a weak (9T2796) and a Strong Heat (8043813)	62

PAGE

10. Comparison of Experimental Time to Rupture With Values Computed from Models With and Without Elevated-Temperature Ultimate Tensile Strength (U) for HEDL Data on Reannealed Heat 55697. 63

11. Comparison of Experimental Time to Rupture With Values Computed from Models With and Without Elevated-Temperature Ultimate Tensile Strength (U) for Several Heats of Type 304 Stainless Steel at 593°C 64

12. Comparison of Experimental Minimum Creep Rate With Values Computed from Models With and Without Elevated-Temperature Ultimate Tensile Strength (U) for 25-mm (1-in.) Plate of Reannealed Reference Heat of Type 304 Stainless Steel . 65

13. Comparison of Experimental Minimum Creep Rate With Values Computed from Models With and Without Elevated-Temperature Ultimate Tensile Strength (U) for a Weak (9T2796) and a Strong Heat (8043813). 66

14. Comparison of Experimental Minimum Creep Rate With Values Computed from Models With and Without Elevated-Temperature Ultimate Tensile Strength (U) for HEDL Data on Reannealed Heat 55697 67

15. Comparison of Experimental Minimum Creep Rate With Values Computed from Models With and Without Elevated-Temperature Ultimate Tensile Strength (U) for Several Heats of Type 304 Stainless Steel 68

16. Prediction of Heat-to-Heat Variations in Rupture Life for Two Heats of Type 304 Stainless Steel. 69

17. Prediction of Heat-to-Heat Variations in Minimum Creep Rate for Heats 8043813 and 9T2796 of Type 304 Stainless Steel . 70

18. Plots Showing Trends in Ultimate Tensile Strength as a Function of Test Temperature for Types 304 and 316 Stainless Steel from Various Sources 74

19. Trends in Ultimate Tensile Strength as a Function of Test Temperature for ORNL Data for Type 304 Stainless Steel . . 75

20. Fits to Experimental ORNL Data for Rupture Life of Type 304 Stainless Steel at 593°C (1100°F). 76

21. Fits to Experimental ORNL Data for Rupture Life of Type 304 Stainless Steel at 649°C (1200°F). 77

PAGE

22. Fits to Experimental ORNL Data for Minimum Creep Rate of Type 304 Stainless Steel at 593°C (1100°F). 78

23. Fits to Experimental ORNL Data for Minimum Creep of Type 304 Stainless Steel at 649°C (1200°F) 79

24. Fits to Experimental US Data for Rupture Life of Type 304 Stainless Steel at 593°C (1100°F). 80

25. Fits to Experimental BSCC Data for Rupture Life of Type 304 Stainless Steel at 650°C (1200°F). 81

26. Comparison of NRIM Stress-Rupture Data at 600, 650, and 700°C (1112, 1202, and 1293°F) for 9 Heats of Type 304 Stainless Steel in As-Received Condition With Predicted Maximum, Average, and Minimum Curves from Rupture Model With Elevated-Temperature Ultimate Tensile Strength (U). . 84

27. Comparison of Experimental Data With Predicted Values of the Plasticity Resource, $e_s = \dot{e}_m t_r$, at 593°C(1100°F). . 97

28. Comparison of Experimental Data With Predicted Values of the Plasticity Resource, $e_s = \dot{e}_m t_r$, at 649°C (1200°F) . 98

29. Comparison of Experimental ORNL Data for the Time to Tertiary Creep, t_{ss}, With Predicted Values at 593°C (1100°F) 102

30. Comparison of Experimental ORNL Data for the Average Creep Rate to Tertiary Creep, $\dot{e}_3$, With Predicted Values at 593°C (1100°F) 103

31. Comparison of Experimental Data With Predicted Values of Time to the Onset of Tertiary Creep at 593°C (1100°F) and 649°C (1200°F) 104

32. Comparison of Experimental Data With Predicted Values of Average Creep Rate to the Onset of Tertiary Creep at 593°C (1100°F) and 649°C (1200°F). 105

33. Comparison of Experimental Data With Predicted Values of Creep Strain to the Onset of Tertiary Creep at 593°C (1100°F) 107

34. Comparison of Experimental Data With Predicted Values of Creep Strain to the Onset of Tertiary Creep at 649°C (1200°F) 108

PAGE

35. Plots of Average Creep Rate and Creep Total Elongation for Type 304 Stainless Steel Data Collected from US and Two Foreign Countries 112

36. Predicted Trends in the Strain to the Onset of Tertiary Creep (No Offset) as a Function of Stress 116

37. Predicted Trends in the Strain to the Onset of Tertiary Creep (No Offset) as a Function of Minimum Creep Rate . . 117

38. Schematic Diagram Showing Results of Fitting Eqn. 49 Directly to an Experimental Creep Curve 124

39. Schematic Illustration of the Properties of the Rational Polynomial Creep Equation 130

40. Fit of the Rational Polynomial Creep Equation to an Experimental Curve at 649°C (1200°F) 134

41. Fit of the Rational Polynomial Creep Equation to an Experimental Curve at 538°C (1000°F). 134

42. Fit of the Rational Polynomial Creep Equation to an Experimental Curve at 593°C (1100°F). 135

43. Fit of the Rational Polynomial Creep Equation to an Experimental Curve at 427°C (800°F) 136

44. Fit of the Rational Polynomial Creep Equation to an Experimental Curve at 482°C (900°F) 136

45. Relationship Between Minimum Creep Rate and Initial Creep Rate for Type 304 Stainless Steel 140

46. Variation of the Rational Polynomial Creep Equation Parameters With Stress at Three Temperatures for Heat 9T2796, 51-mm Plate of Type 304 Stainless Steel 141

47. Comparison of Predictions With Experimental Creep Curves for Type 304 Stainless Steel, Including Predictions of Average Behavior from the Current Equation and from the Blackburn Equation. 143

48. Comparison of Predictions With Experimental Creep Curves for Type 304 Stainless Steel, Including Predictions of Average Behavior from the Current Equation and from the Blackburn Equation With the Testing Conditions: Temperature = 649°C, Stress = 69 MPa. 144

PAGE

49. Heat-to-Heat Variations in Creep Curves of Several Reannealed Heats of Type 304 Stainless Steel 146

50. Illustrative Comparison Among Creep Data at 482°C (900°F) and 427°C (800°F) and Predicted Behavior at 482°C 147

51. Comparison Between an Experimental Variable Load Creep Test for Heat 8043813 With Predicted Behavior Using the Current Creep Equation and the Hypothesis of Strain Hardening . . . 149

52. Comparison of Two Experimental Relaxation Curves for Heat 9T2796 at 593°C With Predicted Behavior Using the Current Creep Equation and the Hypothesis of Strain Hardening 150

53. Predicted Isochronous Stress-Strain Curves at 10^3- and 10^5-hr from the Creep Equation and the Rational Polynomial Equation for Average Stress-Strain Behavior 153

54. Isochronous Stress-Strain Curves at 593°C (1100°F) for Heat 9T2796, 51-mm Plate Predicted by Three Methods 158

55. Comparison of Stress-Temperature Operating Conditions Allowed by ASME Code Case 1592 With the Range of Available Experimental Creep Data for Type 304 Stainless Steel. . . . 165

56. Minimum Creep Rate Data for Heat 9T2796 51-mm Plate of Type 304 Stainless Steel. 171

57. Schematic Illustration of the Region of Interpolation Versus Extrapolation for Creep Data. 177

58. Trends in the Tensile Reduction of Area With Temperature for Weak and Strong Heats of Types 304 and 316 Stainless Steel 183

INTRODUCTION

Austenitic stainless steels have gained worldwide importance as elevated-temperature structural materials, particularly in nuclear power generation systems. This popularity is due to several excellent features of the behavior of these materials, including good elevated-temperature strength, good resistance to sodium corrosion, excellent resistance to superheated steam environments, excellent resistance to carbon transfer, weldability, and relatively low cost [1,2]. Type 304 stainless steel exhibits excellent long-term stability with respect to adverse microstructural changes caused by precipitation reactions [3-7].

The above properties make it possible to design components of type 304 stainless steel for long-term service in temperature regimes where creep and other time-dependent material properties become prime design considerations. Power generation systems require operating times up to and exceeding 100,000 hours, but actual experimental creep data at such times are generally not available. Therefore, it is necessary to predict long-term time-dependent behavior from the results of relatively short-term tests. Most previous work in the extrapolation of creep data has dealt with creep rupture, and many creep-rupture data are available. However, inelastic analysis of actual operating systems also requires a knowledge of the deformation behavior of the components under the expected operating conditions. The prediction of such behavior is a complex problem since, in general, components will be subjected to variable (including cyclic) loads and temperatures and to

multiaxial states of stress. Specific methods have been developed for making such predictions for types 304 and 316 stainless steel and for ferritic 2 1/4 Cr-1 Mo steel [8-11], however. As listed in Ref. [11], the components essential to such predictions are the following: (1) a "flow rule" that relates multiaxial strain-rate components to the corresponding multiaxial stress components; (2) a strain hardening [12] law that describes the behavior under variable stresses; and (3) an expression representing the behavior of the material under isothermal, constant-load uniaxial conditions.

In the current investigation, constant-load isothermal creep strain-time data for several heats of type 304 stainless steel tested in air have been examined over a range of stresses and temperatures to yield an expression for creep strain as a function of time, stress, and temperature. The method presented here allows the creep equation to be based largely upon readily available rupture life and minimum creep rate data. In addition, the method provides a means of accounting for the substantial heat-to-heat variations in properties which are prevalent in this material [13]. The method involves development of analytical expressions for rupture life, minimum creep rate, and time and strain to the onset of teritary creep—all useful design properties in themselves. Predictions made by the equation developed herein in conjunction with the hypothesis of strain hardening are compared with experimental relaxation and variable load data for type 304 stainless steel.

Finally, the implications of the results in terms of material behavior and design applications are discussed. Although elevated temperature allowable stress values for this material are given in ASME Code Case 1592 [14], it is shown that the current equations provide an improved method of performing the complicated calculations involved in the inelastic analysis of elevated-temperature components.

CHAPTER I

DESCRIPTION OF DATA USED

The data used in this investigation fall into several specific categories. These are: (1) time to rupture (t_r) data; (2) reported minimum creep rate ($\dot{e}_m$) data; (3) various forms of creep ductility data (e_t, e_2, or e_{ss}); (4) data for the time to tertiary creep (t_2 or t_{ss}); and (5) actual experimental creep curves. Figure 1 defines the various quantities examined. All data were derived from constant-load isothermal tests.

All material was listed in the original sources as annealed, although it was not clear in all cases whether the material used was mill annealed by the vendor (and tested by the laboratory in the as-received condition), or reannealed in the laboratory before testing. As-received material can contain residual cold work due to straightening and forming operations occurring after the mill anneal. This cold work can cause significant variations in yield strength, and as-received material typically exhibits a 0.2% offset yield strength of about 35 MPa greater than reannealed material [15,16]. However, heat treatment of this material causes little significant microstructural change other than the removal of such residual cold work and perhaps a small amount of grain growth [17]. The ultimate tensile strength and creep properties of type 304 stainless steel are virtually equivalent in the as-received and reannealed conditions [15].

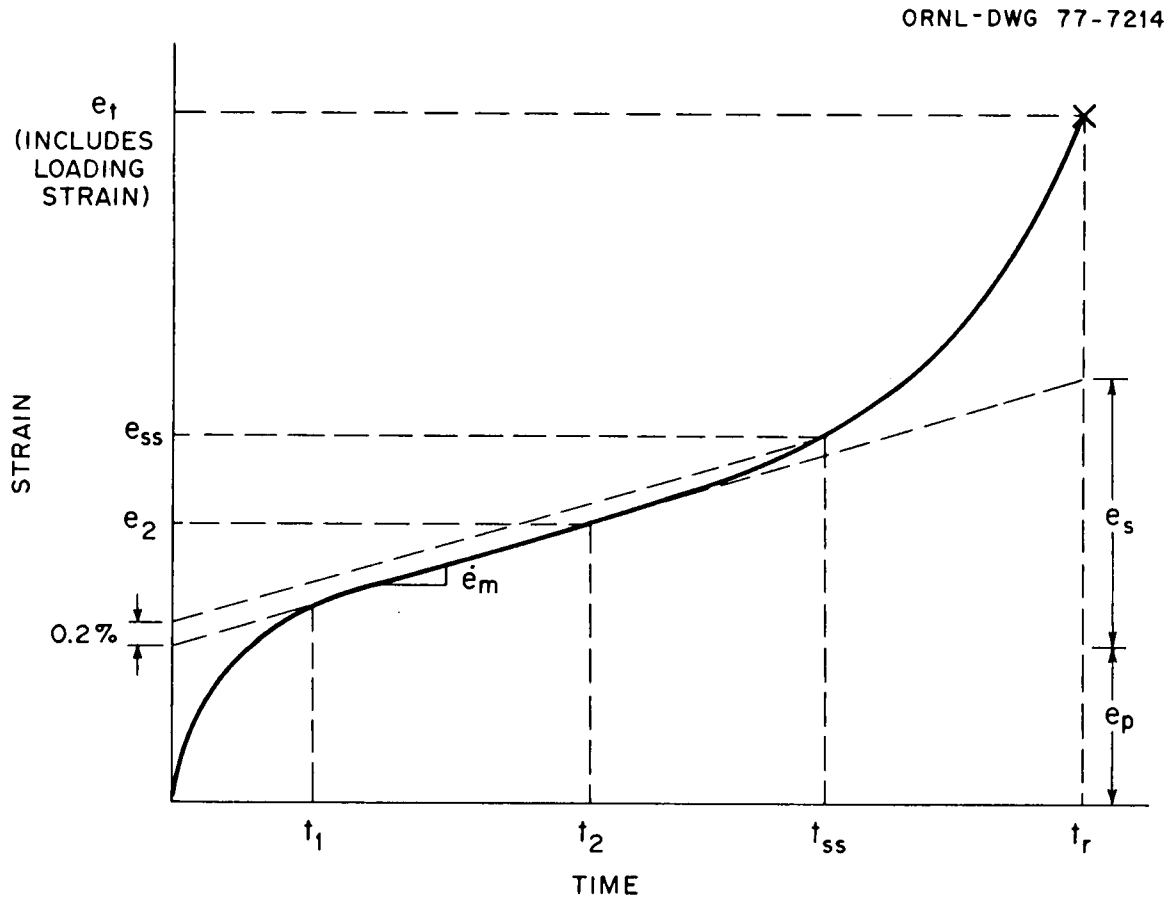

Figure 1. Schematic Illustration of the Various Quantities Used to Characterize the Creep Behavior of Type 304 Stainless Steel.

Rupture life (t_r) data were derived from a variety of international sources, which are described in Ref. [18]. Analysis has shown that ultimate tensile strength is significantly reflected in the creep and creep-rupture behavior of this material [13,19,20]. In fact, it will be shown later in this report that many of the heat-to-heat variations in the creep properties of this material can be described in terms of variations in ultimate tensile strength. Therefore, it was necessary to use only rupture data from heats of material for which ultimate tensile strength data were also available. The data used included data from British [21], Japanese [22] and American [13,23-29] sources, including a large number of data recently generated at Oak Ridge National Laboratory (ORNL)[13,25-28]. Table I summarizes the rupture data. The various heats of material tested were too numerous for each one to be described individually, although Table II describes the various heats for the ORNL data.

Minimum or secondary creep rate ($\dot{e}_m$) data were available from American sources only. These data were usually derived from the same heats of material for which rupture life data were used. Presumably, the values of minimum creep rate were all graphically determined from experimental creep curves. These data, as were the rupture data, were comprised of data from the American literature (US)[23,24,29] and from the testing program at Oak Ridge National Laboratory (ORNL)[13,25-28]. Table III summarizes the minimum creep rate data.

In an effort to fully characterize the creep properties of type 304 stainless steel, various indices of creep ductility have also been examined. These ductility quantities involve the strain incurred before

TABLE I

SUMMARY OF RUPTURE LIFE DATA USED

Data Set[a]	Source (Reference No.)	Number of Data	Temperature Range (°C)	Stress Range (MPa)	Rupture Life Range (hr)	Tensile Data[b] Strain Rate (S^{-1})
BSCC	21	28	600-700	62-215	23-16151	c
NRIM	22	133	600-750	47-215	30-20902	1.25×10^{-3}[d]
US	23,24,29	146	538-816	28-345	10-65028	8.3×10^{-4}[e]
ORNL	13,25-28	205	482-760	52-345	10-29253	6.7×10^{-4}

[a]The data set will be referred to by this label hereafter in this report.

[b]Strain rate at which corresponding ultimate tensile strength data were generated.

[c]Strain rate not given, but assumed to be some standard rate.

[d]Strain rates were 5×10^{-5} S^{-1} up to 1% extension, then 1.25×10^{-3}.

[e]Strain rates specified as 8.3×10^{-5} S^{-1} to the determination of the yield strength, then 8.3×10^{-4} S^{-1} thereafter.

TABLE II

SUMMARY OF CHEMICAL ANALYSIS OF 20 HEATS OF TYPE 304 STAINLESS STEEL IN ORNL TESTING PROGRAM

Heat Symbol	Chemical Element, %																				
	C	N	P	B	O	H	Ni	Mn	Cr	Si	Mo	S	Nb	V	Ti	Ta	W	Cu	Co	Pb	Sn
796	0.047	0.031	0.029		0.0110	0.0006	9.58	1.22	18.5	0.47	0.10	0.012	0.008	0.037	0.003	<0.0005	0.022	0.10	0.05	0.01	0.02
807	0.029	0.021	0.024	0.0005	0.010	0.0012	9.67	1.26	18.8	0.50	0.20	0.023	0.0015	0.012	0.002	<0.0005	0.020	0.11	0.03	0.01	0.01
797	0.059	0.055	0.028	0.0020	0.0075	0.0007	9.78	1.49	18.3	0.60	0.30	0.110	0.0050	0.020	0.005	0.0005	0.050	0.30	0.07	0.002	0.005
283	0.043	0.025	0.018	0.0003	0.0140	0.0009	9.12	1.32	18.2	0.45	0.30	0.020	0.0030	0.030	0.0010	<0.0005	0.021	0.14	0.05	0.01	0.01
926	0.053	0.041	0.020		0.0084	0.0007	9.79	1.16	19.0	0.68	0.10	0.025	0.0180	0.050	0.0100	0.0010	0.030	0.070	0.05	0.010	0.02
187	0.068	0.031	0.018		0.0042	0.0005	9.43	0.83	18.2	0.59	0.07	0.008	0.0020	0.060	0.003	<0.0005	0.015	0.15	0.05	0.01	0.02
697	0.057	0.034	0.016		0.0150	0.0005	9.38	0.91	18.5	0.50	0.05	0.037	0.0030	0.030	0.002	<0.0005	0.011	0.10	0.05	0.01	0.02
866	0.044	0.022	0.023	0.0002	0.0096	0.0010	8.98	1.51	18.5	0.47	0.2	0.007	0.0010	0.018	0.0005	0.0005	0.007	0.13	0.04	0.01	0.01
544	0.063	0.019	0.023	0.0002	0.0081	0.0006	9.12	0.99	18.4	0.47	0.2	0.006	0.0050	0.025	0.017	0.0006	0.026	0.12	0.05	0.01	0.01
330	0.068	0.031	0.018		0.0042	0.0005	9.43	0.83	18.2	0.59	0.07	0.008	0.0100	0.025	0.002	<0.0005	0.0060	0.15	0.05	0.01	0.02
845	0.057	0.024	0.023	0.0002	0.0092	0.0013	9.28	0.92	18.4	0.53	0.10	0.006	0.0100	0.050	0.008	<0.0005	0.007	0.11	0.07	0.01	0.01
779	0.065	0.023	0.024	0.0002	0.0056	0.0009	9.46	0.94	18.1	0.47	0.20	0.005	0.0035	0.029	0.010	0.0020	0.043	0.16	0.02	0.01	0.01
390	0.066	0.086	0.018	0.0020	0.0052	<0.0001	8.75	1.57	18.6	0.60	0.30	0.006	0.0160	0.020	0.001	0.0006	0.043	0.20	0.07	0.0007	0.002
414	0.073	0.058	0.016		0.0190	0.0004	9.52	0.94	18.7	0.69	0.10	0.015	0.0100	0.025	0.002	<0.0005	0.027	0.10	0.05	0.01	0.02
551	0.043	0.027	0.022	0.0010	0.0220	0.0013	9.40	1.20	18.5	0.59	0.30	0.018	0.0140	0.050	0.025	<0.0005	0.049	0.25	0.08	0.01	0.01
737	0.064	0.075	0.026	0.00005	0.0072	<0.0001	9.01	1.71	18.3	0.50	0.30	0.012	0.0140	0.031	0.001	<0.0005	0.016	0.50	0.07	<0.0003	0.0050
380	0.063	0.068	0.018		0.0260	0.0009	8.30	0.97	18.4	0.55	0.07	0.010	0.0100	0.028	0.004	<0.0005	0.016	0.10	0.05	0.01	0.02
686	0.050	0.043	0.025		0.0091	0.0005	9.46	1.23	18.4	0.53	0.20	0.016	0.0030	0.019	0.006	<0.0005	0.021	0.10	0.05	0.01	0.02
813	0.062	0.033	0.044	0.0003			8.95	1.87	17.8	0.48	0.32	0.004	0.0200	0.022	0.002	<0.0005	0.02				
121	0.065	0.140	0.019	0.00005	0.0026	0.0011	9.19	1.92	18.1	0.30	0.14	0.010	0.0010	0.035	0.016	<0.0005	0.015	0.07	0.07	<0.0003	0.002

TABLE III

SUMMARY OF MINIMUM CREEP RATE DATA USED

Data Set	Source (Reference No.)	Number of Data	Temperature Range (MPa)	Stress Range (MPa)	Minimum Creep Rate Range (%/hr)	Tensile Data Strain Rate (S^{-1})
US	23,24,29	82	538-816	28-345	0.000015-31.3	8.3×10^{-4}[a]
ORNL	13,25-28	226	482-760	52-345	0.000021-15.7	6.7×10^{-4}

[a]Strain rate specified as 8.3×10^{-5} S^{-1} to the determination of the yield strength, then 8.3×10^{-4} S^{-1} thereafter.

rupture and the strain incurred before the onset of tertiary creep. Table IV lists the heats of material for which creep ductility was examined in detail, while Table V gives the initial specimen gage lengths and heat treatments for those heats. Table VI defines the ranges covered by those data.

Data for the time to the onset of tertiary creep (t_3) were obtained from the same heats of material described in Tables IV and V, plus additional data from the ORNL heat-to-heat variations program [13,26]. Values of the time to tertiary creep were determined both by the time to first deviation from linear secondary creep (hereinafter referred to as t_2) and by a 0.2% strain offset from the linear secondary creep portion (hereinafter referred to as t_{ss}).

Since the principal purpose of this investigation was to develop an analytical creep strain-time expression, an important part of the data base was a collection of experimental creep strain-time curves. Such curves were available in quantity only for the data from the ORNL program. Table VII defines the ranges of the available creep data from this program. In addition, analytical fits to experimental curves from the data of Ref. [29] were available.

TABLE IV

COMPOSITIONS AND PRODUCT FORMS OF MATERIALS INVESTIGATED IN DUCTILITY ANALYSIS

Heat	Reference	Product Form	Content, wt %[a]												
			C	Mn	P	S	Si	Cr	Ni	Co	Mo	Cu	N	Nb+Ta	Ti
			Type 304 Stainless Steel												
9T2796	28	25.4-mm plate	0.051	1.37	0.041	b	0.4	18.5	9.87	0.1	0.3	0.24	0.031	b	b
9T2796	13,25	50.8-mm plate	0.047	1.22	0.029	0.012	0.47	18.5	9.58	0.05	0.10	0.10	0.031	b	b
55697	29	7-mm rod	0.052	1.1	0.011	0.01	0.52	18.92	9.52	0.035	0.12	0.10	0.052	b	b
8043813	27	25.2-mm plate	0.062	1.87	0.04	0.0043	0.48	17.8	8.95	0.20	0.32	0.20	0.033	b	b
ASTM A 240, 479	30,31	Plate, rod	0.08[c]	2.0[c]	0.045[c]	0.03[c]	1.0[c]	17-19	8-10						

[a] All analyses include balence iron.

[b] Not reported.

[c] Maximum allowed.

TABLE V

HEAT TREATMENTS AND SPECIMEN GAGE LENGTHS
OF MATERIALS STUDIED IN DUCTILITY ANALYSIS

Heat, Description	Initial Gage Length (mm)	Treatment	Time (hr)	Temperature (°C)	Cooling Method
		Type 304 Stainless Steel			
9T2796, 25-mm plate	57.2[a]	Anneal	0.5	1093	Air cool
9T2796, 51-mm plate	57.2	Anneal	0.5	1093	Air cool
8043813	57.2[a]	Anneal	0.5	1065	Air cool
55697	31.8	Anneal	1.0	1066	Rapid air cool

[a]Some high-stress and/or low-temperature tests were run on 31.8-mm-gage-length specimens.

TABLE VI

SUMMARY OF DUCTILITY DATA USED

Heat[a]	Number[b] of Data	Temperature Range (°C)	Stress Range (MPa)
9T2796(25.4 mm)	58	482-816	34-345
9T2796(50.8 mm)	20	538-704	55-317
55697	45	538-649	110-345
8043813	24	538-816	117-379

[a]See Table IV, page 11, for chemical compositions.

[b]The number of data available for different ductility criteria varied slightly. The number given represents the total number of tests from which ductility data of any sort were derived.

TABLE VII

SUMMARY OF CREEP DATA USED

Heat[a]	Number of Data	Temperature Range (°C)	Stress Range (MPa)	Maximum Test Time (hr)
9T2796(25.4 mm)	67	538-871	34-272	13,000
9T2796(50.8 mm)	60	427-704	14-207	46,000
8043813	24	593-704	41-276	3200

[a]See Table IV, page 11, for chemical compositions.

CHAPTER II

ANALYSIS OF RUPTURE LIFE AND MINIMUM CREEP RATE DATA

The importance of creep in elevated-temperature design is well established. Two of the most commonly reported and used material properties as determined from creep tests are the rupture life (total test time to rupture) and steady-state or "minimum" creep rate (slope of the linear stage portion of a classical creep curve such as that shown in Figure 1, page 5). The analysis of stress-rupture data has been widely studied for many years. Some methods have attempted to rely upon fundamental considerations of material behavior, but the current state of understanding of the creep behavior of complex structural alloys requires that most methods be empirical in nature. Recognizing this fact, a method is presented here through which standard techniques of linear regression analysis can be applied to stress-rupture and minimum creep rate data.

Review of Previous Techniques

Various forms of graphical, numerical, parametric, and algebraic procedures have been proposed and used with varying degrees of success. The most widely investigated methods have involved the so-called "time-temperature parameters," in which some parametric combination of rupture life, t_r, and temperature, T, is expressed as a function of stress, σ, only:

$$P(t_r, T) = f(\sigma) \quad . \tag{1}$$

A plot of the time-temperature parameter, P, against stress then defines the rupture behavior as a single two-dimensional "master curve," thus simplifying the analysis. Moreover, short-time high-temperature data can supposedly be used to estimate long-time behavior at lower temperatures. Time-stress, stress-temperature, and time-stress-temperature parameters are also possible, with the total number of proposed parameters now standing in the dozens. Several comprehensive reviews of various parametric techniques are available [32-35].

The large number of possible analytical procedures makes the choice of the method to use in a particular situation a formidable task. One possible solution to this problem is the development of flexible "generalized" parameters such as that proposed by Manson [36]. Also possible are numerical techniques based on a pointwise-defined mesh of material properties. These techniques, such as the "minimum-commitment method" proposed by Manson [33], or the use of finite-difference recurrence relations [37], allow the data to numerically determine the interrelationships among stress, temperature, and time. Thus, the analyst is not required to specify a strict functional form beforehand.

A standard method for selecting mathematical models to represent phenomena in a wide range of applications involves the use of linear regression analysis. Application of this technique to the analysis of creep and creep-rupture data thus appears to be a logical step. In fact, such techniques have been used for a variety of mechanical

properties of 2 1/4 Cr-1 Mo steel [38], including rupture data. Rummler [39] has proposed the use of regression analysis of rupture data, although he was concerned only with fitting data and not with extrapolation. The technique proposed here is basically similar to that used previously for 2 1/4 Cr-1 Mo steel. The essential features of this technique and results for type 304 stainless steel are presented below.

Techniques of Regression Analysis

Regression analysis is widely used in science, engineering, and industry, and many excellent summaries of the subject are available, such as Refs. [40] and [41]. A general description of the subject will not be given here, although a brief introduction is necessary for an understanding of the remainder of this chapter.

It should be remembered that the term "regression analysis" does not imply a single rigidly defined analytical approach. In a sense, it represents more of a general philosophy toward the analysis of data. This philosophy basically involves first the identification of the relevant response (dependent) and predictor (independent) variables. Then, the predictor variables are used to form a model that best describes the variations in the response variable within the framework of the particular problem at hand. The exact method by which the final model is chosen can vary widely depending upon the preference of the individual analyst. There is no single "best" method. This chapter illustrates a few possible approaches.

The need to summarize large masses of data by simple analytical relationships is obvious for elevated-temperature design. For the present purposes, it will be assumed that such relationships can be stated in the form

$$y_i = \sum_j \beta_j x_{ij} + \varepsilon_i \ , \tag{2}$$

where the y_i are the values of the response variable and the x_{ij} are the values of the predictor variables that may include combinations of known constants, stress, temperature, or other important factors. The β_j are the coefficients multiplying the predictor variables, while ε_i is an error term reflecting the random variation in y. Due to the nature of the creep test, the rupture life (t_r), or minimum creep rate ($\dot{e}_m$), or some transformation thereof should be used as the response variable.

Equation (2) assumes that the chosen model is exactly correct and that the β_j have some exact, though unknown, values.

In practice, this ideal situation is not found. In the case of creep and creep-rupture data for complex alloys, the current state of understanding of the processes involved does not allow an identification of the "correct" physical model. Rather, the optimum empirical model is sought, although it is not expected to be physically exact. The coefficients β_j are then estimated by the method of least squares.

Label the estimated values of the β_j as b_j. Then we have

$$\hat{y}_i = \sum_j b_j x_{ij} \ , \tag{3}$$

where $\hat{y}_i$ is the predicted value of the response variable (log t_r or log $\dot{e}_m$) for the ith observation. The difference between predicted and experimental values is given by

$$E_i = y_i - \hat{y}_i \ , \tag{4}$$

and is denoted the ith residual. The least squares technique seeks to minimize the sum of squares of the residuals, RSS, given by

$$RSS = \sum_i E_i^2 = \sum_i (y_i - \hat{y}_i)^2 \ . \tag{5}$$

Additionally, it is assumed that the residuals are normally distributed about zero. As long as a model such as Eqn. 2 is linear in the coefficients, RSS may be minimized by simple techniques, such as are described elsewhere [40,41]. First, however, an appropriate model must be identified.

Several specific decisions must be made during the process of performing a regression analysis for a particular set of data. These include the following steps.

1. The goals of the analysis must be established. For instance, is fitting the data sufficient, or is extrapolation required? Are the fits meant to describe individual heats of material, or is it necessary to develop a general description of the behavior of a material based on a multiheat set of data? What are the important variables whose effects must be described? Is the requirement that of predicting time to failure at a given stress or stress to failure at a given time?

2. The base of relevant data must be located, collected, and screened. In the case of a multiheat data base, some sets of data may

still have to be treated separately. Data for different heats from different sources with different thermomechanical processing histories may display fundamentally different behavior. These differences may preclude simultaneous treatment of the different data sets. On the other hand, while a regression model may not precisely describe heat-to-heat and heat treatment effects, a model that reflects these effects at least to some degree may be of more general use than one that ignores them entirely. Also, can future heats be expected to display a distribution of behavior similar to that found in the heats for which data are available?

3. A model must be selected. This step can be a complicated one in general, especially in the case of creep and creep-rupture data, which can be "messy" in terms of regression analysis. For example, data at higher temperatures are generally collected at lower stresses. This intercorrelation between stress and temperature can make it difficult to isolate the effects of the individual variables. Also, data for different heats are generally not available at the same stress-temperature conditions.

4. Before actual use, the resulting model must be evaluated and limitations placed on its application. Where appropriate, upper and lower bounds on behavior may be established.

The goal of the current analysis is to develop design equations for type 304 stainless steel. Thus, the analysis involves both extrapolation and multiheat data sets. This situation can cause problems, since many regression models can yield meaningless predictions outside the range of available data. In the case of creep

data, metallurgical instabilities or mechanism changes can cause problems when extrapolating (see Chapter V). Moreover, in the ideal limit, regression analysis assumes that scatter in the data about the predicted mean is due only to random variation. Heat-to-heat variations in properties introduce a new nonrandom source of variation. These problems are not thought to be insurmountable, but they indicate the importance of extreme caution.

The data base which will be used in the current analysis was described in the last chapter. Note that we will be using ultimate tensile strength (U) terms in the various predictive models developed. However, U is not a uniquely defined property even for a given heat of material at a given temperature, but depends upon the testing technique used to generate the tensile data. In particular, at temperatures where creep effects are important, strain rate is an important variable [16]. As can be seen in Table I, page 7, of the last chapter, four major sets of stress-rupture data were available for analysis, labeled BSCC, NRIM, US, and ORNL data. Only US and ORNL minimum creep rate data were available. The ultimate tensile strength data were generated at different strain rates for each of these four data sources. Therefore, for consistency, data from each of these sets were analyzed separately.

The remainder of this chapter is devoted to model selection and evaluation.

Techniques of Model Selection

Various standard techniques for selecting optimum regression models are available. These include the methods of forward selection, backward elimination, stepwise regression, and several others [40]. However, most methods have the common characteristic that they seek to isolate a single optimum model based on statistical considerations. In the case of creep and rupture data, such isolation is probably not appropriate. Rather, it is preferable to isolate several potential models and to choose one based on criteria such as physical reasonableness and analytical behavior when extrapolated. The most straightforward way of determining such a list of candidate models is simply to perform all possible regressions involving a preselected set of predictor variables. This solution is complicated by the fact that the definition of "best" model can become subjective. The method does, however, provide the analyst with a variety of options.

Before choosing a list of predictor variables, one must decide upon a choice of dependent variable. This choice has caused a surprising amount of controversy in the case of rupture data, with some authors favoring time as the dependent variable, and others favoring stress. Depending upon the methods and goals of a particular analysis, perhaps there is some question about the choice of dependent variable. However, in performing a regression analysis, the nature of the creep test forces time to rupture and minimum creep rate (or some transformations thereof) to be considered as the respective dependent variables. Here, we have chosen to use log t_r and log $\dot{e}_m$ as dependent

variables since the logarithmic transformation appears to yield variables that display a normal distribution about the mean at given levels of the predictor variables. Moreover, this normal distribution appears to have a constant variance as a function of the predictor variables. Both of these conditions (normal distribution and constant variance) are implied assumptions of the linear regression techniques used here.

The important factors in determining the value of log $\dot{e}_m$ or log t_r appear to be applied stress (σ), temperature (T) , and heat-to-heat variability. Previous investigators [13,19,20] have shown that the elevated-temperature ultimate tensile strength can be an effective indicator of heat-to-heat variations in creep and rupture behavior. We have assumed that the ultimate tensile strength (U) can be used as a third factor in order to decrease the uncertainty caused by heat-to-heat variations in strength, since these variations can be quite large [13]. Thus, we have

$$y = f(\sigma, T, U) \tag{6}$$

where y is log t_r or log $\dot{e}_m$ and the function f is formed by some linear combination of terms which are themselves functions of σ, T, and U, plus one constant intercept form. Each term is multiplied by a coefficient whose value is determined by a least-squares fit to the data.

This approach contains an infinite set of possible functions. However, we are interested here in fitting large multiple heat sets of

data for design purposes. Any final model chosen must not only fit the data, but must yield reasonable and consistent extrapolations beyond the range of the data in stress, time, and temperature. These considerations greatly reduce the set of terms that must be considered. Such practical considerations also greatly reduce the number of terms that should be allowed to appear in any one model.

Even so, the number of models that must be considered is huge. For example, in the present analyses, we considered a possible total of sixteen terms, plus a constant term. (These terms will be enumerated later.) Moreover, the models considered were limited to those containing a constant term plus one to six terms in σ, T, and U. The total number of models thus under consideration was

$$N = \binom{16}{6} + \binom{16}{5} + \binom{16}{4} + \binom{16}{3} + \binom{16}{2} + \binom{16}{1} \tag{7}$$

where $\binom{m}{k}$ represents the total possible number of combinations of m terms taken k at a time, $\binom{m}{k} = \frac{m!}{k!(m-k)!}$. Thus the total number of models we considered was 14,892!

Fortunately, methods are available for increasing computational efficiency in the choice of subset regression models. We used the method of LaMotte and Hocking [42,43], as implemented by a computer program based on their SELECT subroutine.

The program first rejects many models at each level (number of terms) as being inferior based on statistical criteria. The remaining models at that level are ranked according to the coefficient of determination, R^2. The statistic R^2 (%) is defined by

$$R^2 = 100\left(1 - \frac{RSS}{CTSS}\right) . \tag{8}$$

RSS is the residual sum of squares, given by Eqn. 5. The corrected total sum of squares, CTSS, is given by

$$CTSS = \sum_{i=1}^{N} (y_i)^2 - \frac{\left(\sum_{i=1}^{N} y_i\right)^2}{N} , \tag{9}$$

where N is the total number of data. The value of R^2 represents the percentage of the variation in the experimental data that can be described by a particular model.

Input to the computer program thus consists of the experimental data and a list of possible terms. Output consists of a ranked list (according to R^2) of the ten best models at each level (number of terms). These lists will in general not identify a single "best" model, but will merely indicate a list of candidate models. The final model selection can then be based on a combination of criteria, including fits to data, simplicity, physical reasonableness, consistent extrapolation, etc.

Identification of Candidate Models

The first step in the analysis for each of the six subject data sets (BSCC, NRIM, US, and ORNL rupture data and US and ORNL minimum rate data) was to use the SELECT subroutine to identify candidate models for describing the stress-rupture behavior of this material according to Eqn. 6. After several preliminary runs, a total of sixteen terms

were identified for input to the computer program. They are listed in Table VIII. These terms reflect the requirement that the final equation be simple and extrapolable. Temperature appears in the various terms only as 1/T, rather than as more complicated functions. Since creep is a thermally activated process, such a temperature dependence is certainly reasonable. The ultimate tensile strength for this material at a given strain rate can be approximately described as a cubic polynomial in temperature [16]. The ultimate tensile strength terms thus provide a more flexible means of describing any temperature dependence. Note that only first order terms in stress (σ) or log σ appear in Table VIII. Graphical analysis of the current data in terms of isothermal plots of log t_r or log $\dot{e}_m$ vs log σ showed no inflections in these plots. In fact, these curves appeared to be describable by straight lines. If any curvature of these lines is reflected in the data, it would be described by a model containing both σ and log σ terms. Thus, the relatively simple terms given in Table VIII should be capable of providing simple models that well describe trends in the data, while exhibiting no inflections or analytical instabilities when extrapolated beyond the data base.

Each of the six available data sets (four rupture and two minimum creep rate) was individually subjected to analysis using the SELECT procedure. In addition, the US and ORNL rupture data for type 304 stainless steel were rerun together for comparison purposes. Data from the US, BSCC, and NRIM sources for type 316 stainless steel were also analyzed. The results of analyses for that material are reported elsewhere [44].

TABLE VIII

TERMS USED IN CHOOSING CANDIDATE MODELS THROUGH SELECT

Term Number	Term[a]
1	$1/T$
2	σ
3	σ/T
4	$\log \sigma$
5	$(\log \sigma) /T$
6	$(\log \sigma) / (TU)$
7	U
8	$1/U$
9	$U \sigma$
10	σ/U
11	$1/(TU)$
12	$U \log \sigma$
13	$\frac{1}{U} \log \sigma$
14	$\sigma /(TU)$
15	$\log (\sigma/U)$
16	U/T

[a] T = Temperature (K),

σ = Stress (MPa),

U = Ultimate Tensile Strength at Temperature (MPa).

Since the SELECT program ranks candidate models according to the R^2 statistic, models with more terms will have inherent advantage over those with fewer terms. Therefore, one must limit the number of terms in the selected models based on a compromise between statistical fit to data and simplicity. An example of the variation of R^2 with number of nonconstant terms from SELECT for the ORNL rupture data is shown in Figure 2, where R^2 for the best and tenth best model at each level is plotted against the number of nonconstant terms in that model. Figure 2 shows that R^2 increases very rapidly in going from one to two nonconstant terms, but increases little more in going beyond three terms. Another useful statistic for examining these fits is the standard error of estimate, SEE, given by

$$SEE = \sqrt{\frac{RSS}{N - \nu}} \tag{10}$$

where N is again the total number of data and ν is the total number of terms in the model. As shown in Figure 3 SEE improves (decreases) very little in going beyond three terms. Another interesting aspect of Figures 2 and 3 is the very small magnitude of the statistical difference between the best and tenth best model at each level. Based on plots such as Figures 2 and 3, models with three nonconstant terms were chosen for extensive study. Table IX shows the ten best three-term models for each of the above six data sets, plus the ORNL-US combined rupture data. The numbers in parenthesis to the right of some of the models in Table IX indicate the number of that model as used in subsequent analysis. Models were chosen for further study on the basis of fits to one or more data sets and of physical reasonableness. Models

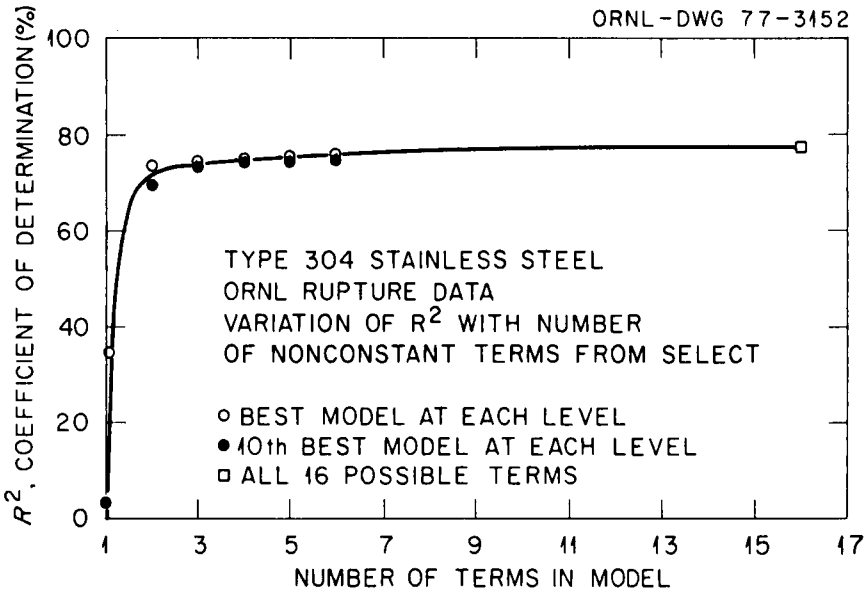

Figure 2. Variation in the Coefficient of Determination, R^2, With Number of Nonconstant Terms in Regression Models for the ORNL Rupture Life Data.

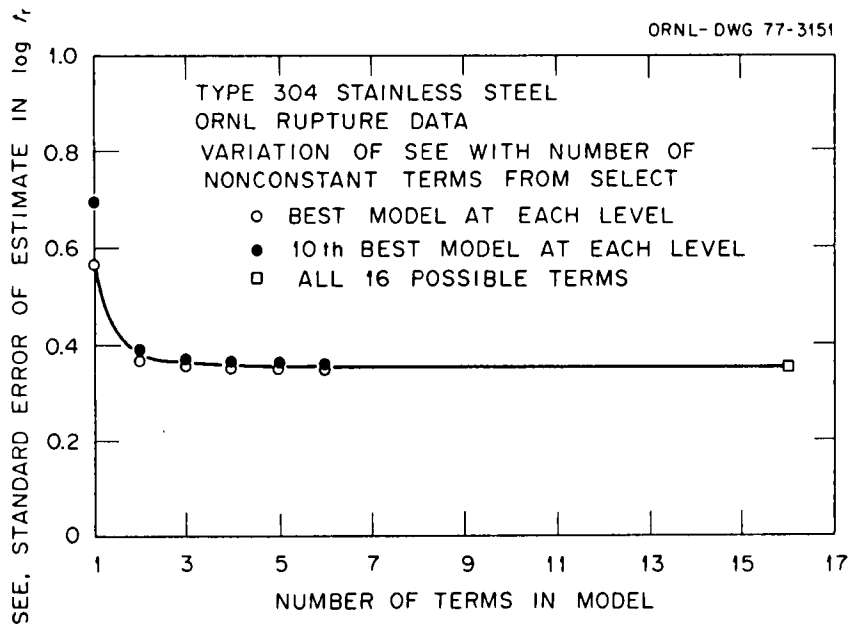

Figure 3. Variation in the Standard Error of Estimate, SEE, With Number of Nonconstant Terms in Regression Models for the ORNL Rupture Life Data.

TABLE IX

TEN LEADING THREE NONCONSTANT TERM MODELS AS IDENTIFIED BY SELECT FOR EACH DATA SET

Terms[a]	R^2 [b]	
ORNL Rupture Life Data		
16,12, 5	74.37	(1)[c]
16, 1,12	74.28	(2)
3, 4,16	74.09	(3)
16, 1, 5	73.94	(4)
4,14,16	73.91	
16, 4, 2	73.88	(5)
15,16, 2	73.75	
9, 4,16	73.70	(6)
15,14,16	73.64	
3,15,16	73.63	
US Rupture Life Data		
10, 3, 1	89.92	
16,14,10	89.83	
9,10, 1	89.80	
9, 2, 1	89.73	
7,14,10	89.57	
12,14,10	89.47	
14,10, 1	89.46	
16,12,10	89.46	
16, 7,10	89.44	
16, 4, 2	89.44	(5)
BSCC Rupture Life Data		
11, 7,12	87.19	(7)
6, 7,15	86.89	
6, 7, 4	86.73	
7,11,15	86.11	
1,12,16	86.09	(2)
6,12,15	86.06	
16,13,15	86.05	
12, 5,16	86.02	(1)
6,16,15	85.91	
9,16, 4	85.84	
NRIM Rupture Life Data		
9, 1, 2	89.34	
11,10,16	88.73	
7,10,16	88.60	

TABLE IX (continued)

Terms[a]	R^2 [b]	
4, 5,14	88.28	(8)
7,14,16	88.23	
4, 5,10	88.23	(9)
8, 1,10	88.02	
7,11,10	87.95	
11, 1,10	87.78	
6,15,16	87.76	
ORNL Minimum Creep Rate Data		
16, 1,12	84.61	(2)
16,12, 5	83.67	(1)
11, 7,12	83.14	(7)
14,16,12	82.98	(10)
15, 6, 7	82.74	
16, 4, 2	82.70	
3,16, 2	82.69	
16,12, 2	82.65	
3, 7, 2	82.64	
9,16, 4	82.62	(6)
US Minimum Creep Rate Data		
12, 4, 9	95.87	
3,12, 4	95.79	(11)
2,12, 4	95.77	
2, 4,16	95.75	(5)
3, 4,16	95.75	(12)
14, 4,16	95.73	
4, 9,16	95.72	(6)
10, 4,16	95.65	(3)
14,12, 4	95.57	
14,15, 1	95.53	(13)
US-ORNL Combined Rupture Life Data		
4,10,16	76.50	(3)
4,14,16	76.29	
4, 2,16	76.02	(5)
15,10,16	75.99	(14)
4, 3,16	75.95	(12)
10, 3,16	75.89	
14,10,16	75.87	
14,10, 7	75.73	
9,10,16	75.71	
9, 4,16	75.70	(6)

[a]As listed in Table VIII, page 26.

[b]Coefficient of Determination. R^2 defines the percent of variations in the data that is described by the model.

[c]Numbers in parenthesis indicate the number of the given model in the final list of candidate models, as listed in subsequent analysis.

which lacked an explicit temperature term were exluded from further study. Also excluded were models in which log t_r was linear in σ, since an extrapolation to zero stress would yield a finite rupture life from such a model.

In selecting models for further study, it was decided to consider rupture life and minimum creep rate models simultaneously, since the candidate models for these two properties were generally similar in form. Models for both types 304 and 316 stainless steel were treated together. A total of fourteen three-nonconstant term models were selected on the basis of the SELECT results for rupture life and minimum creep rate of type 304. A fifteenth, two-term model was chosen for further study because of previous use [13,19]. Model 16, also a two-nonconstant term model, was chosen for study on the basis of simplicity and fits to data. Models 17-27 were chosen for type 316 stainless steel in the same way that Models 1-14 were chosen for type 304 stainless steel. Finally, Models 28-32 were chosen for comparison, these models being forms of the common Larson-Miller (LM) [45], Manson-Succop (MS)[46], and Orr-Sherby-Dorn (OSD)[47] time-temperature parameters. Model 27, chosen through SELECT, is also a form of the OSD parameter. The final list of thirty-two candidate models is given in Table X.

Obviously, the list in Table X could have been made longer or shorter. The SELECT results indicate that one is certainly not likely to describe the current data sets much better than with the models in this list, although there are several other models that could have been included.

TABLE X

LIST OF CANDIDATE MODELS USED TO DESCRIBE RUPTURE LIFE AND MINIMUM CREEP RATE DATA

1. $\log y = \alpha_0 + \frac{\alpha_1}{T} \log \sigma + \frac{\alpha_2 U}{T} + \alpha_3 U \log \sigma$

2. $\log y = \alpha_0 + \alpha_1/T + \frac{\alpha_2 U}{T} + \alpha_3 U \log \sigma$

3. $\log y = \alpha_0 + \alpha_1 \log \sigma + \frac{\alpha_2 \sigma}{U} + \alpha_3 U/T$

4. $\log y = \alpha_0 + \alpha_1 U/T + \alpha_2/T + \frac{\alpha_3}{T} \log \sigma$

5. $\log y = \alpha_0 + \alpha_1 \log \sigma + \alpha_2 \sigma + \alpha_3 U/T$

6. $\log y = \alpha_0 + \alpha_1 \log \sigma + \alpha_2 U\sigma + \alpha_3 U/T$

7. $\log y = \alpha_0 + \alpha_1 /(UT) + \alpha_2 U + \alpha_3 U \log$

8. $\log y = \alpha_0 + \alpha_1 \log \sigma + \frac{\alpha_2}{T} \log \quad + \frac{\alpha_3}{TU}$

9. $\log y = \alpha_0 + \alpha_1 \log \sigma + \frac{\alpha_2}{T} \log \sigma + \frac{\alpha_3}{T} \sigma$

10. $\log y = \alpha_0 + \frac{\alpha_1}{TU} \sigma + \alpha_2 U/T + \alpha_3 U \log \sigma$

11. $\log y = \alpha_0 + \alpha_1 \sigma/T + \alpha_2 U \log \sigma + \alpha_3 \log \sigma$

12. $\log y = \alpha_0 + \alpha_1 \log \sigma + \alpha_2 \sigma/T + \alpha_3 U/T$

13. $\log y = \alpha_0 + \alpha_2 \sigma /(TU) + \alpha_2 \log (\sigma/U) + \alpha_3/T$

14. $\log y = \alpha_0 + \alpha_1 \log (\sigma/U) + \alpha_2 \sigma/U + \alpha_3 U/T$

15. $\log y = \alpha_0 + \alpha_1 \log \sigma + \alpha_2 U$

16. $\log y = \alpha_0 + \alpha_1 \log \sigma + \alpha_2 U/T$

TABLE X (continued)

17. $\log y = \alpha_0 + \alpha_1\sigma + \alpha_2 \log \sigma + \alpha_3 \log \sigma/T$

18. $\log y = \alpha_0 + \alpha_1\sigma + \frac{\alpha_2}{U} \log \sigma + \alpha_3 /T$

19. $\log y = \alpha_0 + \alpha_1\sigma + \alpha_2 \log (\sigma/U) + \alpha_3 /T$

20. $\log y = \alpha_0 + \alpha_1 \log \sigma + \frac{\alpha_2}{T} \log \sigma + \alpha_3\sigma U$

21. $\log y = \alpha_0 + \alpha_1 \log \sigma + \alpha_2 \sigma/T \frac{\alpha_3}{T} \log \sigma$

22. $\log y = \alpha_0 + \alpha_1 \log \sigma + \alpha_2 \sigma U + \alpha_3 /T$

23. $\log y = \alpha_0 + \alpha_1 \log \sigma + \alpha_2 /T + \alpha_3 \sigma/(TU)$

24. $\log y = \alpha_0 + \frac{\alpha_1}{U} \log \sigma + \frac{\alpha_2}{TU} \log \sigma + \alpha_3 \sigma /(TU)$

25. $\log y = \alpha_0 + \alpha_1 \log \sigma + \alpha_2 U/T + \alpha_3 U \log \sigma$

26. $\log y = \alpha_0 + \alpha_1 \sigma /U + \alpha_2 \log (\sigma/U) + \alpha_3 /T$

27. $\log y = \alpha_0 + \alpha_1 \log \sigma + \alpha_2 \sigma + \alpha_3 /T$

28. $\log y = \alpha_0 + \alpha_1 \log \sigma + \alpha_2 \sigma /T + \alpha_3 /T$

29. $\log y = \alpha_0 + \frac{\alpha_1}{T} \log \sigma + \alpha_2 \sigma /T + \alpha_3 /T$

30. $\log y = \alpha_0 + \alpha_1 \log \sigma + \alpha_2 /T$

31. $\log y = \alpha_0 + \alpha_1 \log \sigma + \alpha_2 T$

TABLE X (continued)

32.	$\log y = \alpha_0 + \frac{\alpha_1}{T} \log \sigma + \alpha_2 / T$

Note: y = minimum creep rate or rupture life; T = temperature (K); σ = stress (MPa). U = ultimate tensile strength at temperature (MPa); $\alpha_0 - \alpha_3$ = constants to be estimated by least squares.

Evaluation of Candidate Models

The 32 candidate models were studied as follows. First, each model was fit by a least squares technique to each of the six basic data sets. Then, each data set was divided into two portions: rupture data into short-term ($t_r \leq 2000$ hr) and long-term ($t_r > 2000$ hr) data, and minimum creep rate data into high rate ($\dot{e}_m \geq 0.001\%/hr$) and low rate ($\dot{e}_m < 0.001\%/hr$) data. Each of the models was next fit to the short time and high rate data sets. Predictions from the models thus obtained were then compared with the long time and low rate data to assess the extrapolability of the various models.

Tables XI and XII present the best-fit values of the coefficients from each of the 32 models listed in Table X for the four complete rupture life and two complete minimum creep rate data sets respectively. Tables XIII and XIV then show the relative successes obtained in fitting these models to the complete data sets in terms of R^2. Finally, Tables XV and XVI show the values of the root mean square error, RMSE, for each of the models obtained by predicting the long time and low rate data from fits to the short time and high rate data.

$$RMSE = \left(\frac{RSS}{N}\right)^{\frac{1}{2}} \tag{11}$$

where N is the total number of data, and RSS the residual mean square. N and RSS refer to the predicted (long time/low rate) data only. Since the models were not fit directly to the long time/low rate data, the

TABLE XI

BEST FIT VALUES OF THE COEFFICIENTS IN THE CANDIDATE MODELS FOR RUPTURE LIFE

Model[a]	α_0	α_1	α_2	α_3
ORNL Data				
1	0.57164E 01	-0.39149E 04	0.32601E 02	-0.73034E-02
2	0.17499E 02	-0.19782E 05	0.62477E 02	-0.21474E-01
3	0.68238E 01	-0.30856E 01	-0.30696E 01	0.11554E 02
4	0.10085E 00	0.17477E 02	0.95896E 04	-0.58833E 04
5	0.72143E 01	-0.40327E 01	-0.73095E-02	0.15262E 02
6	0.85326E 01	-0.50893E 01	-0.13614E-04	0.16734E 02
7	-0.13424E 02	0.14372E 07	0.81838E-01	-0.21507E-01
8	0.37520E 01	-0.52116E 01	0.55252E 04	-0.57080E 04
9	0.24885E 01	-0.23925E 01	0.36604E 04	-0.70614E 01
10	0.15176E 01	-0.34496E 04	0.22242E 02	-0.69045E-02
11	0.12855E 02	-0.47562E 01	0.10109E-01	-0.75057E 01
12	0.79272E 01	-0.45755E 01	-0.51099E 01	0.15888E 02
13	-0.93274E 01	-0.27193E 04	-0.29207E 01	0.11282E 05
14	-0.67699E 00	-0.43632E 01	-0.19307E 01	0.82819E 01
15	0.99715E 01	-0.64475E 01	0.21329E-01	0.0
16	0.11337E 02	-0.64000E 01	0.14755E 02	0.0
17	0.56978E 01	-0.13737E-01	-0.80948E 01	0.68691E 04
18	0.12607E 01	-0.11656E-01	-0.47263E 03	0.59133E 04
19	-0.92370E 01	0.23165E-02	-0.70631E 01	0.83044E 04
20	0.11013E 02	-0.10948E 02	0.65009E 04	-0.88710E-05
21	0.68851E 01	-0.98262E 01	-0.10745E 02	0.78241E 04
22	-0.31714E 01	-0.48628E 01	-0.26686E-05	0.14756E 05
23	-0.83205E 01	-0.23948E 00	0.12681E 05	-0.47144E 04
24	0.70545E 01	-0.10035E 04	0.60216E 06	-0.36123E 04
25	0.12188E 02	-0.69175E 01	0.12097E 02	0.17552E-02
26	-0.70949E 01	-0.37312E 01	-0.21397E 01	0.98057E 04
27	-0.78886E 01	-0.23951E 01	-0.86600E-02	0.15324E 05
28	0.28638E 02	-0.37067E 01	-0.52129E-02	-0.19064E-01
29	-0.14630E 02	-0.33745E 04	-0.44569E 01	0.23539E 05
30	-0.22443E 01	-0.51421E 01	0.14340E 05	0.0
31	0.31167E 02	-0.54310E 01	-0.18660E-01	0.0
32	-0.14174E 02	-0.48771E 04	0.25668E 05	0.0
US Data				
1	0.48168E 01	-0.28756E 04	0.37010E 02	-0.11928E-01
2	0.12139E 02	-0.12867E 05	0.56316E 02	-0.21767E-01
3	0.76023E 01	-0.34220E 01	-0.32216E 01	0.11652E 02
4	-0.45283E 01	0.13008E 02	0.16142E 05	-0.63286E 04
5	0.79928E 01	-0.43161E 01	-0.75253E-02	0.14945E 02
6	0.88909E 01	-0.51492E 01	-0.15494E-04	0.16424E 02
7	-0.11877E 02	0.13543E 07	0.76442E-01	-0.20840E-01
8	0.66829E 01	-0.73987E 01	0.63682E 04	-0.58174E 04
9	0.55808E 01	-0.48610E 01	0.46722E 04	-0.71464E 01

Table XI (continued)

Model[a]	α_0	α_1	α_2	α_3
10	0.20373E 01	-0.28072E 04	0.29550E 02	-0.11775E-01
11	0.12212E 02	-0.55556E 01	0.98219E-02	-0.70730E 01
12	0.87473E 01	-0.48932E 01	-0.49875E 01	0.15465E 02
13	-0.91659E 01	-0.27328E 04	-0.39472E 01	0.10970E 05
14	-0.42587E-01	-0.39937E 01	-0.25269E 01	0.76752E 01
15	0.99919E 01	-0.63208E 01	0.20162E-01	0.0
16	0.11852E 02	-0.67170E 01	0.15136E 02	0.0
17	0.66591E 01	-0.18848E-01	-0.89641E 01	0.77146E 04
18	-0.33152E 01	-0.16106E-01	-0.26191E 03	0.95552E 04
19	-0.10654E 02	-0.46064E-02	-0.56058E 01	0.11109E 05
20	0.10246E 02	-0.11954E 02	0.83261E 04	-0.30691E-04
21	0.80722E 01	-0.11023E 02	-0.14613E 02	0.88223E 04
22	-0.58298E 01	-0.46984E 01	-0.17462E-04	0.17794E 05
23	-0.62079E 01	-0.20252E 01	0.14281E 05	-0.43922E 04
24	0.53559E 01	-0.15281E 04	0.14529E 07	-0.54210E 04
25	0.90443E 01	-0.48836E 01	0.25043E 02	-0.66998E-02
26	-0.69027E 01	-0.42188E 01	-0.27631E 01	0.97970E 04
27	-0.76300E 01	-0.27874E 01	-0.12239E-01	0.16640E 05
28	0.31196E 02	-0.40918E 01	-0.84976E-02	-0.20056E-01
29	-0.15287E 02	-0.40783E 04	-0.63829E 01	0.26242E 05
30	-0.93749E 00	-0.63316E 01	0.15664E 05	0.0
31	0.35630E 02	-0.67599E 01	-0.20157E-01	0.0
32	-0.15318E 02	-0.61742E 04	0.29730E 05	0.0
NRIM Data				
1	0.47446E 01	-0.25656E 04	0.42911E 02	-0.15642E-01
2	0.84187E 01	-0.81973E 04	0.59331E 02	-0.25025E-01
3	0.96019E 01	-0.44219E 01	-0.29391E 01	0.11822E 02
4	-0.74762E 01	0.10547E 02	0.21028E 05	-0.68945E 04
5	0.10138E 02	-0.53371E 01	-0.67400E-02	0.14931E 02
6	0.11256E 02	-0.62270E 01	-0.10439E-04	0.15826E 02
7	-0.17292E 02	0.22296E 07	0.93624E-01	-0.25224E-01
8	0.91789E 01	-0.95308E 01	0.73401E 04	-0.58988E 04
9	0.84867E 01	-0.75410E 01	0.58580E 04	-0.66907E 01
10	0.24505E 01	-0.34894E 04	0.33990E 02	-0.13961E-01
11	0.13362E 02	-0.76191E 01	0.96554E-02	-0.74160E 01
12	0.10768E 02	-0.58066E 01	-0.44592E 01	0.15230E 02
13	-0.94165E 01	-0.33448E 04	-0.41453E 01	0.11574E 05
14	0.25143E 01	-0.18657E 01	-0.58323E 01	0.68597E 01
15	0.11207E 02	-0.67003E 01	0.19017E-01	0.0
16	0.12574E 02	-0.68598E 01	0.14469E 02	0.0
17	0.12315E 02	-0.12134E-01	-0.14313E 02	0.99220E 04
18	-0.45501E 01	-0.21867E-01	-0.32551E 03	0.11986E 05
19	-0.11353E 02	-0.29163E-02	-0.64201E 01	0.11495E 05
20	0.15567E 02	-0.16454E 02	0.99042E 04	-0.81101E-05
21	0.13049E 02	-0.15391E 02	-0.96933E 01	0.10505E 05

TABLE XI (continued)

Model[a]	α_0	α_1	α_2	α_3
22	-0.27288E 01	-0.72963E 01	0.55089E-05	0.19437E 05
23	-0.62088E 01	-0.31623E 01	0.16748E 05	-0.44885E 04
24	0.61440E 01	-0.19028E 04	0.18390E 07	-0.75254E 04
25	0.89846E 01	-0.46460E 01	0.28343E 02	-0.86644E-02
26	-0.64710E 01	-0.54294E 01	-0.24988E 01	0.10139E 05
27	-0.56890E 01	-0.61474E 01	-0.34465E-02	0.20616E 05
28	0.39519E 02	-0.70948E 01	0.33553E-03	-0.23120E-01
29	-0.18765E 02	-0.73034E 04	0.23821E 01	0.35402E 05
30	-0.41964E 01	-0.69379E 01	0.20334E 05	0.0
31	0.39420E 02	-0.70160E 01	-0.23142E-01	0.0
32	-0.18899E 02	-0.67273E 04	0.34644E 05	0.0
BSCC Data				
1	0.26969E 01	-0.28987E 04	0.45433E 02	-0.12967E-01
2	0.97994E 01	-0.12820E 05	0.67031E 02	-0.23806E-01
3	0.10066E 02	-0.67149E 01	0.24391E 00	0.20264E 02
4	-0.55547E 01	0.19644E 02	0.14974E 05	-0.63089E 04
5	0.80915E 01	-0.54704E 01	-0.35215E-02	0.20065E 02
6	0.78307E 01	-0.55860E 01	-0.12133E-04	0.21703E 02
7	-0.26905E 02	0.33744E 07	0.10773E 00	-0.23705E-01
8	-0.21622E 01	-0.34660E 01	0.77323E 04	-0.11459E 05
9	-0.33029E 01	0.28845E 00	0.48645E 04	-0.12980E 02
10	-0.10339E 00	-0.37308E 04	0.34658E 02	-0.10619E-01
11	0.15627E 02	0.47532E 01	0.10609E-01	-0.97040E 01
12	0.88196E 01	0.59358E 01	-0.16027E 01	0.20107E 02
13	-0.16739E 02	-0.92598E 04	0.11289E 01	0.22528E 05
14	-0.54461E 01	-0.79047E 01	0.17688E 01	0.13456E 02
15	0.62818E 01	-0.51086E 01	0.23705E-01	0.0
16	0.97380E 01	-0.64639E 01	0.19980E 02	0.0
17	0.21546E 01	-0.25116E-01	-0.80221E 01	0.91928E 04
18	0.48309E 01	-0.10955E-01	-0.10285E 04	0.60666E 04
19	-0.13402E 02	0.27722E-01	-0.14620E 02	0.64450E 04
20	0.24399E 02	-0.13617E 02	0.12983E 04	0.97292E-04
21	0.37296E 01	-0.10443E 02	-0.20162E 02	0.10554E 05
22	0.19908E 02	-0.12399E 02	0.94254E-04	0.46393E 04
23	-0.19722E 02	0.44616E 01	0.16989E 05	-0.11149E 05
24	0.98808E 01	-0.18156E 04	0.95880E 06	-0.35611E 04
25	0.91049E 01	-0.61149E 01	0.23568E 02	0.19958E-02
26	-0.10464E 02	-0.11722E 02	0.28799E 01	0.17996E 05
27	-0.16061E 02	-0.42445E-01	-0.18826E-01	0.19927E 05
28	0.28904E 02	-0.85748E 00	-0.16219E-01	-0.23808E-01
29	-0.18870E 02	-0.10635E 04	-0.13916E 02	0.24236E 05
30	-0.59158E 01	-0.47778E 01	0.17428E 05	0.0
31	0.33190E 02	-0.49768E 01	-0.21422E-01	0.0
32	-0.16951E 02	-0.46770E 04	0.28201E 05	0.0

[a]From Table X, pages 34-36.

TABLE XII

BEST FIT VALUES OF THE COEFFICIENTS IN THE CANDIDATE MODELS FOR MINIMUM CREEP RATE

Model[a]	α_0	α_1	α_2	α_3
ORNL Data				
1	-0.27646E 01	0.33463E 04	-0.51840E 02	0.16162E-01
2	-0.14809E 02	0.19365E 05	-0.80584E 02	0.28802E-01
3	-0.97988E 01	0.64336E 01	0.17071E 01	-0.19303E 02
4	0.89478E 01	-0.18416E 02	-0.20283E 05	0.75696E 04
5	-0.70556E 01	0.52861E 01	0.93188E-02	-0.21887E 02
6	-0.85695E 01	0.65453E 01	0.17918E-04	-0.23770E 02
7	0.26067E 02	-0.27020E 07	-0.12077E 00	0.28861E-01
8	-0.52362E 01	0.95799E 01	-0.86034E 04	0.63352E 04
9	-0.44835E 01	0.69546E 01	-0.66166E 04	0.73560E 01
10	0.76886E 00	0.28746E 04	-0.42992E 02	0.15954E-01
11	-0.15812E 02	0.42974E 01	-0.13899E-01	0.10510E 02
12	-0.87542E 01	0.64038E 01	0.53388E 01	-0.22442E 02
13	0.16506E 02	0.33992E 04	0.37573E 01	-0.17033E 05
14	0.31511E 01	0.55066E 01	0.23256E 01	-0.12347E 02
15	-0.10085E 02	0.80828E 01	-0.29505E-01	0.0
16	-0.12330E 02	0.83111E 01	-0.21216E 02	0.0
17	-0.62801E 01	0.18499E-01	0.12784E 02	-0.10771E 05
18	0.13194E 02	0.18387E-01	0.28272E 03	-0.17847E 05
19	0.18345E 02	0.43372E-02	0.64360E 01	-0.16813E 05
20	-0.12921E 02	0.16945E 02	-0.10879E 05	0.16873E-04
21	-0.78952E 01	0.15055E 02	0.14307E 02	-0.11983E 05
22	0.10228E 02	0.65240E 01	0.59320E-05	-0.23670E 05
23	0.13982E 02	0.18444E 01	-0.20173E 05	0.48705E 04
24	-0.42806E 01	0.23925E 04	-0.22466E 07	0.56944E 04
25	-0.73910E 01	0.53197E 01	-0.36437E 02	0.10062E-01
26	0.13933E 02	0.41534E 01	0.33102E 01	-0.15004E 05
27	0.15420E 02	0.35422E 01	0.11199E-01	-0.23882E 05
28	-0.39918E 02	0.51719E 01	0.64244E-02	0.28837E-01
29	0.25011E 02	0.47679E 04	0.56248E 01	-0.35275E 05
30	0.81644E 01	0.71540E 01	-0.22760E 05	0.0
31	-0.42993E 02	0.72965E 01	0.28298E-01	0.0
32	0.24457E 02	0.66707E 04	-0.37992E 05	0.0
US Data				
1	-0.42162E 01	0.32073E 04	-0.41910E 02	0.13561E-01
2	-0.27111E 01	0.21388E 04	-0.57043E 02	0.27072E-01
3	-0.92434E 01	0.53876E 01	0.24094E 01	-0.15924E 02
4	0.76618E 01	-0.15281E 02	-0.19298E 05	0.71617E 04
5	-0.92823E 01	0.59056E 01	0.60365E-02	-0.18257E 02
6	-0.95923E 01	0.64031E 01	0.13868E-04	-0.19677E 02

TABLE XII (continued)

Model[a]	α_0	α_1	α_2	α_3
7	0.21503E 02	-0.25801E 07	-0.97857E-01	0.24240E-01
8	-0.10866E 02	0.12060E 02	-0.83126E 04	0.50080E 04
9	-0.10323E 02	0.10090E 02	-0.68306E 04	0.58818E 01
10	-0.11575E 01	0.12312E 04	-0.48266E 02	0.22653E-01
11	-0.13578E 02	0.69145E 01	-0.13768E-01	0.91193E 01
12	-0.94586E 01	0.61566E 01	0.45062E 01	-0.18860E 02
13	0.14542E 02	0.21022E 04	0.60458E 01	-0.14091E 05
14	0.27313E 01	0.58559E 01	0.18569E 01	-0.10593E 02
15	-0.93618E 01	0.72802E 01	-0.26513E-01	0.0
16	-0.11780E 02	0.76024E 01	-0.18556E 02	0.0
17	-0.11620E 02	0.17576E-01	0.14650E 02	-0.10292E 05
18	-0.99625E 01	0.12844E-01	0.10415E 04	-0.13838E 04
19	0.16352E 02	0.65257E-02	0.64642E 01	-0.15442E 05
20	-0.13399E 02	0.18857E 02	-0.13144E 05	0.47254E-04
21	-0.12332E 02	0.16520E 02	0.14435E 02	-0.11583E 05
22	0.12026E 02	0.64508E 01	0.25827E-04	-0.26231E 05
23	0.77443E 01	0.49045E 01	-0.19973E 05	0.33831E 04
24	-0.11692E 02	0.63048E 03	0.43007E 06	0.31434E 04
25	-0.77787E 01	0.48045E 01	-0.32709E 02	0.10282E-01
26	0.13147E 02	0.25520E 01	0.58416E 01	-0.12984E 05
27	0.99367E 01	0.54890E 01	0.10874E-01	-0.22888E 05
28	-0.42931E 02	0.63312E 01	0.82325E-02	0.28876E-01
29	0.23564E 02	0.64024E 04	0.51371E 01	-0.37601E 05
30	0.49067E 01	0.83564E 01	-0.22238E 05	0.0
31	-0.46457E 02	0.85940E 01	0.28965E-01	0.0
32	0.23503E 02	0.78739E 04	-0.39825E 05	0.0

[a]From Table X, pages 34-36.

TABLE XIII

VALUES OF THE COEFFICIENTS OF DETERMINATION FROM THE CANDIDATE MODELS FOR RUPTURE LIFE

Model No.	ORNL Data	US Data	NRIN Data	BSCC Data
1	74.37	88.89	85.84	86.02
2	74.28	88.16	84.48	86.09
3	73.63	89.11	86.59	85.64
4	73.94	88.91	87.47	85.80
5	73.88	89.43	86.77	85.73
6	73.70	89.21	86.49	85.84
7	73.36	86.24	87.03	87.19
8	68.86	88.85	87.88	79.37
9	69.15	89.34	87.89	80.05
10	72.50	88.76	85.14	84.95
11	72.23	84.12	84.46	82.79
12	74.09	89.00	86.54	85.68
13	68.73	89.08	86.05	71.42
14	73.60	88.11	84.80	85.09
15	73.16	85.28	83.57	82.10
16	71.32	85.62	85.95	85.63
17	54.32	79.53	83.74	27.80
18	62.95	79.97	75.87	81.62
19	67.12	87.44	85.38	78.25
20	47.24	68.91	81.56	61.79
21	55.49	80.10	83.69	27.84
22	52.78	75.27	83.39	62.60
23	67.49	87.99	86.53	77.88
24	64.02	79.96	79.56	81.33
25	71.40	86.73	86.94	85.71
26	68.57	89.38	86.45	70.90
27	56.19	80.91	83.42	27.86
28	57.42	81.74	82.83	28.32
29	57.15	81.28	82.87	27.87
30	52.68	70.95	83.20	25.66
31	56.10	76.87	82.83	26.62
32	55.86	78.00	82.75	26.35

TABLE XIV

VALUES OF THE COEFFICIENTS OF DETERMINATION FROM THE CANDIDATE MODELS FOR MINIMUM CREEP RATE

Model No.	ORNL Data	US Data
1	83.67	94.54
2	84.61	93.90
3	81.21	95.65
4	81.53	95.42
5	82.70	95.75
6	82.62	95.72
7	83.14	92.92
8	79.10	93.61
9	78.30	93.18
10	82.98	94.21
11	75.82	95.79
12	82.15	95.75
13	78.79	95.53
14	79.01	95.41
15	76.80	94.64
16	80.85	94.55
17	72.67	92.94
18	73.64	90.61
19	77.76	95.43
20	67.46	92.39
21	73.22	93.30
22	71.42	93.95
23	78.43	94.66
24	67.53	91.53
25	82.15	94.90
26	78.53	95.41
27	73.83	94.27
28	72.83	94.39
29	73.96	94.56
30	71.22	90.36
31	71.93	92.13
32	73.05	93.48

TABLE XV

VALUES OF THE ROOT MEAN SQUARE ERROR OBTAINED BY PREDICTING THE LONG TIME RUPTURE LIFE DATA FROM FITS TO THE SHORT TIME DATA[a]

Model	ORNL Data (18 tests)	US Data (44 tests)	NRIM Data (71 tests)	BSCC Data (12 tests)
1	0.413	0.185	0.122	0.381
2	0.420	0.223	0.141	0.380
3	0.466	0.285	0.142	0.301
4	0.425	0.172	0.108	0.402
5	0.424	0.244	0.126	0.308
6	0.414	0.224	0.129	0.292
7	0.380	0.274	0.121	0.233
8	0.598	0.346	0.136	0.663
9	0.630	0.347	0.140	0.639
10	0.484	0.245	0.152	0.443
11	0.525	0.470	0.174	0.315
12	0.418	0.241	0.134	0.330
13	0.476	0.246	0.132	0.700
14	0.443	0.318	0.325	0.278
15	0.464	0.307	0.154	0.261
16	0.480	0.282	0.132	0.288
17	0.844	0.637	0.174	1.341
18	0.657	0.571	0.318	0.508
19	0.592	0.214	0.135	0.514
20	0.994	1.004	0.234	0.857
21	0.783	0.587	0.172	1.346
22	0.800	0.655	0.208	0.826
23	0.572	0.312	0.140	0.779
24	0.688	0.6490	0.268	0.517
25	0.512	0.206	0.115	0.378
26	0.506	0.288	0.266	0.704
27	0.723	0.499	0.173	1.344
28	0.653	0.420	0.211	1.343
29	0.656	0.431	0.188	1.344
30	0.792	0.828	0.165	1.355
31	0.679	0.532	0.161	1.342
32	0.676	0.476	0.156	1.342

[a]Long time: t_r > 2000 hr.

TABLE XVI

VALUES OF THE ROOT MEAN SQUARE ERROR OBTAINED BY PREDICTING THE LOW RATE MINIMUM CREEP RATE DATA FROM FITS TO THE HIGH RATE DATA[a]

Model	ORNL Data (17 tests)	US Data (33 tests)
1	0.536	0.444
2	0.415	0.722
3	0.932	0.920
4	0.792	0.314
5	0.741	0.702
6	0.676	0.530
7	0.624	0.872
8	1.074	2.208
9	1.222	2.404
10	0.658	0.709
11	1.568	0.756
12	0.791	0.596
13	0.867	0.594
14	1.199	0.539
15	1.296	0.343
16	0.754	0.381
17	0.982	2.175
18	1.152	2.736
19	0.704	0.510
20	1.126	1.742
21	0.895	1.891
22	0.830	0.920
23	0.968	1.328
24	2.042	1.601
25	0.589	0.420
26	0.995	0.640
27	0.758	1.178
28	0.850	0.713
29	0.688	0.686
30	0.846	0.934
31	0.862	0.674
32	0.696	0.558

[a](High Rate: $\dot{\epsilon}_m$ > 0.001%/hr.)

value of R for these data is meaningless—thus the use of the RMSE statistic for these comparisons.

The next step in the analysis is the selection of an optimum model for each of the six data sets. By virtue of the way in which the original terms for SELECT were chosen, most of the candidate models behave "reasonably" when extrapolated. In terms of fits to data, several models are virtually equivalent for each data set. Thus, any of several models could easily be chosen for each data set. There are many ways through which an optimum model might be chosen. The simple procedure used here for each data set was as follows. First, define the RSS value for each model from the fit to each total data set as RSS_f and the RSS value from the extrapolation to the long time/low rate data as RSS_e. Let N_f be the total number of data in each total data set and N_e be the total number of data in each long time/low rate data set. For each data set a new RMSE value, RMSE*, was calculated from

$$RMSE^* = \frac{RSS_f + RSS_e}{N_f + N_e} . \tag{12}$$

Also, in order to assess the overall applicability of each model to type 304 stainless steel, the four rupture life data sets were summed and the two minimum creep rate data sets were summed to yield RMSE** as

$$RMSE^{**} = \frac{\sum RSS_f + \sum RSS_e}{\sum N_f + \sum N_e} . \tag{13}$$

Tables XVII and XVIII show the results of these summations, including the rankings of the models for each individual data set.

TABLE XVII

VALUES OF THE POOLED ROOT MEAN SQUARE ERROR FROM FITS TO THE RUPTURE LIFE DATA AND FROM PREDICTIONS OF LONG TIME DATA FROM FITS TO SHORT TIME DATA
(LONG TIME : t_r > 2000)

Model	ORNL Data	US Data	NRIM Data	BSCC Data
1	0.148	0.122	0.094	0.170
2	0.149	0.136	0.106	0.169
3	0.156	0.144	0.098	0.147
4	0.151	0.144	0.098	0.177
5	0.151	0.132	0.092	0.149
6	0.151	0.129	0.094	0.144
7	0.150	0.162	0.089	0.121
8	0.188	0.160	0.091	0.281
9	0.189	0.157	0.093	0.271
10	0.162	0.137	0.107	0.193
11	0.167	0.223	0.117	0.163
12	0.150	0.135	0.095	0.156
13	0.179	0.135	0.097	0.324
14	0.154	0.159	0.168	0.143
15	0.158	0.177	0.114	0.149
16	0.167	0.168	0.097	0.144
17	0.273	0.294	0.120	0.689
18	0.219	0.276	0.199	0.225
19	0.195	0.140	0.100	0.241
20	0.317	0.455	0.149	0.409
21	0.263	0.278	0.119	0.691
22	0.276	0.329	0.133	0.396
23	0.192	0.158	0.098	0.297
24	0.217	0.294	0.168	0.229
25	0.170	0.143	0.088	0.170
26	0.182	0.143	0.142	0.327
27	0.255	0.252	0.120	0.690
28	0.244	0.228	0.136	0.688
29	0.245	0.234	0.128	0.790
30	0.276	0.400	0.118	0.702
31	0.252	0.289	0.119	0.694
32	0.252	0.268	0.117	0.695

TABLE XVIII

VALUES OF THE POOLED ROOT MEAN SQUARE ERROR FROM FITS TO THE MINIMUM CREEP RATE DATA AND FROM PREDICTIONS OF LOW RATE DATA FROM FITS TO HIGH RATE DATA (HIGH RATE: $\dot{e}_m$ > 0.001%/hr)

Model	ORNL Data	US Data
1	0.215	0.272
2	0.196	0.368
3	0.269	0.379
4	0.256	0.211
5	0.239	0.314
6	0.236	0.265
7	0.226	0.438
8	0.302	0.803
9	0.321	0.871
10	0.230	0.357
11	0.372	0.328
12	0.249	0.284
13	0.291	0.289
14	0.312	0.276
15	0.342	0.240
16	0.260	0.254
17	0.365	0.811
18	0.366	1.034
19	0.290	0.267
20	0.432	0.702
21	0.352	0.720
22	0.368	0.424
23	0.302	0.522
24	0.503	0.684
25	0.235	0.256
26	0.302	0.305
27	0.337	0.490
28	0.354	0.353
29	0.330	0.341
30	0.371	0.523
31	0.365	0.402
32	0.341	0.333

The choice of optimum models for minimum creep rate and rupture life for the ORNL data is particularly important. Later in this report it will be shown that the models for $\dot{e}_m$ and t_r can be useful in developing a complete creep strain-time equation. Since most available creep curves are from the ORNL data, the creep equation will be based primarily on those data. Based on the above criteria, Model 1 is the best rupture life model and the second best minimum creep rate model. Interestingly, Model 2 is the best minimum creep rate model and the second best rupture life model. Clearly, either of these models could be used to describe both rupture life and minimum creep rate. Note that based on the entire available data base, Model 1 yielded an RMSE** value of 0.49 for $\dot{e}_m$ (the best of all models) and of 0.35 for t_r (the second best of all models). Model 2 yielded RMSE** values of 0.51 for $\dot{e}_m$ and of 0.36 for t_r. Clearly, there is very little advantage in either model over the other (or in fact, over several others, such as Models 5, 6, 7). However, since Model 1 ranked ahead of Model 2 in the overall comparisons for both properties, Model 1 was selected as optimum for both properties for the ORNL data.

For the US data, based on RMSE* values, Model 4 ranked first for both $\dot{e}_m$ and t_r, and thereby was considered optimum for both properties. Note that Model 4 ranked first for t_r in the overall RMSE** values and second for $\dot{e}_m$ in the overall RMSE** values.

Model 4 also ranked first for the NRIM rupture data, while Model 7 ranked first for the BSCC data. Conclusions based on the BSCC data may be questionable due to lack of data (thus the wide variation in the

successes of various models for these data), but the values RMSE* and RMSE** contain an inherent weighting factor to take the number of data into account.

The above individual data set comparisons indicate Models 1 and 4 as perhaps the two most outstanding from the original list of 32 candidates, which themselves came from an original possible list of over 14,000. The properties of these two models will therefore be described here.

First, both models predict that log σ vs log t_r and log σ vs log $\dot{e}_m$ isotherms will be linear, which is not surprising for a material with the long-term stability of type 304 stainless steel. The slopes of these linear isotherms are given by

$$\left(\frac{\partial \log y}{\partial \log \sigma}\right)_T = \frac{\alpha_1}{T} + \alpha_3 U \ , \tag{14}$$

for Model 1 (y is $\dot{e}_m$ or t_r, the α's are coefficients as in Tables XI, pages 38-40, and XII, pages 41-42). For Model 4, these slopes are given by

$$\left(\frac{\partial \log y}{\partial \log \sigma}\right)_{T,U} = \alpha_3 \ . \tag{15}$$

Thus, one immediately sees a strong difference between these two models. For Model 4, the slope is constant for all heats at all temperatures. For Model 1, the slope is a function of both U and T. For the ORNL data, the value of this slope can vary from -9.05 for t_r and 12.44 for $\dot{e}_m$ for maximum strength material at 427°C to -5.08 for t_r and 5.80 for

$\dot{e}_m$ for minimum strength material at 704°C. Maximum and minimum strength refer to the value U as will be defined in this chapter.

Constant stress plots of log t_r or log e_m vs. 1/T are also linear for both models. The slope of these iso-stress lines is given by

$$\left[\frac{\partial \log t_r}{\partial (1/T)}\right]_{\sigma,U} = \alpha_1 \log \sigma + \alpha_2 U \tag{16}$$

for Model 1, and by

$$\left[\frac{\partial \log t_r}{\partial (1/T)}\right]_{\sigma,U} = \alpha_1 U + \alpha_2 \tag{17}$$

for Model 4. Thus, the slope is a function both of σ and U for Model 1, but is a function only of U for Model 4. Therefore Model 4 can in a sense be viewed as a "U-modified" OSD parameter [47], since that parameter implies such a slope to be constant.

The dependence of log t_r and log $\dot{e}_m$ upon U is also linear in both cases, the slope of this dependence being given by

$$\left(\frac{\partial \log y}{\partial U}\right)_{\sigma,T} = \frac{\alpha_2}{T} + \alpha_3 \log \sigma \tag{18}$$

for Model 1 and by

$$\left(\frac{\partial \log y}{\partial U}\right)_{\sigma,T} = \frac{\alpha_1}{T} \tag{19}$$

for Model 4.

While both Models 1 and 4 express log $\dot{e}_m$ or log t_r as functions of σ, T, and U (as they should), those models can be solved directly for stress. For Model 1, this solution yields

$$\log \sigma = \frac{(\log y - \alpha_0 - \alpha_2 \frac{U}{T})}{(\alpha_1/T + \alpha_3 U)} . \tag{20}$$

$$\log \sigma = \frac{(\log y - \alpha_0 - \alpha_1 U/T - \alpha_2/T)}{(\alpha_3/T)} . \tag{21}$$

Effects of Ultimate Tensile Strength

Of the 32 candidate models listed in Table X, page 34, only Models 17, 21, 27, 28, 29, 30, 31, and 32 lack terms reflecting ultimate tensile strength. The first three of these were obtained from a separate analysis of type 316 stainless steel data [44], while the last five were chosen for study simply because they are forms of widely used parametric models. It is not surprising that none of these models fare very well in comparison to the entire list of models. In terms of fits to the six total data sets, the best any of the above "non-U" models do for R^2 is Model 29, which ranks 14th best for the US minimum creep rate data. For rupture data, the best non-U model is Model 17 which ranks 19th for the NRIM rupture data. For the extrapolated data the best non-U model, Model 29, ranks 7th among the models for the ORNL low minimum creep rate data, while Model 32 ranks 18th for the NRIM long rupture life data. Table XIX illustrates the comparisons between the best models with U terms and the best non-U models for each data set.

TABLE XIX

COMPARISON OF RESULTS OBTAINED USING MODELS WITH AND WITHOUT ULTIMATE TENSILE STRENGTH TERMS

	Fits				Extrapolations			
	Best U Model[a]		Best Non-U Model[a]		Best U Model[a]		Best Non-U Model[a]	
Data Set	Model No.	R (%)	Model No.	R (%)	Model No.	RMSE	Model No.	RMSE
ORNL(t_r)	1	74.37	28	57.42	7	.617	28	.808
US(t_r)	5	89.44	28	81.74	4	.415	28	.648
NRIM(t_r)	8	88.28	17	83.73	4	.329	32	.395
BSCC(t_r)	30	87.19	28	28.32	7	.483	32	1.16
ORNL($\dot{e}_m$)	2	84.61	29	73.96	2	.644	29	.830
US($\dot{e}_m$)	32	95.79	29	94.56	4	.560	32	.747

[a]From the list of candidate models given in Table X, page 34.

Figure 4 compares results obtained for the ORNL data using Model 1 (with U), and using Model 27, a leading non-U model.

Two conclusions can be drawn from the above comparisons. First, the models with U terms are in general superior to those without U terms. This superiority is particularly pronounced for the ORNL data, which is not surprising in view of the fact that these data were specifically generated to study heat-to-heat variations in properties [13]. Also, it is certain that the ORNL U data were all generated at a constant strain rate, while this fact is not as clear for the other data—particularly the US and BSCC data. As will be discussed below, the success obtained with models containing U terms is largely attributable to the fact that the heat-to-heat variations in U provide a measure of heat-to-heat variations in creep and creep-rupture properties. A second conclusion is that our technique identified models much better than the standard time-temperature parameters studied, although the three standard parameters considered here form a small subset of the total number of parameters that have been proposed.

Interestingly, both Models 1 and 4 predict a linear relationship between log $\dot{e}_m$ or log t_r and U, consistent with the results given in Refs. [19] and [20]. The predictions of Model 1 concerning this relationship for the ORNL data are compared with the actual data in Figures 5-7. These figures show considerable scatter, but it appears that the model does accurately describe trends in the data. (Included in these figures are data for laboratory reannealed, as-received, and aged data, although only the reannealed data were used in the actual modeling.)

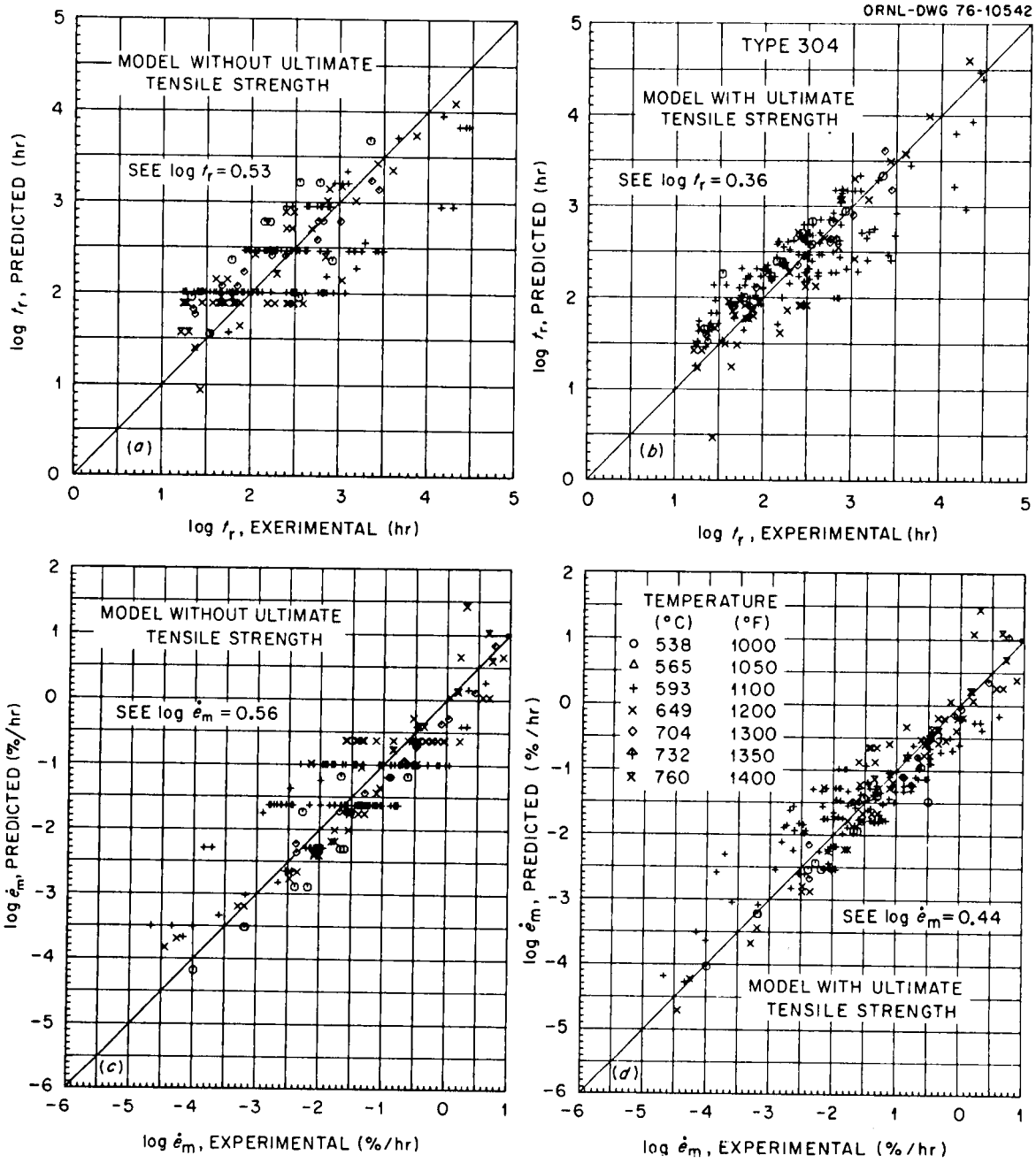

Figure 4. Comparison of Experimental Time to Rupture and Minimum Creep Rate With Predicted Results from Models With and Without Ultimate Tensile Strength for 20 Heats of Type 304 Stainless Steel.

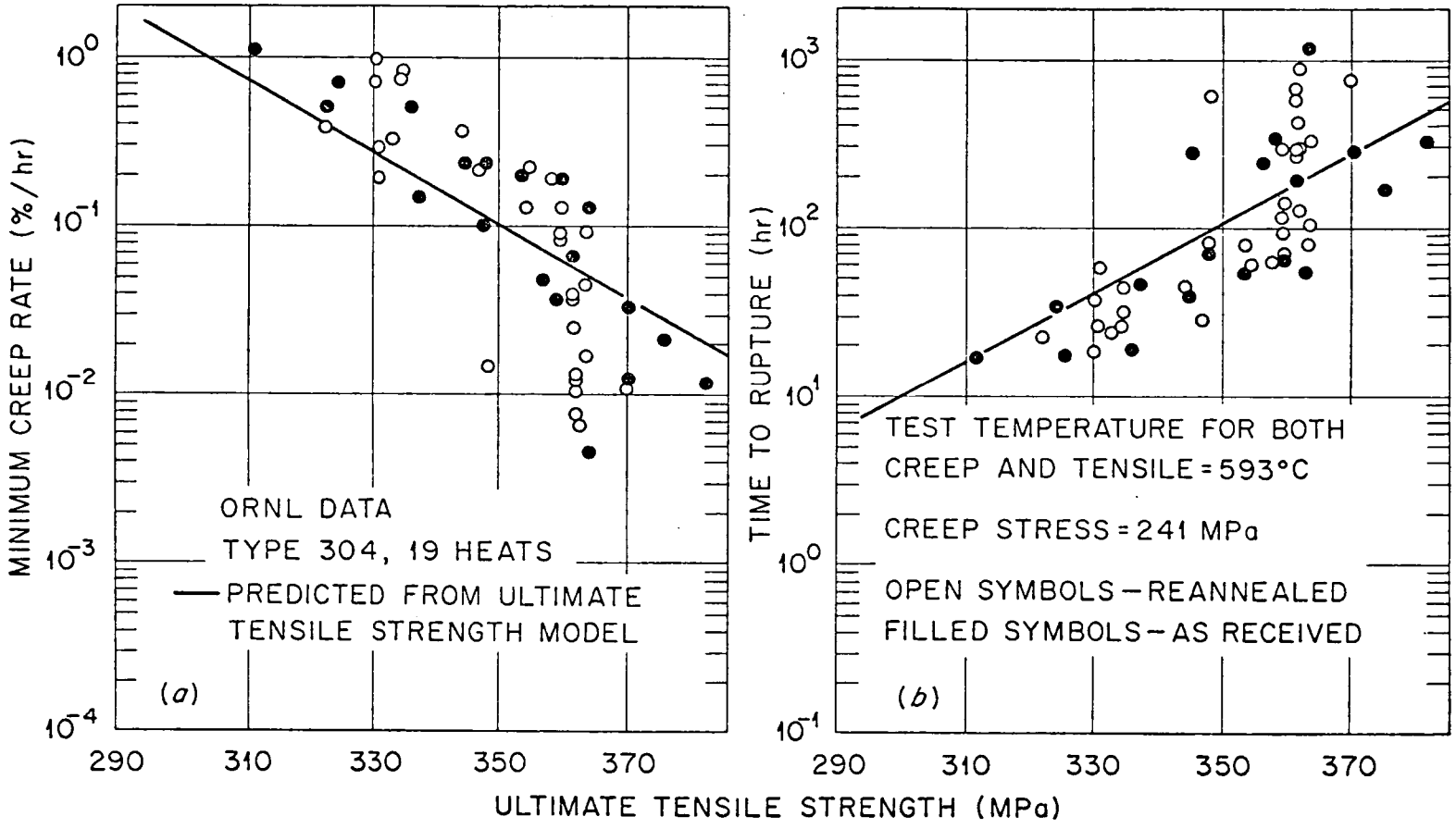

Figure 5. Comparison of Experimental Time to Rupture as a Function of Elevated-Temperature Ultimate Tensile Strength (U) With Values Predicted from Rupture Model with U for Different Heats of Type 304 Stainless; Tests Were at 593°C (1100°F) and 241 MPa (35 ksi).

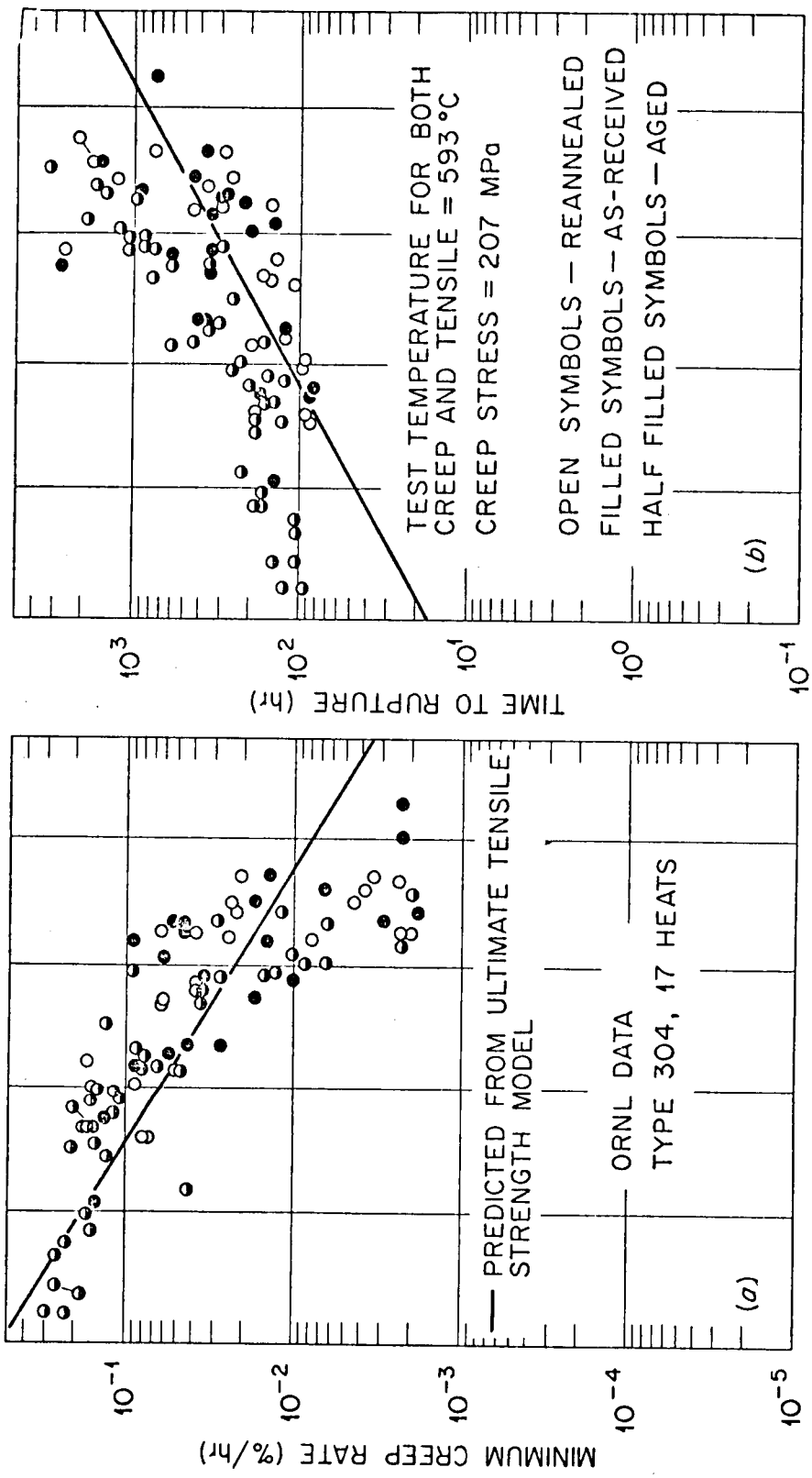

Figure 6. Comparison of Experimental Time to Rupture as a Function of Elevated-Temperature Ultimate Tensile Strength (U) With Values Predicted from Rupture Model With U for Different Heats of Type 304 Stainless; Tests Were at 593°C (1100°F) and 207 MPa (30 ksi).

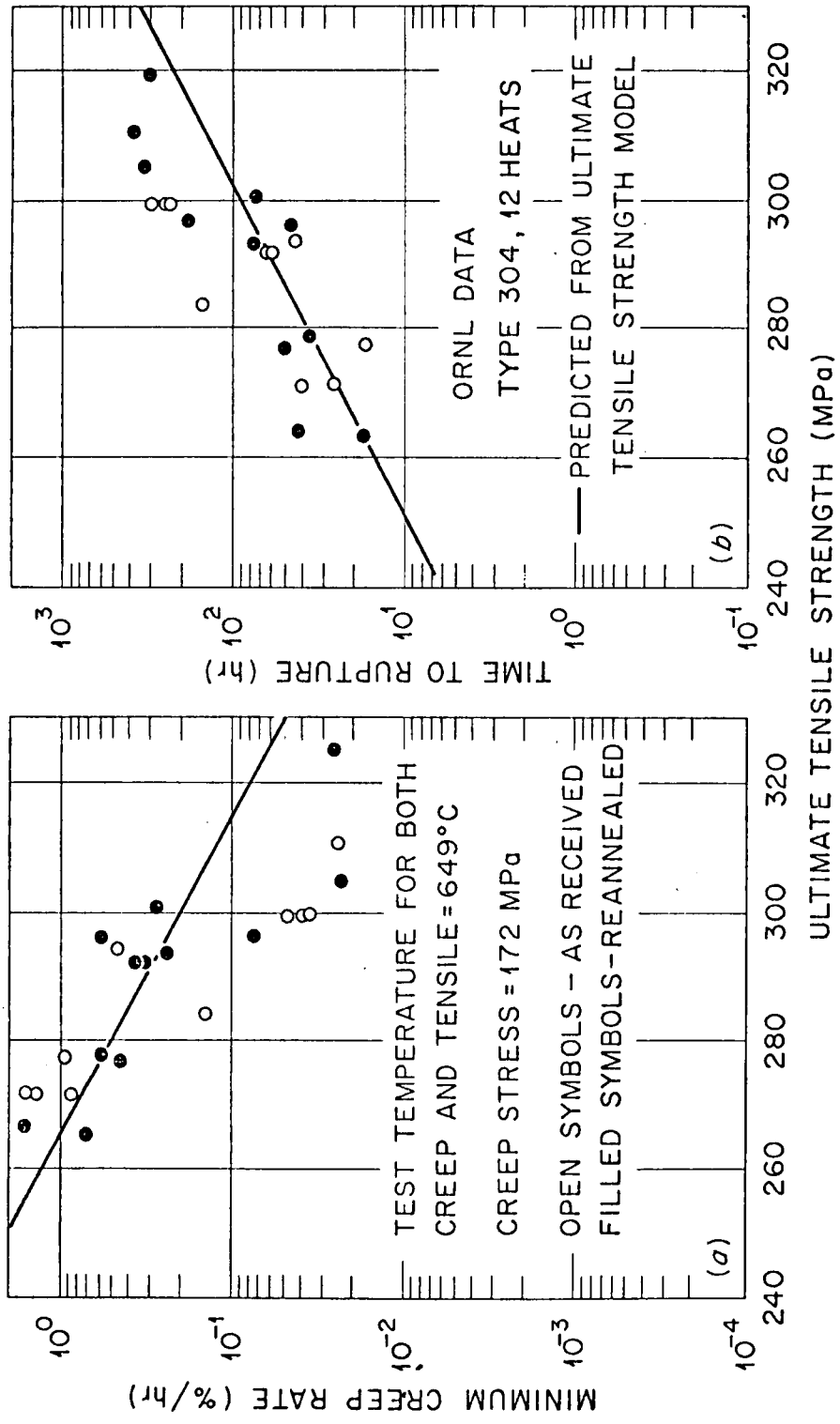

Figure 7. Comparison of Experimental Time to Rupture as a Function of Elevated-Temperature Ultimate Tensile Strength (U) With Values Predicted from Rupture Model With U for Different Heats of Type 304 Stainless; Tests Were at 649°C (1200°F) and 172 MPa (25 ksi).

The improvement in predicting $\dot{e}_m$ and t_r for individual heats can be seen in Figures 8-15, where data for individual heats are compared with the predictions of Model 1 (with a U term) and of Model 27 (a leading model with no U term). Figures 16 and 17 further present comparisons of the behavior of heat 8043813, an unusually strong heat [27] with the behavior of heat 972796 (the so-called ORNL "reference heat"), which is weaker than average [25]. Clearly, the model with an ultimate tensile strength correction significantly decreases the uncertainty in these predictions caused by heat-to-heat variations. However, it is also clear that the model cannot precisely describe the behavior of every individual heat. This expected result is due partially to experimental uncertainty and scatter in measuring U, $\dot{e}_m$, and t_r, and partially to the fact that ultimate tensile strength does not totally describe the complex results of heat-to-heat variations.

Prediction of Mean, Maximum, and Minimum Behavior

Using the above models for minimum creep rate and rupture life as functions of stress, temperature, and ultimate tensile strength, one can estimate the behavior of an average heat, or of a minimum or maximum strength heat if one can first estimate the average minimum, and maximum ultimate tensile strength at each temperature. The models provide a prediction not only of mean values of $\dot{e}_m$ and t_r, but of the spread that can be expected in these values due to heat-to-heat variations in properties.

Reference [16] presents an analysis of ultimate tensile strength as a function of temperature for the ORNL data, while Ref. [18] presents

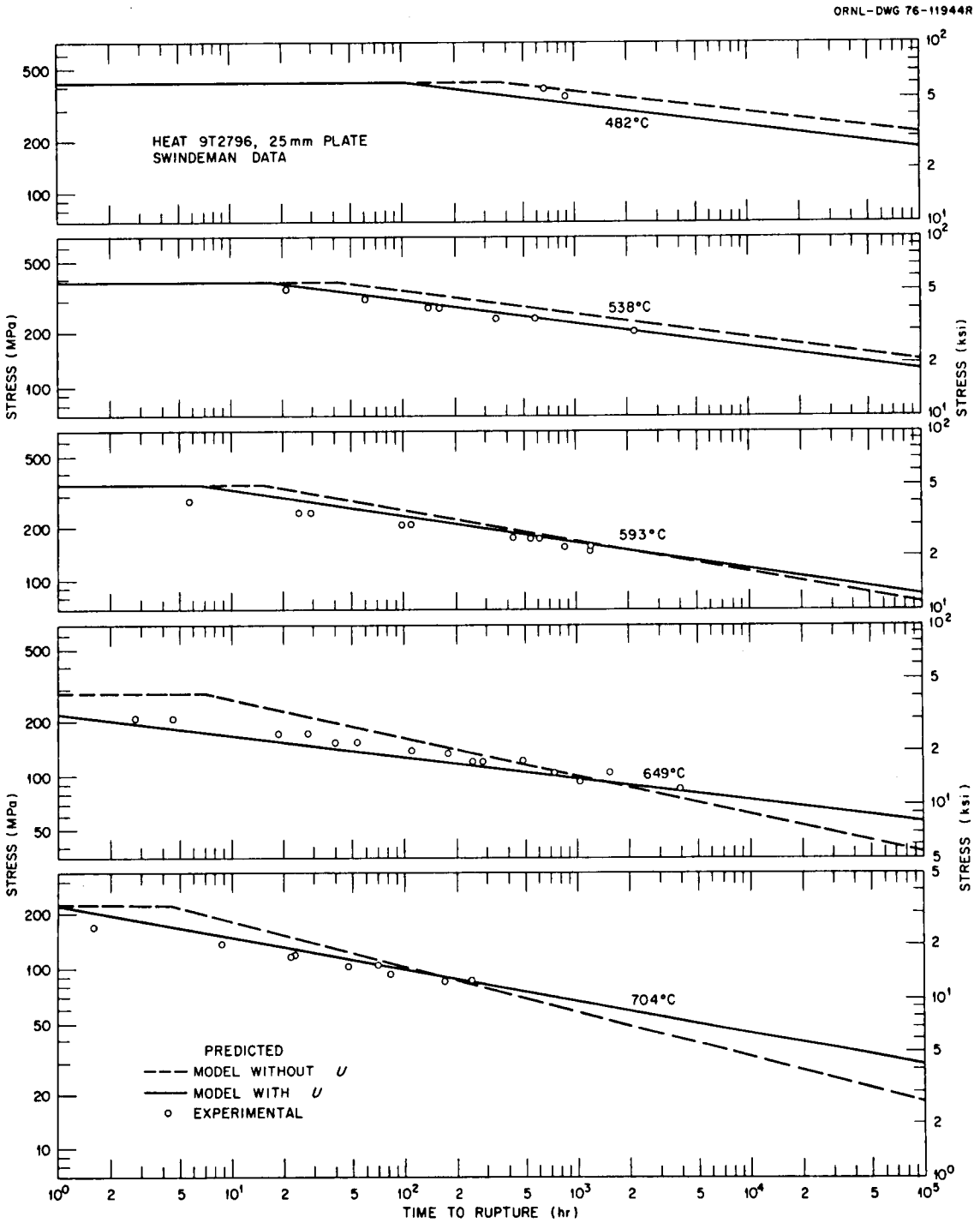

Figure 8. Comparison of Experimental Time to Rupture With Values Computed from Models With and Without Elevated Temperature Ultimate Temperature Strength (U) for 25-mm (1-in.) Plate of Reannealed Heat 9T2796 of Type 304 Stainless Steel.

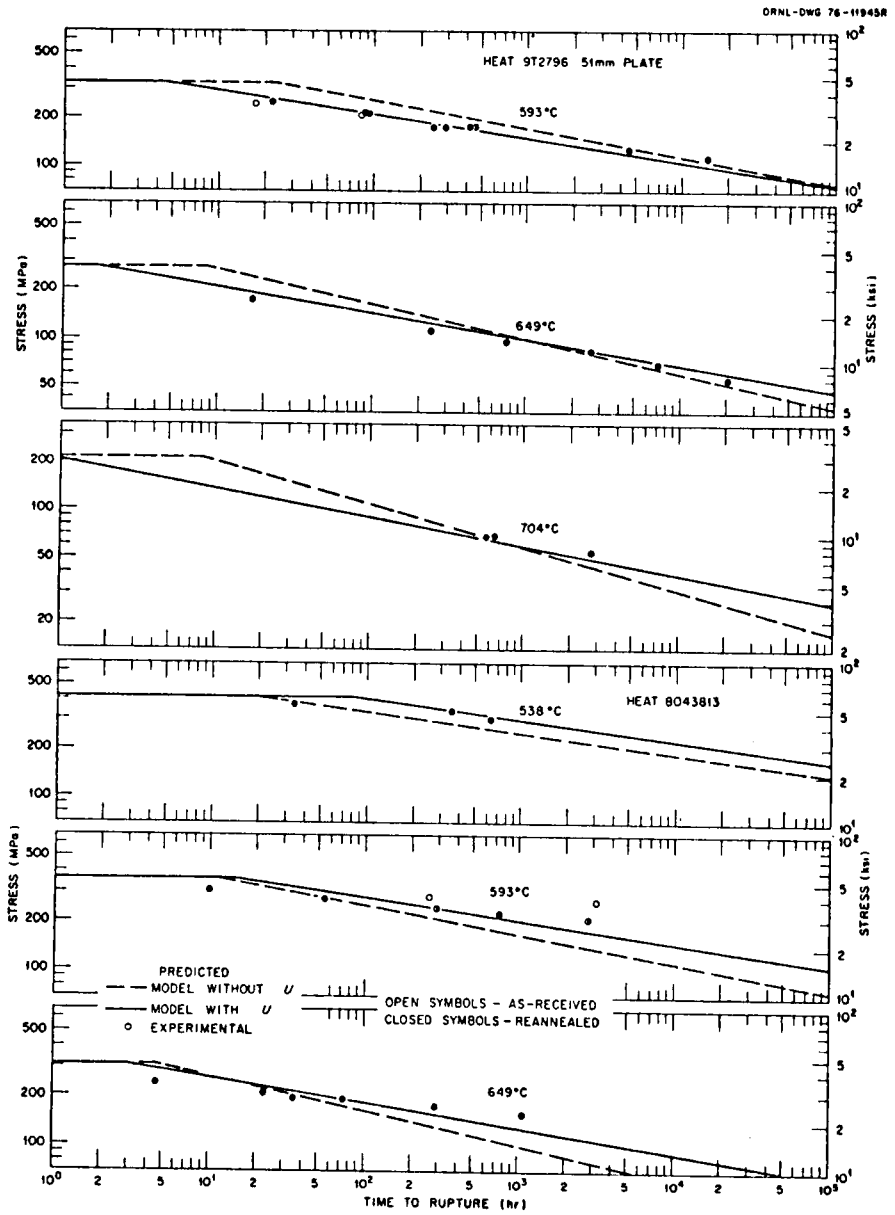

Figure 9. Comparison of Experimental Time to Rupture With Values Computed from Models With and Without Elevated-Temperature Ultimate Tensile Strength (U) for a Weak (9T2796) and a Strong Heat (8043813).

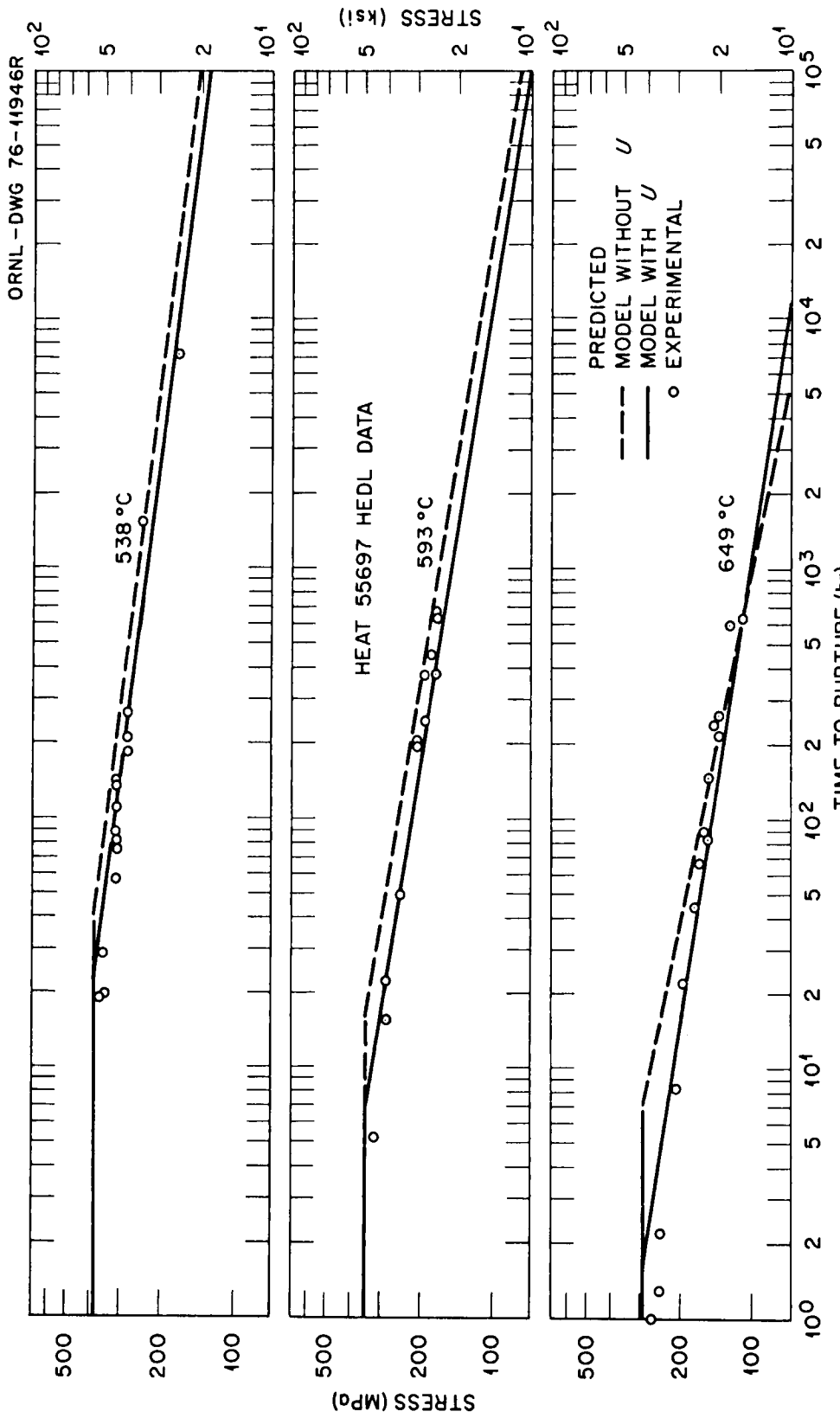

Figure 10. Comparison of Experimental Time to Rupture With Values Computed from Models With and Without Elevated-Temperature Ultimate Tensile Strength (U) for HEDL Data on Reannealed Heat 55697.

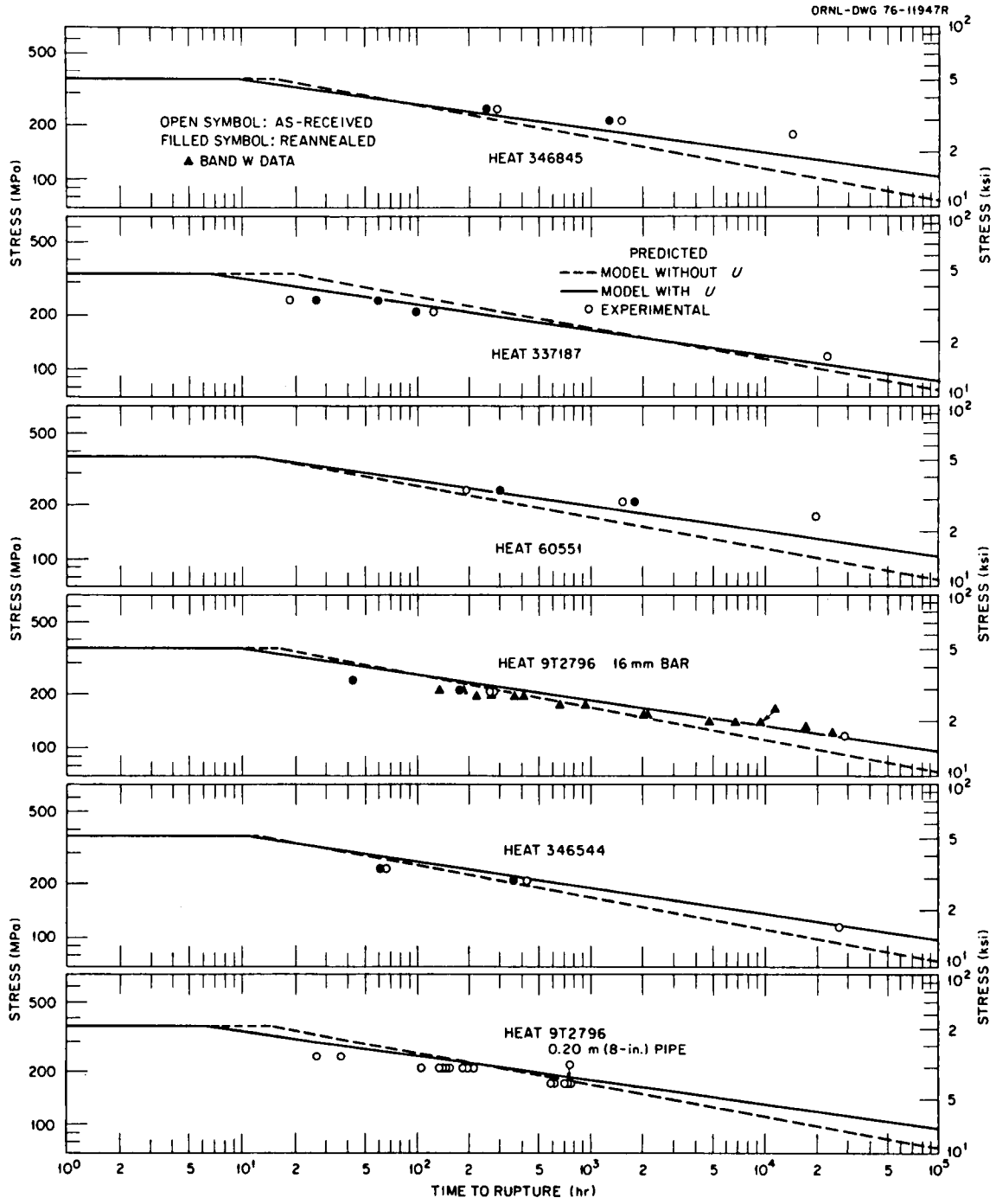

Figure 11. Comparison of Experimental Time to Rupture With Values Computed from Models With and Without Elevated-Temperature Ultimate Tensile Strength (U) for Several Heats of Type 304 Stainless Steel at 593°C. The B and W data were privately supplied by Babcock and Wilcox Corp.

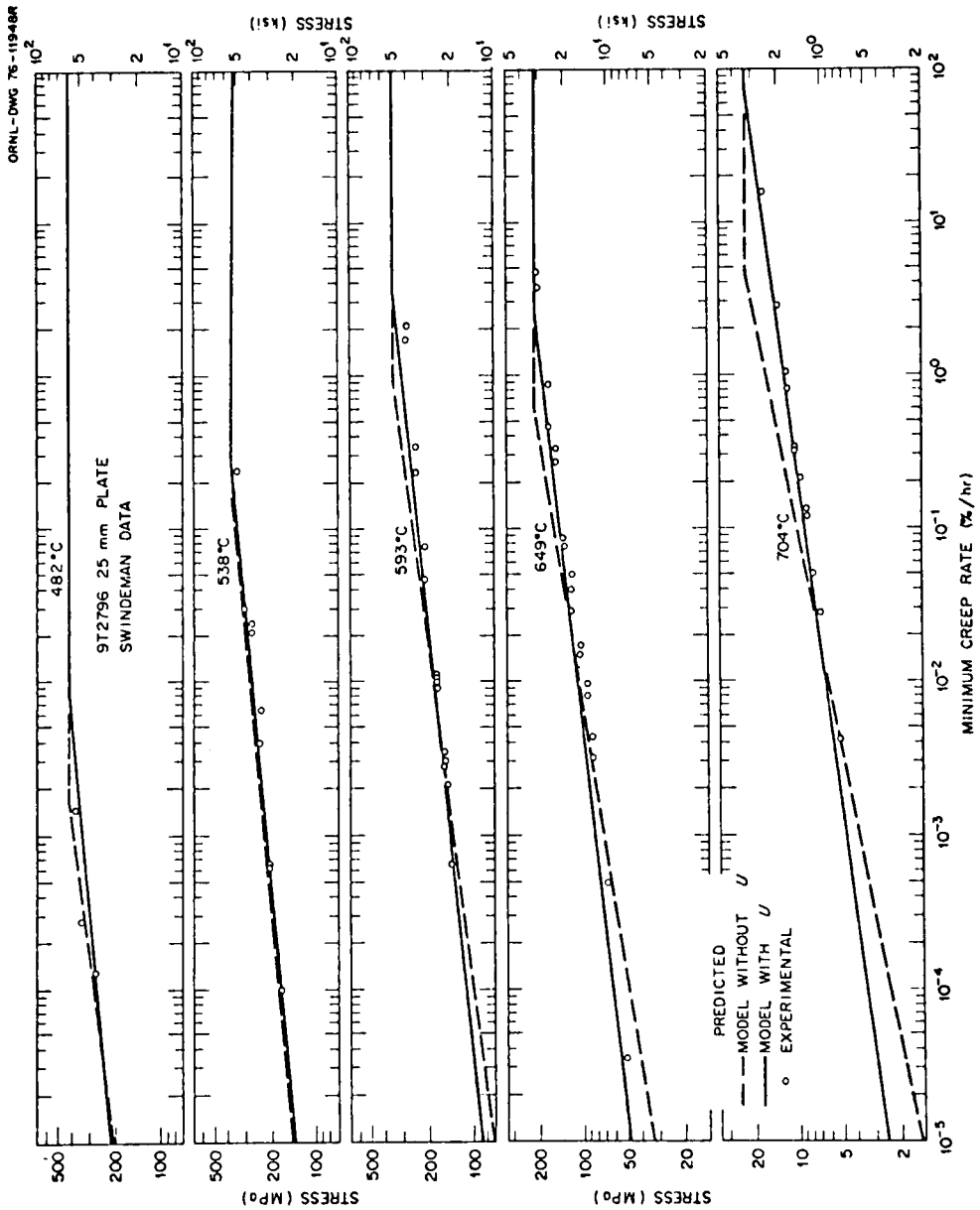

Figure 12. Comparison of Experimental Minimum Creep Rate With Values Computed from Models With and Without Elevated-Temperature Ultimate Tensile Strength (U) for 25-mm (1-in.) Plate of Reannealed Reference Heat of Type 304 Stainless Steel.

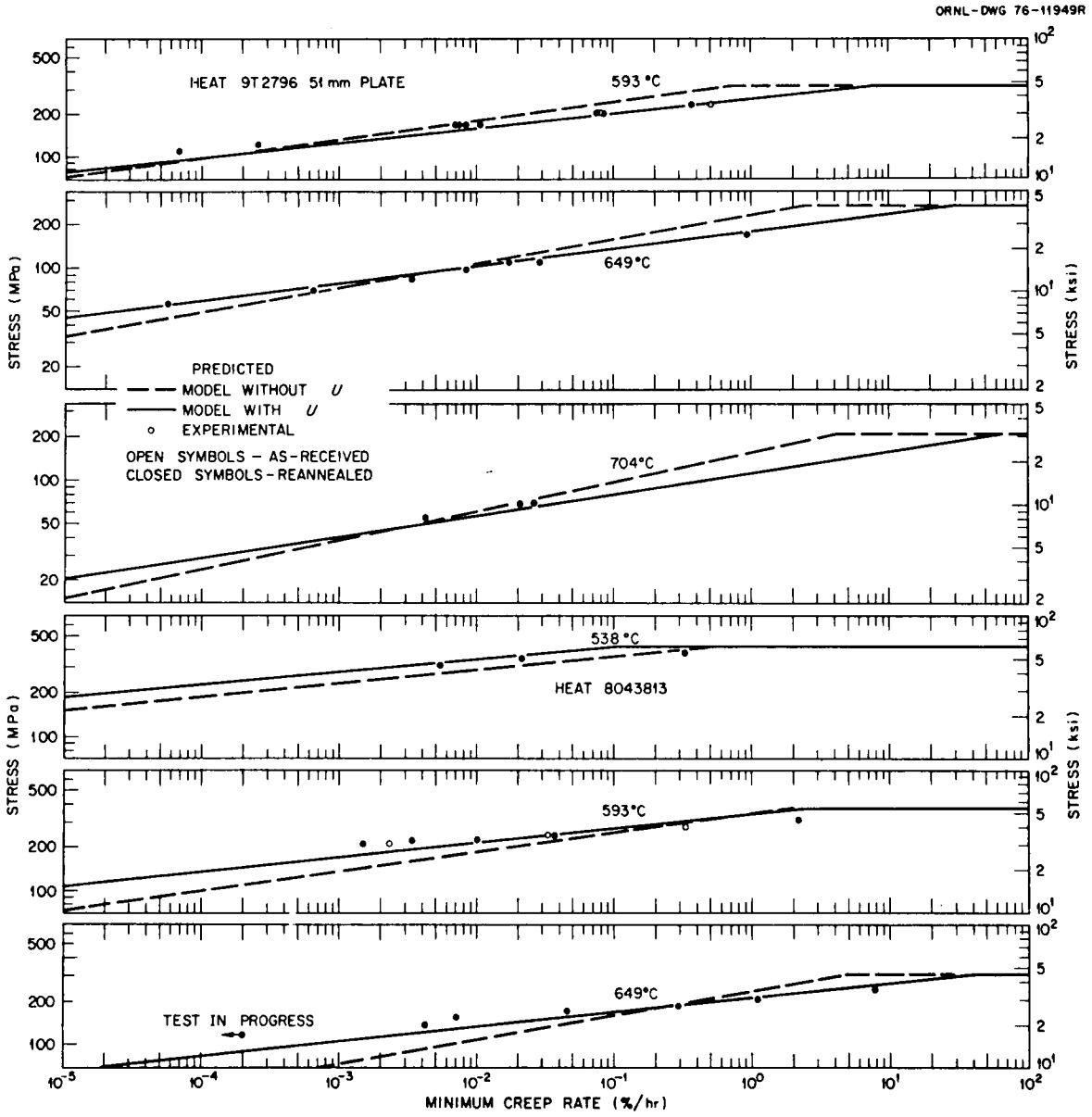

Figure 13. Comparison of Experimental Minimum Creep Rate With Values Computed from Models With and Without Elevated-Temperature Ultimate Tensile Strength (U) for a Weak (9T2796) and a Strong Heat (8043813).

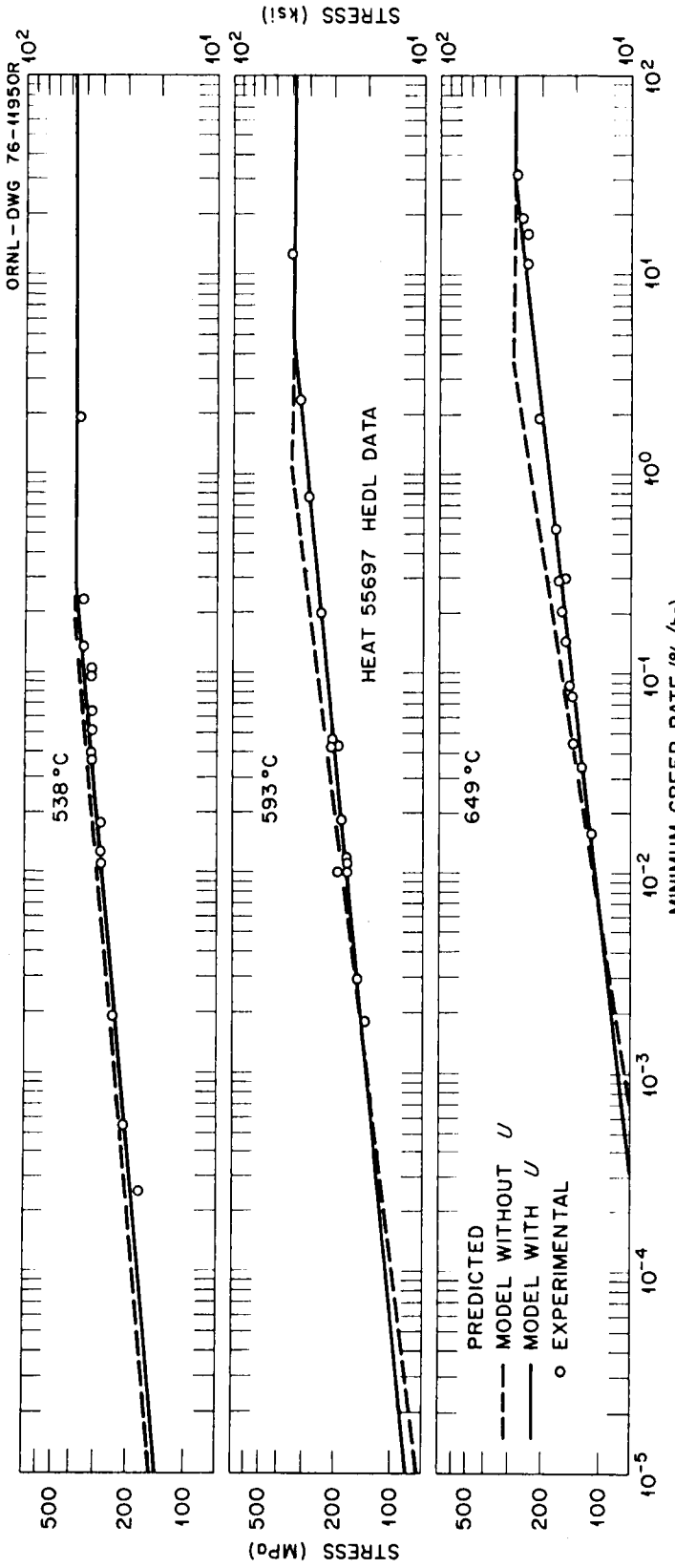

Figure 14. Comparison of Experimental Minimum Creep Rate With Values Computed from Models With and Without Elevated-Temperature Ultimate Tensile Strength (U) for HEDL Data on Reannealed Heat Heat 55697.

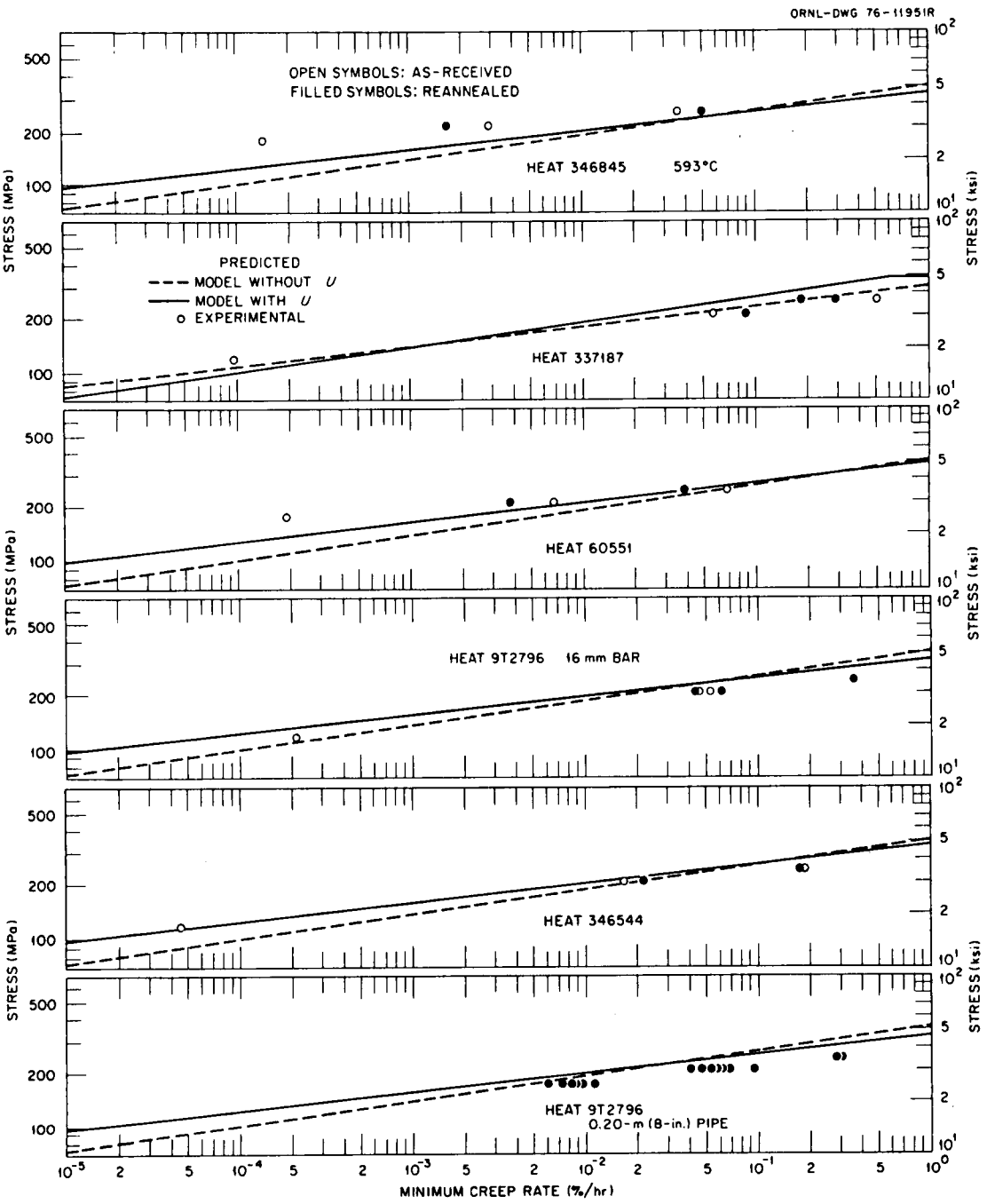

Figure 15. Comparison of Experimental Minimum Creep Rate With Values Computed from Models With and Without Elevated-Temperature Ultimate Tensile Strength (U) for Several Heats of Type 304 Stainless Steel.

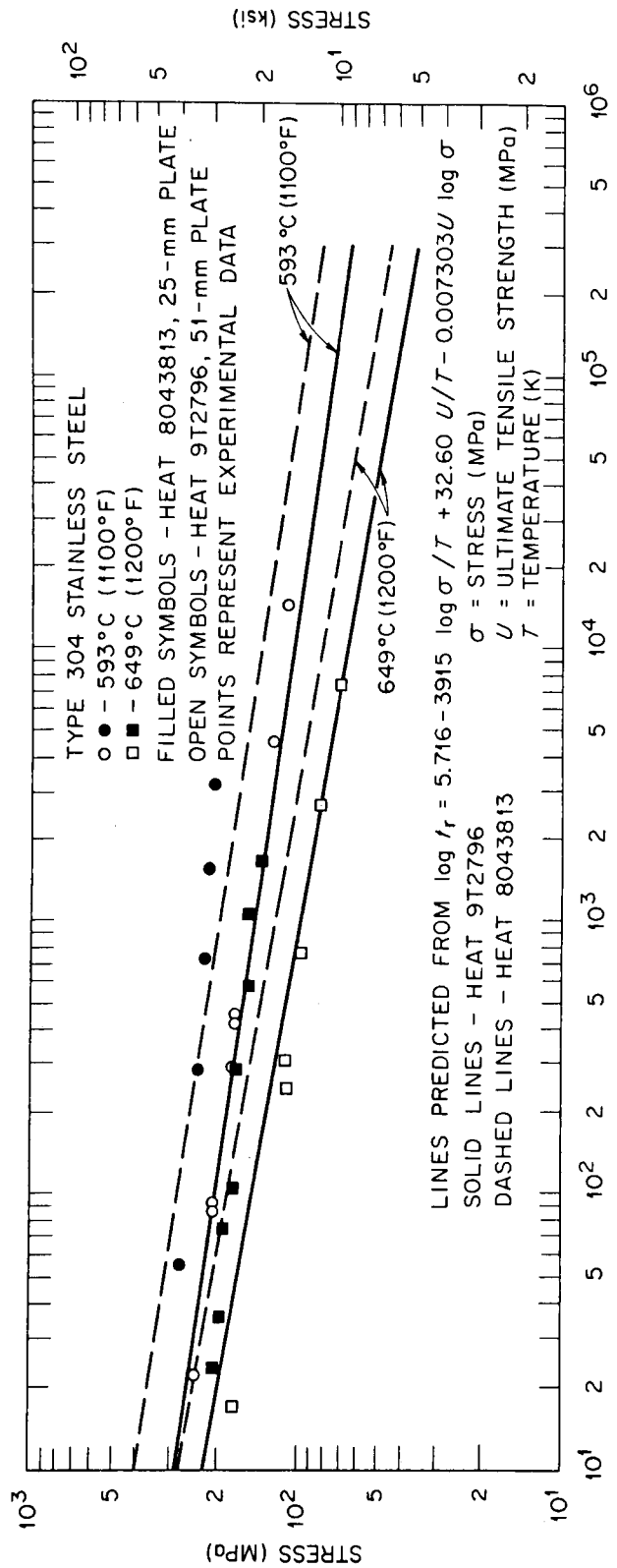

Figure 16. Prediction of Heat-to-Heat Variations in Rupture Life for Two Heats of Type 304 Stainless Steel. Heat 8043813 is a relatively strong heat; heat 972796 is a relatively weak heat.

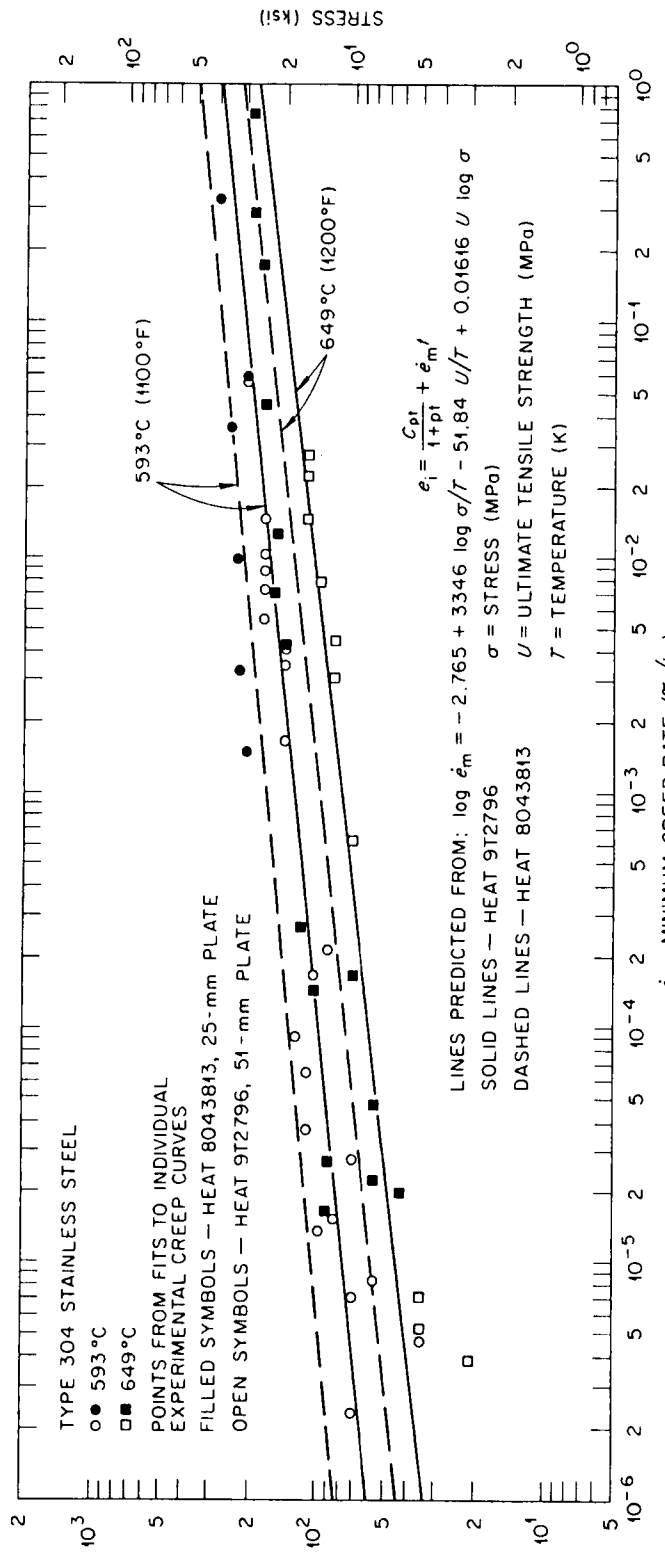

Figure 17. Prediction of Heat-to-Heat Variations in Minimum Creep Rate for Heats 8043813 and 9T2796 of Type 304 Stainless Steel.

such an analysis for the US, NRIM, and BSCC data. For all four data sets, U can be described by a model of the form

$$U = \beta_0 + \beta_1 T + \beta_2 T^2 + \beta_3 T^3 \qquad (22)$$

where the constants β_0, β_1, β_2, and β_3 were estimated by methods of least squares. Table XX presents the values of these constants for each data set, as well as the number of data and SEE value from Eqn. 22 for each data set. The equation for the ORNL data is expressed for temperatures in °C, while the other equations are expressed for temperatures in °F. The so-called maximum and minimum values were obtained by adding or subtracting twice the value of SEE from the predicted mean. These values do not, of course, represent strict physical maxima or minima. Neither do they represent rigorous limits in a statistical sense. They give a convenient measure of the width of the scatter band for engineering purposes. However, this method of defining limits shows reasonably good agreement with statistical upper and lower central tolerance limits [48] for these data sets. At a confidence level of 95%, one expects only 5% of all observations to fall below the lower tolerance limit. Another 5% would be expected to fall above the lower limit. For instance, Table XXI compares the currently defined limits with these more rigorous statistical limits for the ORNL data. The current method is preferred here for convenience and simplicity in application. Figures 18 and 19 illustrate the variation in U with temperature and the two methods for defining limits.

Figures 20-25 illustrate results obtained by inserting the above mean, maximum, and minimum values of U into the optimum model for each

TABLE XX

BEST FIT VALUES OF COEFFICIENTS IN EQUATIONS DESCRIBING ULTIMATE TENSILE STRENGTH AS A FUNCTION OF TEMPERATURE[a]

Data Set	Number of Data	β_0	β	β_1	β_2	β_3	SEE[b]
ORNL[c]	135	88.90	-2.19×10^{-1}		5.95×10^{-4}	-5.65×10^{-7}	3.40
US[d]	272	91.93	-1.13×10^{-1}		1.59×10^{-4}	-7.84×10^{-8}	3.98
NRIM[d]	99	95.44	-1.291		1.90×10^{-4}	-9.55×10^{-8}	2.79
BSCC[d]	218	89.09	-1.09×10^{-1}		1.51×10^{-4}	-7.40×10^{-8}	2.94

[a]Ultimate tensile strength (U) and temperature (T) have been related by $U = \beta_0 + \beta_1 T + \beta_2 T^2 + \beta_3 T^3$ strength values are given in Ksi by these equations. To convert to MPa, the strength is multiplied by 6.895.

[b]Standard error of estimate for U (Ksi) by the equation in note a.

[c]Temperatures in °C.

[d]Temperatures in °F.

TABLE XXI

COMPARISON BETWEEN LOWER CENTRAL TOLERANCE LIMITS ON ULTIMATE TENSILE STRENGTH FOR THE ORNL DATA WITH CURRENT LIMITS

Temperature (°C)	"Lower Limit" Value of Ultimate Tensile Strength (MPa)	
	Lower Central Tolerance Limit	Mean Value Minus 2 × SEE[a]
100	441	452
200	383	397
300	366	377
400	361	369
500	341	349
600	288	296
700	165	183

[a]Mean value given by the equation in Table XX (converted to MPa). Then twice the standard error of estimate is subtracted to give an empirical lower limit.

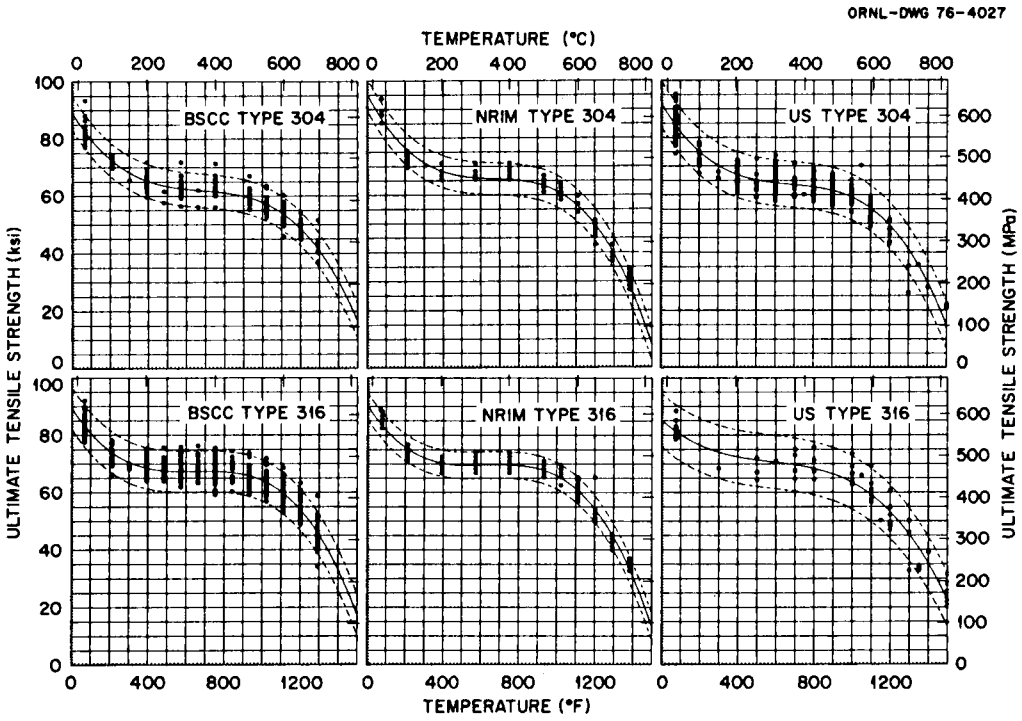

Figure 18. Plots Showing Trends in Ultimate Tensile Strength as a Function of Test Temperature for Types 304 and 316 Stainless Steel from Various Sources. Upper- and lower-limit lines (dashed) are given by ±2SEE.

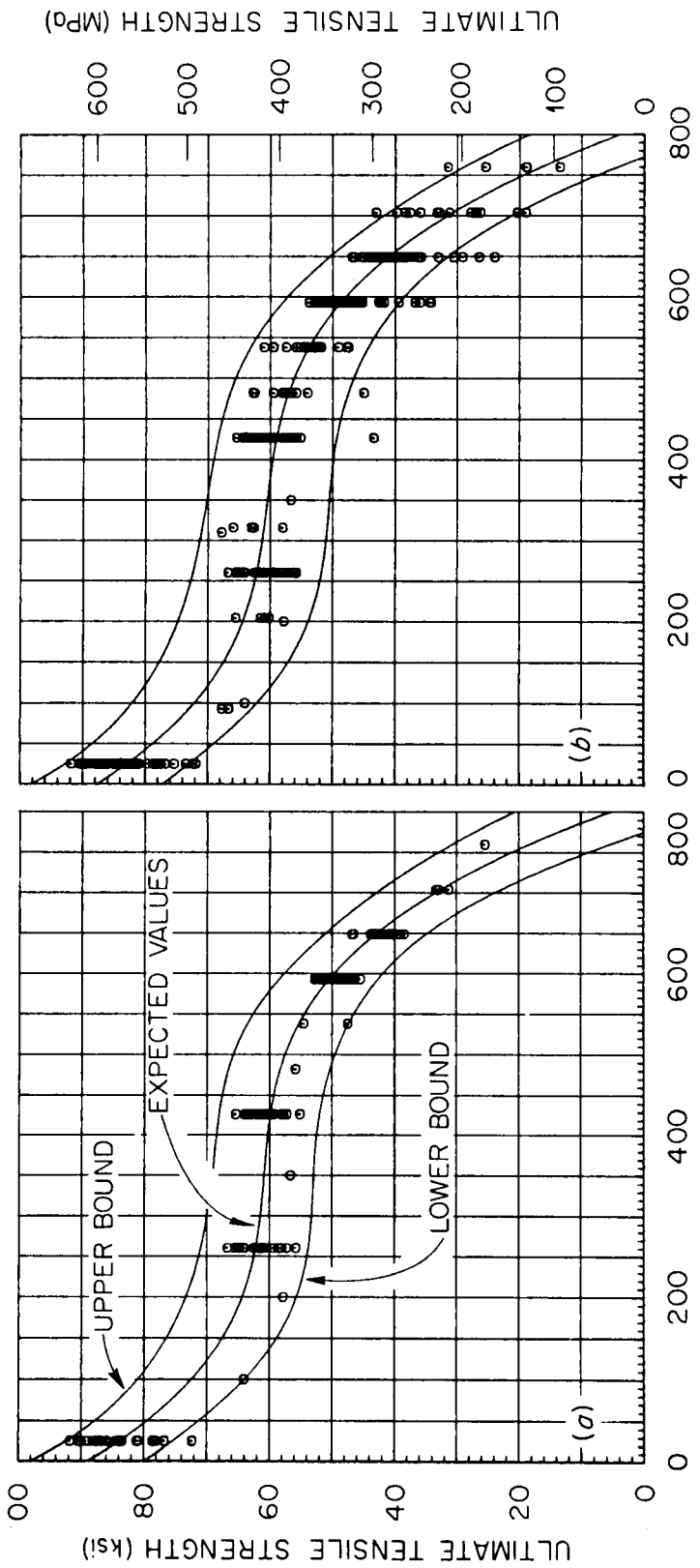

Figure 19. Trends in Ultimate Tensile Strength as a Function of Test Temperature for ORNL Data for Type 304 Stainless Steel. Upper- and lower-limit lines are given by central tolerance limits. (a) Data for a strain rate of 6.7×10^{-4} S^{-1}; (b) Data for strain rates from 6.7×10^{-6} S^{-1} to 6.7×10^{-2} S^{-1}.

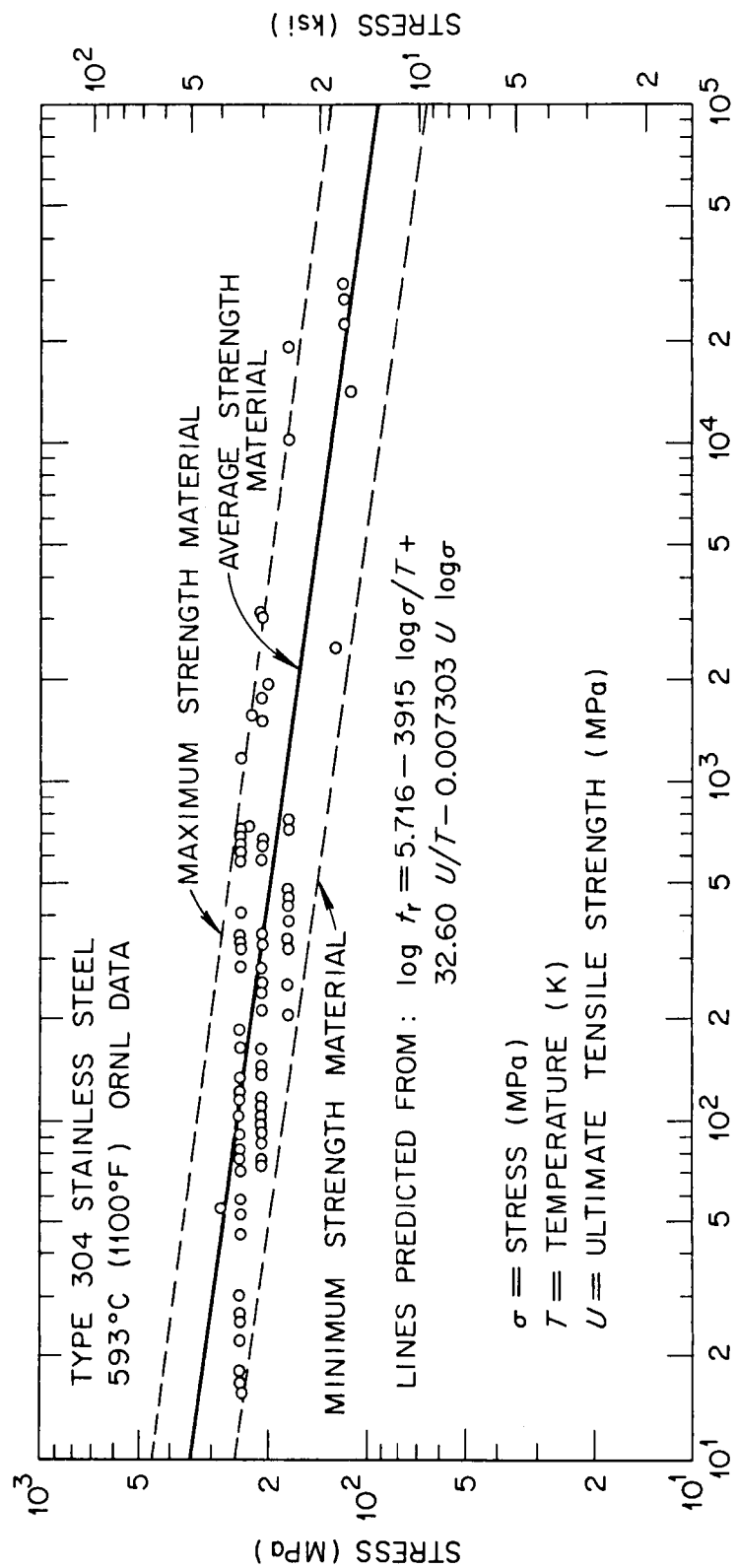

Figure 20. Fits to Experimental ORNL Data for Rupture Life of Type 304 Stainless Steel at 593°C (1100°F). Lines are predictions from Model 1 for estimated average, minimum, and maximum ultimate tensile strength levels.

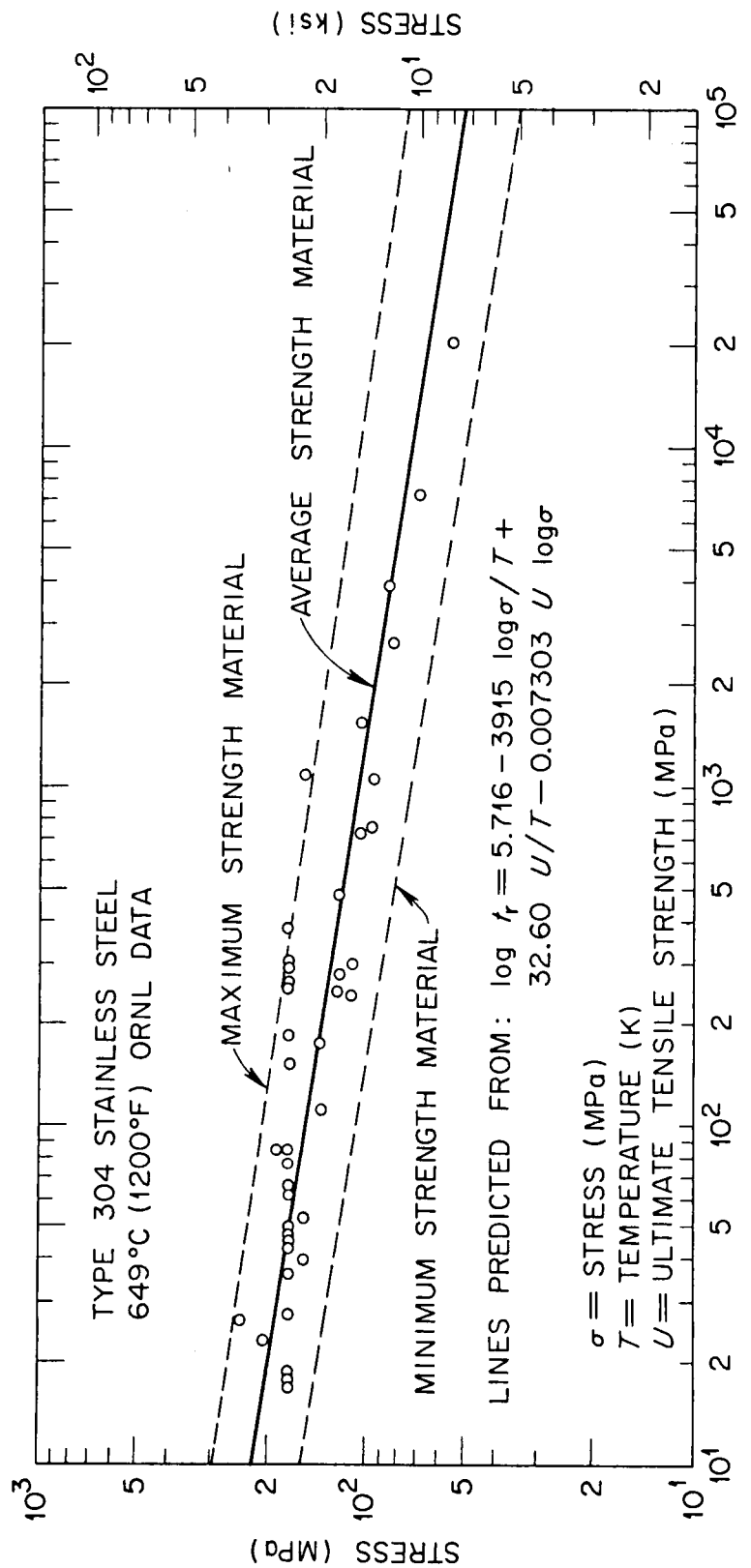

Figure 21. Fits to Experimental ORNL Data for Rupture Life of Type 304 Stainless Steel at 649°C (1200°F). Lines are predictions from Model 1 for estimated average, minimum, and maximum ultimate tensile strength levels.

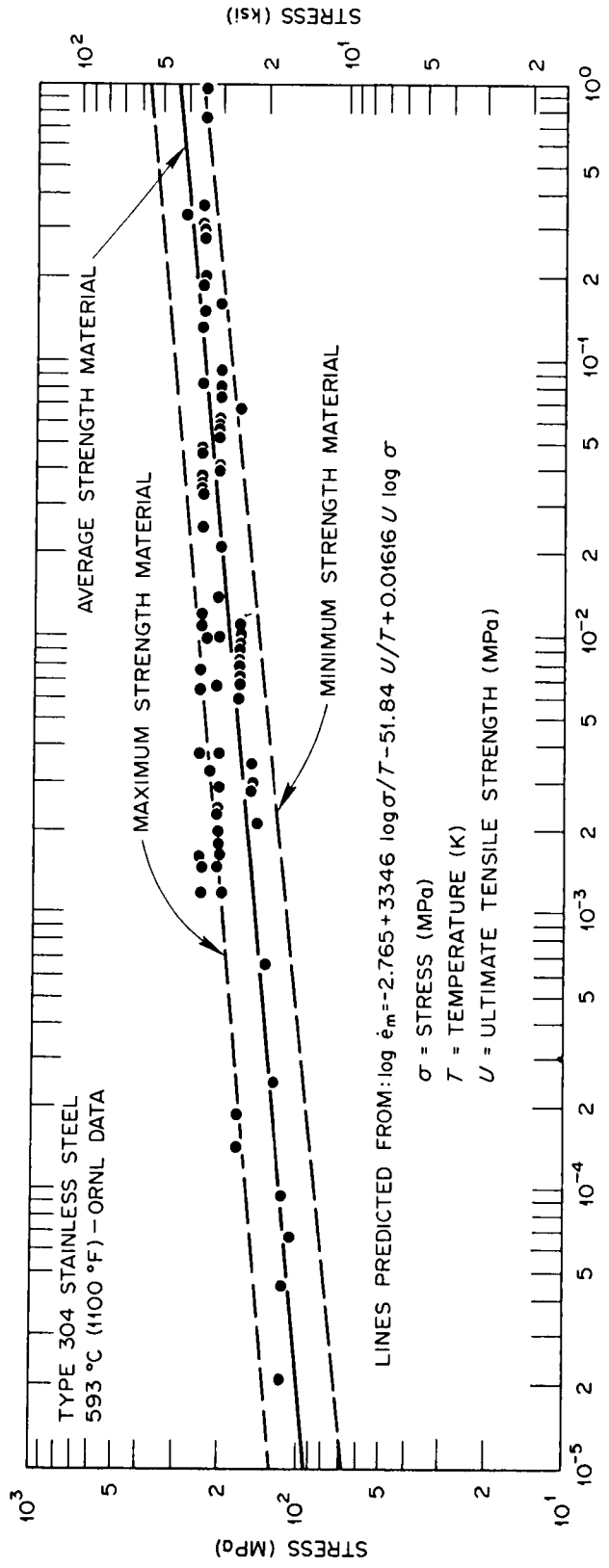

Figure 22. Fits to Experimental ORNL Data for Minimum Creep Rate of Type 304 Stainless Steel at 593°C (1100°F). Lines are predictions from Model 1 for estimated average, minimum, and maximum ultimate tensile strength levels.

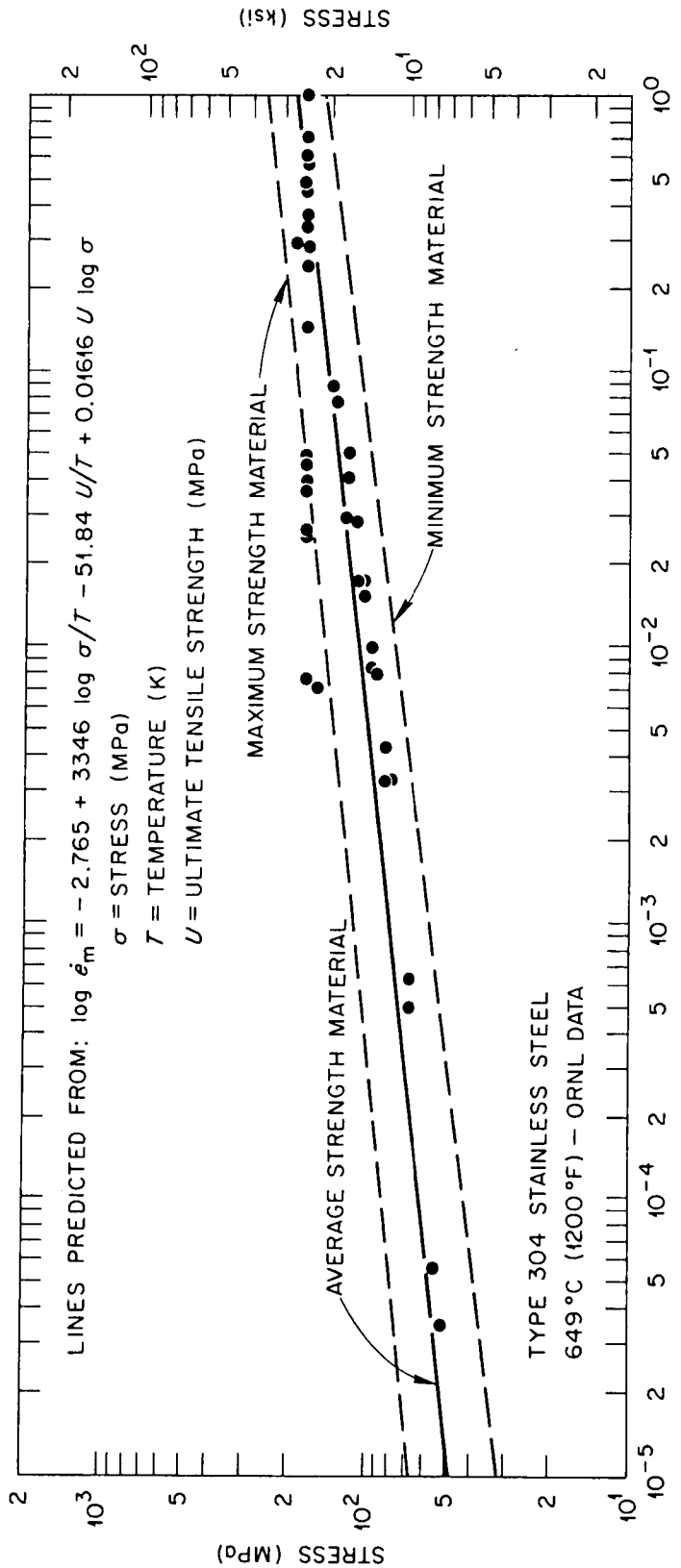

Figure 23. Fits to Experimental ORNL Data for Minimum Creep of Type 304 Stainless Steel at 649°C (1200°F). Lines are predictions from Model 1 for estimated average, minimum, and maximum ultimate tensile strength levels.

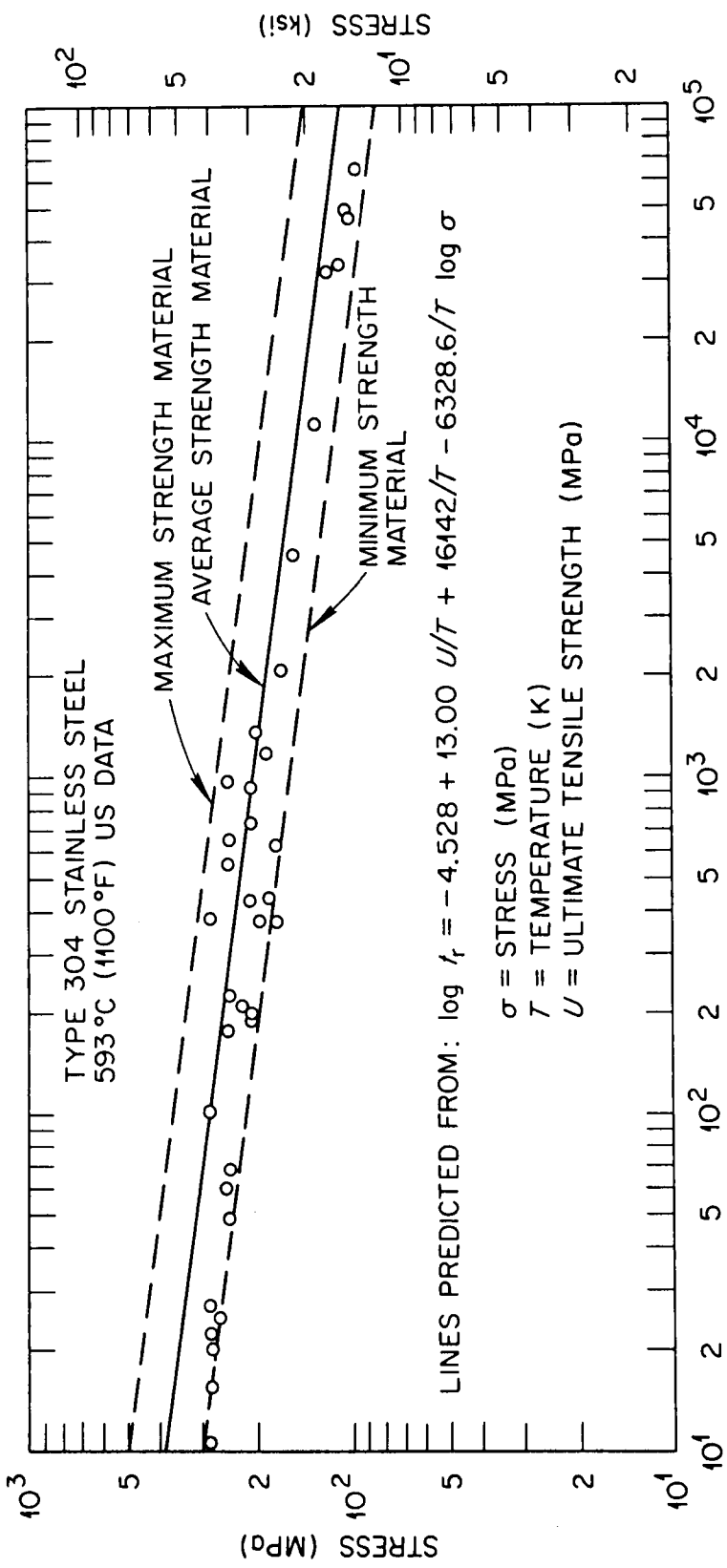

Figure 24. Fits to Experimental US Data for Rupture Life of Type 304 Stainless Steel at 593°C (1100°F). Lines are predictions from Model 1 for estimated average, minimum, and maximum ultimate tensile strength levels.

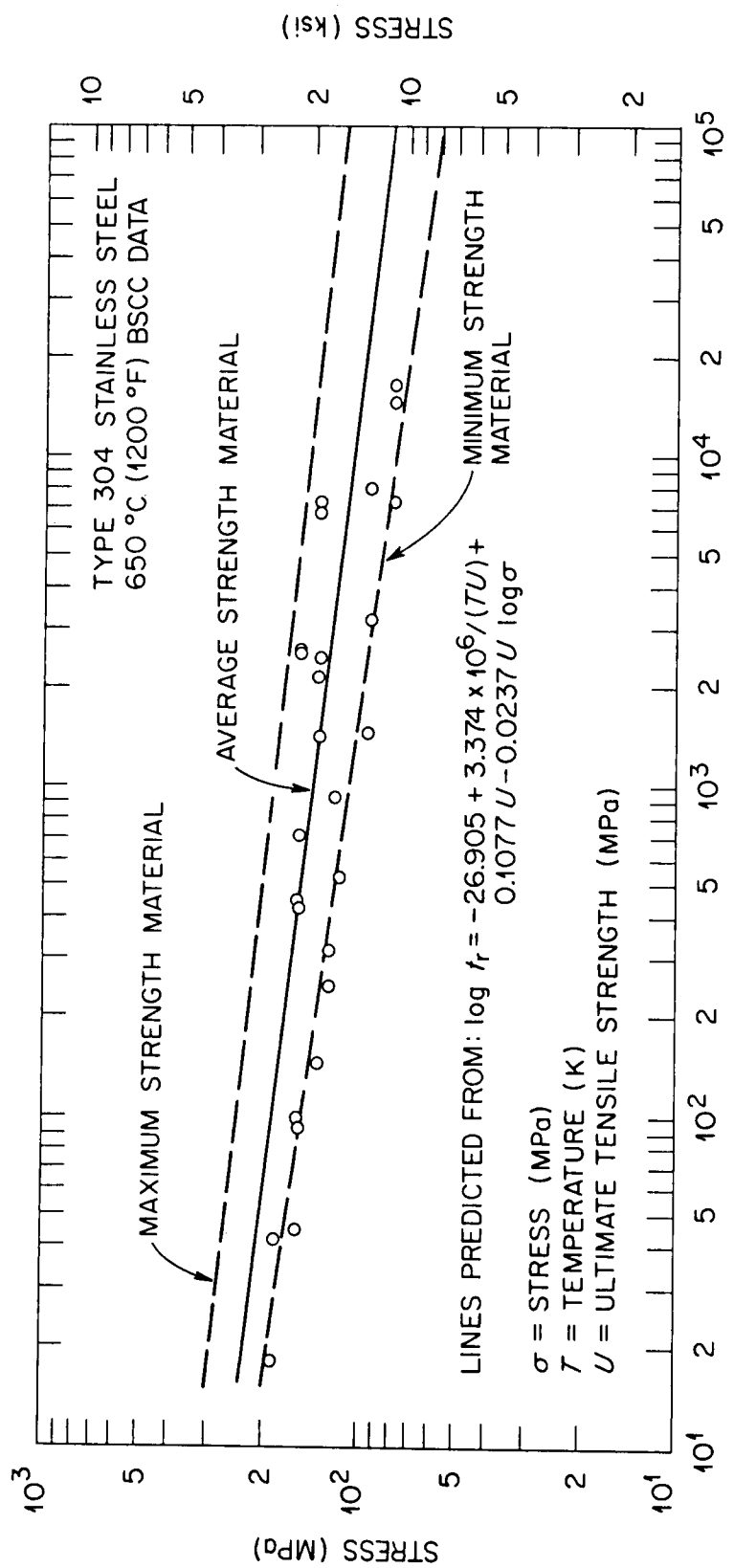

Figure 25. Fits to Experimental BSCC Data for Rupture Life of Type 304 Stainless Steel at 650°C (1200°F). Lines are predictions from Model 1 for estimated average, minimum, and maximum ultimate tensile strength levels.

data set to predict the corresponding creep behavior. Again, these models are Model 1 for the ORNL data, Model 4 for the US data, and Model 7 for the BSCC data. These figures yield two obvious results. First, the predictions of average behavior depict the variations in the data quite accurately. Second, the predictions of maximum and minimum behavior correspond very closely to the upper and lower limits of the scatter bands of the data.

Strain Rate Effects

As discussed above and in detail in Ref. [16], the ultimate tensile strength of a given heat of material is a function of the tensile strain rate, at least for temperatures of 538°C or greater. The U values used in establishing the above models were therefore obtained at a constant strain rate for each data set. Unfortunately, this fact appears to limit the applicability of the models. For instance, the ORNL models apply to U values obtained at a constant nominal strain rate of 6.7×10^{-4} sec^{-1}. If one knows the value of U for a given heat at some other strain rate, the models cannot directly predict creep behavior using this value of U.

Fortunately, the strain rate dependence of U at a given temperature can be simply quantified as

$$U = U_o + B \log \dot{e} \tag{23}$$

where $\dot{e}$ is the tensile strain rate, U_o is the ultimate tensile strength at a strain rate of unity, and B is a temperature-dependent constant.

As explained in Ref. [16], U_o differs for different heats, but B should be relatively free of heat-to-heat variations.

Knowing the value of U at any strain rate, $\dot{e}$, one can use Eqn. 23 to calculate the corresponding value, U*, at a strain rate of 6.7×10^{-4} sec^{-1} by the relation

$$U^* = U + B \log(6.7 \times 10^{-4}/\dot{e}) \ . \tag{24}$$

Figure 26 shows results obtained by comparing Model 1 from the ORNL rupture data to the NRIM rupture data, after correcting the NRIM U values to the corresponding values for e = 6.7×10^{-4} by the above procedure. The agreement between predictions and data is excellent. Therefore, this simple procedure appears to provide a simple, effective means of extending the applicability of the current models to various strain rates.

The above models are extremely useful in predicting rupture life and minimum creep rate behavior for type 304 stainless steel. It will be shown in the following chapters that these models can also provide a means of predicting creep ductility and creep strain-time behavior.

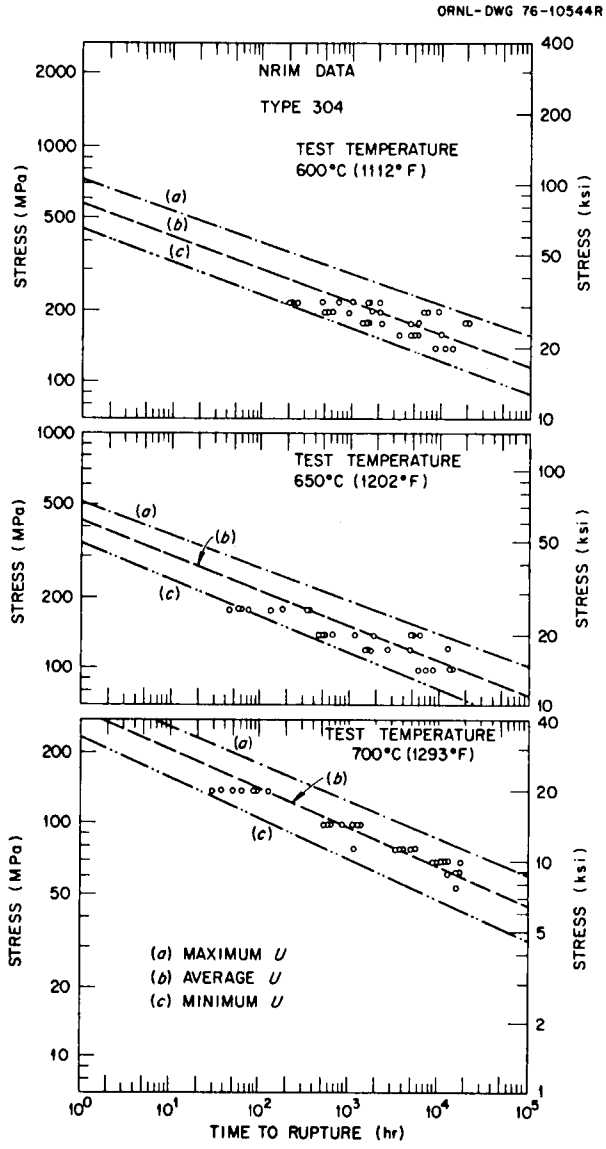

Figure 26. Comparison of NRIM Stress-Rupture Data at 600, 650, and 700°C (1112, 1202, and 1293°F) for 9 Heats of Type 304 Stainless Steel in As-Received Condition With Predicted Maximum, Average, and Minimum Curves from Rupture Model With Elevated-Temperature Ultimate Tensile Strength (U).

CHAPTER III

ANALYSIS OF CREEP DUCTILITY DATA

Many of the previous investigations into the interpretation and analysis of creep data have focused only on the time to rupture, and many methods for the correlation and extrapolation of rupture life data have been proposed. Current elevated-temperature design rules [49], also require a knowledge of the time to the onset of tertiary creep and time to reach a specified strain. These design rules also include an inelastic strain limit which forbids the accumulation of more than 1% total inelastic membrane (through-thickness) strain. This limit is independent of stress and temperature history and of material; however, a strain limit based on actual material ductility could be very useful. Knowledge of time-dependent ductility can be useful in various applications, such as optimizing design conditions or materials selection. Ductility can also give fundamental insights into material behavior.

Booker et al. [50-52] studied techniques for the quantitative analysis of creep ductility data for types 304 and 316 stainless steel, ferritic 2 1/4 Cr-1 Mo steel, and nickel-base Inconel alloy 718. The type 304 stainless steel data examined in those studies are characterized in Table IV, page 11, Table V, page 12, and Table VI, page 13. Three ductility criteria will be discussed here: (1) the

creep strain to rupture, e_r; (2) the creep strain to the onset of tertiary creep, e_3; and (3) the plasticity resource, $e_s = \dot{e}_m t_r$.

The quantities e_r, e_3, and e_s all exhibit considerable scatter. However, based on a concept introduced by Smith [53] for rupture ductility, average strain rates corresponding to each of these ductility criteria were defined as

$$\dot{e}_r = e_r/t_r \tag{25}$$

$$\dot{e}_3 = e_3/t_3 \tag{26}$$

$$\dot{e}_m = e_s/t_r \tag{27}$$

where t_3 is the time to the onset of tertiary creep. As described in Chapter I and shown in Figure 1, page 5, t_3 may be either t_{ss} or t_2 and e_3 is the corresponding strain. The quantities $\dot{e}_r$, t_r, $\dot{e}_3$, t_3, and $\dot{e}_m$ all exhibit much less scatter than the above ductility criteria and therefore can be analyzed with more confidence. Knowing those quantities e_r, e_3, and e_s can then be calculated indirectly, since

$$e_r = \dot{e}_r t_r \tag{28}$$

and so on.

The analyses in Refs. [50-52] employed two techniques, both based upon the above concept of average strain rates. The first procedure, given in Ref. [50], is similar to the parametric analysis introduced by Goldhoff [54] for rupture ductility. This procedure involves separate analysis of the appropriate time (t_3 or t_r) and of

the appropriate strain rate ($\dot{e}_r$, $\dot{e}_3$, or $\dot{e}_m$) by some parametric or other procedure such as those commonly used in the analysis of rupture life data. These analyses yield the time and rate as functions of stress and temperature, after which they can simply be multiplied together to yield the appropriate ductility as a function of these variables. Booker et al. [50] applied this procedure only to single heat data sets (Table IV, page 11), although the use of ultimate tensile strength in developing multiheat creep models appears to be promising.

The second technique, described in Refs. [51,52], involves empirical relationships among various criteria. In particular, those results used relationships of the form

$$\dot{e}_m = F\, t_r^{-\lambda} \tag{29}$$

$$\dot{e}_3 = B\, \dot{e}_m^{\alpha} \tag{30}$$

$$\dot{e}_3 = D\, t_r^{-\gamma} \tag{31}$$

$$\dot{e}_r = C\, \dot{e}_m^{\rho} \tag{32}$$

and

$$\dot{e}_r = E\, t_r^{-\delta} \tag{33}$$

where F, λ, D, γ, E, and δ are temperature-dependent constants, while B, α, C, and ρ are independent of temperature. Note that Eqn. 29 is merely the widely used Monkman-Grant [55] equation, except that F and λ are temperature dependent.

Equations 29-33 allow one to calculate the various strain rates $\dot{e}_m$, $\dot{e}_3$, and $\dot{e}_r$ from either $\dot{e}_m$ or t_r. Knowledge of the values of t_r and $\dot{e}_m$ or $\dot{e}_r$ then yields e_s or e_r. Additionally, Ref. [56] presents an equation of the form

$$t_3 = At_r^{\beta} \tag{34}$$

where A and β are temperature independent constants, and t_3 is either t_2 or t_{ss}. Thus, a knowledge of t_r can be used to estimate t_3, which can be combined with $\dot{e}_3$ to yield e_3. Tables XXII-XXVII present the results obtained in Refs. [51,52, and 56] by fitting Eqns. 29-34 to data for the four above-mentioned materials. Those references include additional details, including attempts to analytically model the temperature dependence of Eqns. 29, 31, and 33.

The models developed for $\dot{e}_m$ and t_r in the last chapter directly yield a model for the plasticity resource, e_s, as a function of stress (σ), temperature (T), and ultimate tensile strength (U). For instance, using Model 1, $\dot{e}_m$ and t_r can be described by

$$\log t_r = 5.716 - \frac{3915}{T} \log \sigma + 32.60\ U/T - 0.007303\ U \log \sigma \tag{35}$$

and

$$\log \dot{e}_m = -2.765 + \frac{3346}{T} \log \sigma - 51.84\ U/T + 0.01616\ U \log \sigma \ . \tag{36}$$

Then, since $\log e_s = \log \dot{e}_m + \log t_r$, e_s is described by a model of the same form:

$$\log e_s = 2.951 - \frac{569}{T} \log \sigma - 19.24\ U/T + .008857\ U \log \sigma \ . \tag{37}$$

TABLE XXII

RELATIONSHIP BETWEEN MINIMUM CREEP RATE AND RUPTURE LIFE[a]

Data Set	Temperature (°C)	Number of Points	F	λ	RMS	R^2
304 Stainless	538	24	8.604	1.115	0.237	94.0
	593	41	15.991	1.180	0.214	96.4
	649	45	24.522	1.119	0.160	97.7
	704	14	28.633	1.086	0.140	98.2
	760	11	31.416	1.042	0.0339	99.5
316 Stainless	538	8	10.452	1.232	0.159	94.6
	593	48	6.410	0.982	0.0949	97.8
	649	12	21.574	1.000	0.0591	99.2
	704	48	32.259	1.038	0.0476	99.3
	760	7	29.207	1.003	0.0183	99.5
	816	36	35.696	1.082	0.0318	99.4
Inconel 718	538	8	13.296	1.378	0.162	98.5
	593	11	2.791	1.211	0.897	90.9
	649	13	1.393	1.142	0.362	95.5
	704	11	2.405	1.165	1.022	81.4
2 1/4 Cr-1 Mo	538	26	7.030	1.075	0.795	65.4
	593	45	97.820	1.414	0.751	81.5
	649	28	36.122	1.316	0.536	84.0

[a]Minimum creep rate, $\dot{e}_m$, and rupture life, t_r have been related by $\dot{e}_m = Ft_r^{-\lambda}$.

TABLE XXIII

RELATIONSHIP BETWEEN MINIMUM CREEP RATE AND AVERAGE CREEP RATE TO TERTIARY CREEP[a]

Data Set	Number of Points	B	α	RMS[b]	R^{2c}	Temperature Range of Data (°C)
304 Stainless	138	1.110	0.974	0.050	99.3	482-816
316 Stainless G[d]	120	1.602	0.995	0.269	95.6	593-816
316 Stainless H[e]	38	1.092	0.991	0.0235	99.6	538-760
Inconel 718 T[f]	18	0.684	0.86	0.254	92.2	538-760
Inconel 718 C[g]	26	1.40	0.985	0.322	96.2	538-704
2 1/4 Cr-1 Mo	117	0.637	0.854	0.241	90.2	482-677

[a]Minimum creep rate, $\dot{e}_m$, and average creep rate to tertiary creep, $\dot{e}_3$, have been related by $\dot{e}_3 = B\dot{e}_m^{\alpha}$.

[b]RMS = $\Sigma Y^2/(n - \nu)$, where n = number of data points and ν = number of coefficients in the model (here $\nu = 2$); ΣY^2 = sum of squared residuals $\Sigma Y^2 = \Sigma(\ln \dot{e}_{3pred} - \ln \dot{e}_{3exp})^2$ where $\ln \dot{e}_{3pred}$ = ln [predicted rate (%/hr)] and $\ln \dot{e}_{3eff}$ = ln [experimentally observed rate (%/hr)].

[c]R^2 = coefficient of determination; R^2 describes how well a regression model describes variations in the data. $R^2 = 100$ signifies complete description, $R^2 = 0.0$ signifies no description. $\sqrt{R^2/100} = R$, the linear correlation coefficient.

[d]Data for total strain.

[e]Data for creep strain only.

[f]Data for total strain.

[g]Data for creep strain only.

TABLE XXIV

RESULTS OF CORRELATION BETWEEN AVERAGE CREEP RATE TO TERTIARY CREEP AND RUPTURE LIFE[a]

Data Set	Temperature (°C)	Number of Points	D	γ	RMS[b]	R^2[c]
304 Stainless	538	24	4.899	1.030	0.174	94.4
	593	37	22.571	1.198	0.202	96.2
	649	44	25.091	1.089	0.172	97.3
	704	14	33.882	1.099	0.124	98.5
	760	11	33.115	1.034	0.048	99.3
316 Stainless G[d]	593	36	30.265	1.078	0.020	99.6
	704	48	49.383	1.081	0.030	99.6
	816	36	42.921	1.103	0.023	99.6
316 Stainless H[e]	538	7	7.131	1.154	0.174	93.5
	593	12	12.783	1.038	0.171	96.5
	649	12	23.220	1.005	0.027	99.6
	760	7	31.690	1.004	0.014	99.6
Inconel 718 T[f]	593	4	2.044	1.048	0.339	94.4
	649	6	27.859	1.442	0.121	97.4
	704	4	0.081	0.710	0.00406	99.5
	760	3	2.545	1.125	0.0566	97.0
Inconel 718 C[g]	538	6	32.394	1.429	0.491	97.0
	593	6	3.968	1.218	0.0636	99.3
	649	8	1.212	1.020	0.0259	99.7
	704	6	6.640	1.232	0.103	98.8
2 1/4 Cr-1 Mo	538	23	3.531	0.903	0.422	73.1
	593	41	51.761	1.280	0.699	77.2
	649	26	18.168	1.185	0.411	83.8

[a]Rupture life, t_r, and average creep rate to tertiary creep, $\dot{e}_3$, are related by $\dot{e}_3 = Dt_r^{-\gamma}$.

[b]RMS = $\Sigma Y^2/(n - \nu)$, where n = number of data points and ν = number of coefficients in the model (here $\nu = 2$); ΣY^2 = sum of squared residuals, $\Sigma Y^2 = \Sigma(\ln \dot{e}_{3pred} - \ln \dot{e}_{3exp})^2$ where $\ln \dot{e}_{3pred}$ = ln [predicted rate (%/hr)] and $\ln \dot{e}_{3exp}$ = ln [experimentally observed rate (%/hr)].

[c]R^2 = coefficient of determination; R^2 describes how well a regression model describes variations in the data. $R^2 = 100$ signifies complete description, $R^2 = 0.0$ signifies no description. $\sqrt{R^2/100} = r$, the linear correlation coefficient.

[d]Data for total strain.

[e]Data for creep strain only.

[f]Data for total strain.

[g]Data for creep strain only.

TABLE XXV

RELATIONSHIP BETWEEN MINIMUM CREEP RATE AND AVERAGE CREEP RATE TO RUPTURE[a]

Data Set	Temperature Range of Data (°C)	Number of Points	C	δ	RMS[b]	R^2[c]
304 Stainless	482-816	142	2.20	0.927	0.251	96.4
316 Stainless G	593-816	120	3.18	1.026	0.044	99.3
316 Stainless H	538-760	37	2.52	0.899	0.290	94.8
Inconel 718 T	538-760	19	4.20	0.756	0.413	71.0
Inconel 718 C	538-704	27	1.71	0.813	0.062	94.5
2 1/4 Cr-1 Mo[d]	482-677	126	1.34	0.650	0.741	64.6

[a]Minimum creep rate, $\dot{e}_m$, and average creep rate to rupture, $\dot{e}_r$, have been related by $e_r = C\dot{e}_m^{\rho}$

[b]RMS in terms of $\ln(\dot{e}_r)$.

[c]Coefficient of determination.

[d]Data in this case represent total strain.

TABLE XXVI

RELATIONSHIP BETWEEN AVERAGE CREEP RATE TO RUPTURE AND RUPTURE LIFE[a]

Data Set	Temperature (°C)	Number of Points	E	δ	RMS[b]	R^2[c]
304 Stainless	538	24	66.67	1.225	0.098	97.7
	593	40	43.26	1.165	0.095	98.3
	649	45	46.41	1.103	0.130	98.0
	704	14	61.98	1.139	0.140	98.4
	760	11	52.28	1.081	0.100	98.7
316 Stainless G	593	36	11.64	1.022	0.127	97.3
	704	48	85.73	1.030	0.099	98.6
	816	48	127.29	1.151	0.031	99.6
316 Stainless H	538	8	121.04	1.292	0.026	99.2
	593	11	39.34	1.087	0.051	99.1
	649	12	52.05	1.027	0.048	99.3
	760	6	81.05	1.042	0.0006	99.9
Inconel 718 T	593	5	1.30	0.763	0.084	92.6
	649	9	4.29	1.154	0.076	97.6
	704	5	7.34	0.844	0.086	89.0
Inconel 718 C	538	7	2.28	0.124	0.063	98.6
	593	7	3.28	0.954	0.009	99.7
	649	7	3.50	0.939	0.066	98.1
	704	7	8.79	0.978	0.066	96.9
2 1/4 Cr-1 Mo	538	29	143.45	1.151	0.086	95.6
	593	47	185.17	1.213	0.103	95.9
	649	27	147.16	1.198	0.128	94.9

[a]Average creep rate to rupture, $\dot{e}_r$, and rupture life, t_r, have been related by $\dot{e}_r = Et_r^{-\delta}$.

[b]RMS in terms of $\ln(\dot{e}_r)$.

[c]Coefficient of determination.

TABLE XXVII

RESULTS OF CORRELATION BETWEEN TIME TO TERTIARY CREEP AND RUPTURE LIFE[a]

Data Set	Number of Points	A	β	RMS[b]	R^2[c]	Temperature Range Data (°C)
304 Stainless, t_{ss}	277	0.752	0.977	0.090	96.6	482-816
304 Stainless, t_2	233	0.685	0.968	0.117	93.6	538-649
316 Stainless, t_2	183	0.526	1.004	0.071	93.5	538-816
2 1/4 Cr-1 Mo, t_{ss}	126	0.334	1.046	0.067	96.1	482-677
Inconel 718, t_{ss}	63	0.424	1.045	0.080	98.2	538-704
Inconel 718, t_2	52	0.285	1.049	0.142	94.3	538-704

[a]Time to tertiary creep, t_3, and rupture life, t_r, have been related by $t_3 = At_r^{\beta}$; t_3 may be t_{ss} (0.2% offset time to tertiary creep) or t_2 (time to first deviation from linear secondary creep).

[b]RMS = $\Sigma Y^2/(n - \nu)$ where n = number of data points and ν = number of coefficients in the model (here $\nu = 2$); ΣY^2 = sum of squared residuals, $\Sigma Y^2 = \Sigma(\ln t_{3pred} - \ln t_{3exp})^2$ where $\ln t_{3pred}$ = ln [predicted rate (%/hr) and $\ln t_{3exp}$ = ln [experimentally observed rate (%/hr)].

[c]R^2 = coefficient of determination; R^2 describes how well a regression model describes variations in the data. $R^2 = 100$ signifies complete description, $R^2 = 0.0$ signifies no description. $\sqrt{R^2/100} = r$, the linear correlation coefficient.

Figures 27 and 28 illustrate results obtained using this model to predict e_s for heats 9T2796 and 8043813 of type 304 stainless steel. As expected, the amount of scatter is large, but the model describes trends in the data well. Note that the predicted (and observed) magnitude of heat-to-heat variation in e_s is smaller than in either $\dot{e}_m$ or t_r. This decrease is caused by the fact that stronger heats have larger values of t_r and smaller values of $\dot{e}_m$. These opposing effects tend to cancel out, thus decreasing the variation in $e_s = \dot{e}_m t_r$. This effect appears to be generally true for creep ductility data, i.e., scatter is large for a given heat, but the differences between different heats are relatively small. Since Eqn. 36 is the result of an exhaustive modeling procedure for $\dot{e}_m$, it is felt to be superior to Eqn. 29 in describing $\dot{e}_m$.

The above procedure may also be used to model variations in e_r and e_3 by separately modeling $\dot{e}_r$, t_r, $\dot{e}_3$, and t_3. By way of illustration, only e_3 will be treated here.

The modeling procedure described in the last chapter resulted in a list of 32 candidate models that appeared to be equally applicable to data for $\dot{e}_m$ or t_r. The approach here has been to use these same models for examining the quantities t_{ss} and $\dot{e}_3$ for the ORNL data. The source of these data is described in Chapter II. Table XXVIII gives the values of the coefficients appearing in these 32 models (see Table X, page 34), and Table XXIX shows the values of the coefficient of determination (R^2) obtained by fitting each model to the available data for t_{ss} and $\dot{e}_3$. Interestingly, Model 1, chosen as optimum for $\dot{e}_m$ and t_r, again ranks first (in terms of R^2) for the $\dot{e}_3$ data, and ranks very close to

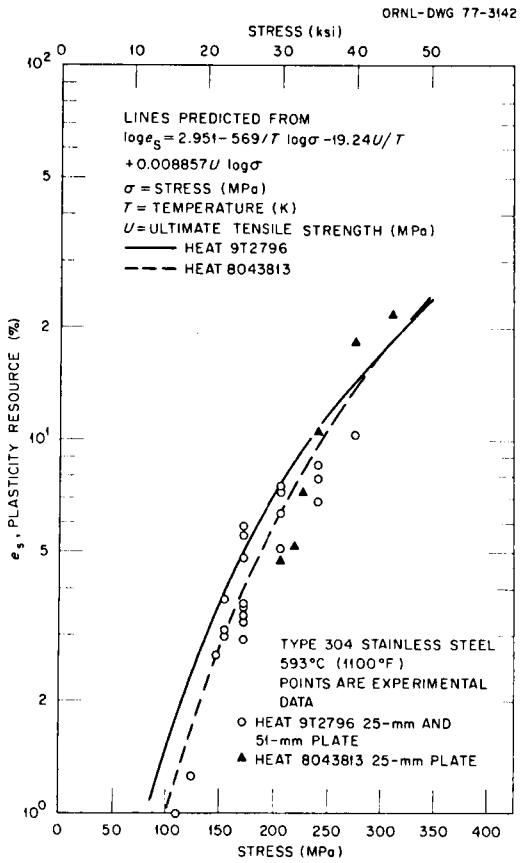

Figure 27. Comparison of Experimental Data With Predicted Values of the Plasticity Resource, $e_s = \dot{e}_m t_r$, at 593°C (1100°F). Shown are predictions for heat 8043813 (a strong heat) and for heat 9T2796 (a weak heat).

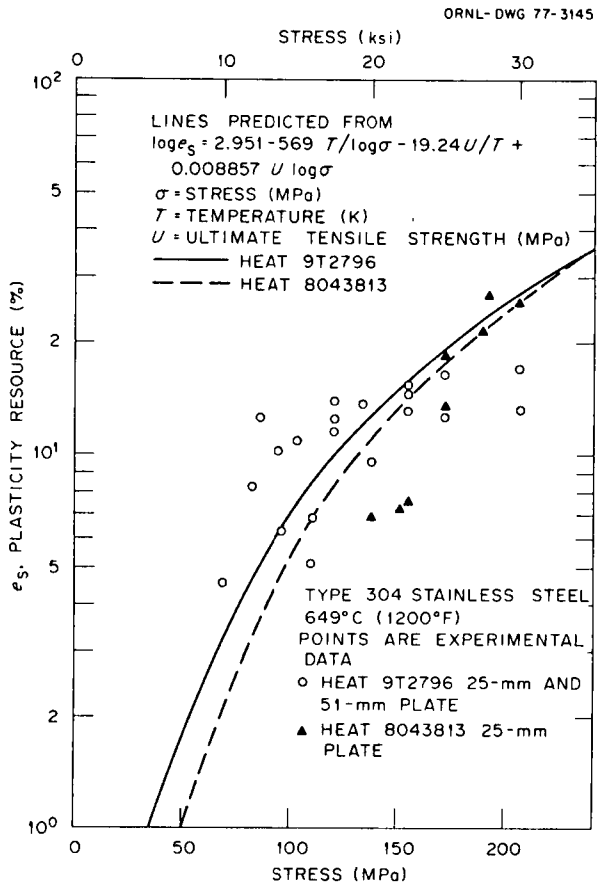

Figure 28. Comparison of Experimental Data With Predicted Values of the Plasticity Resource, $e_s = \dot{e}_m t_r$, at 649°C (1200°F). Shown are predictions for heat 8043813 (a strong heat) and for heat 9T2796 (a weak heat).

TABLE XXVIII

BEST FIT VALUES OF THE COEFFICIENTS IN THE CANDIDATE MODELS FOR TIME TO TERTIARY CREEP

Model[a]	α_0	α_1	α_2	α_3
1	0.47303E 01	-0.33313E 04	0.29834E 02	-0.68761E-02
2	0.14418E 02	-0.16397E 05	0.54669E 02	-0.18847E-01
3	0.71040E 01	-0.36322E 01	-0.19533E 01	0.11837E 02
4	-0.97089E 00	0.15355E 02	0.95432E 04	-0.52157E 04
5	0.74497E 01	-0.42867E 01	-0.44594E-02	0.14150E 02
6	0.82664E 01	-0.49384E 01	-0.81747E-05	0.15032E 02
7	-0.14409E 02	0.16267E 07	0.76245E-01	-0.18900E-01
8	0.40715E 01	-0.56332E 01	0.54624E 04	-0.48132E 04
9	0.29965E 01	-0.32582E 01	0.38980E 04	-0.59650E 01
10	0.11494E 01	-0.28765E 04	0.21604E 02	-0.68717E-02
11	0.12351E 02	-0.29968E 01	0.93408E-02	-0.72904E 01
12	0.78299E 01	-0.45899E 01	-0.31933E 01	0.14553E 02
13	-0.93286E 01	-0.19720E 04	-0.31541E 01	0.10615E 05
14	-0.12016E 01	-0.44049E 01	-0.12342E 01	0.80315E 01
15	0.85925E 01	-0.57054E 01	0.19802E-01	0.0
16	0.99444E 01	-0.57208E 01	0.13837E 02	0.0
17	0.64401E 01	-0.10283E-01	-0.83883E 01	0.65008E 04
18	0.46788E-01	-0.10380E-01	-0.41681E 03	0.62397E 04
19	-0.89119E 01	0.32643E-02	-0.66724E 01	0.77624E 04
20	0.10771E 02	-0.10560E 02	0.60665E 04	-0.45144E-05
21	0.72062E 01	-0.96574E 01	-0.82486E 01	0.72573E 04
22	-0.23935E 01	-0.48361E 01	0.14585E-05	0.13604E 05
23	-0.78617E 01	-0.67610E 00	0.12460E 05	-0.38462E 04
24	0.62990E 01	-0.10332E 04	0.66663E 06	-0.32364E 04
25	0.10940E 02	-0.63270E 01	0.10758E 02	0.20425E-02
26	-0.76056E 01	-0.28541E 01	-0.24310E 01	0.95635E 04
27	-0.64713E 01	-0.29363E 01	-0.55245E-02	0.14441E 05
28	0.27869E 02	-0.41160E 01	-0.23728E-02	-0.17998E-01
29	-0.13838E 02	-0.36105E 04	-0.22989E 01	0.22775E 05
30	-0.28988E 01	-0.46843E 01	0.13831E 05	0.0
31	0.29014E 02	-0.48963E 01	-0.17819E-01	0.0
32	-0.13600E 02	-0.43791E 04	0.23857E 05	0.0

[a]Table X, page 34, Time to Tertiary Creep.

TABLE XXIX

BEST FIT VALUES OF THE COEFFICIENTS IN THE CANDIDATE MODELS FOR AVERAGE CREEP RATE TO TERTIARY CREEP

Model[a]	α_0	α_1	α_2	α_3
1	-0.26253E 01	0.31406E 04	-0.44107E 02	0.12963E-01
2	-0.12120E 02	0.15891E 05	-0.68041E 02	0.24336E-01
3	-0.95386E 01	0.64928E 01	0.78192E 00	-0.18601E 02
4	0.76194E 01	-0.17172E 02	-0.17351E 05	0.66593E 04
5	-0.91511E 01	0.64455E 01	0.27538E-02	-0.19561E 02
6	-0.96692E 01	0.68527E 01	0.49889E-05	-0.20087E 02
7	0.22404E 02	-0.23690E 07	-0.10169E 00	0.23970E-01
8	-0.48879E 01	0.92618E 01	-0.82556E 04	0.57715E 04
9	-0.35908E 01	0.64037E 01	-0.63709E 04	0.71376E 01
10	0.72981E 00	0.25646E 04	-0.37484E 02	0.13697E-01
11	-0.16100E 02	0.27507E 00	-0.12381E-01	0.10581E 02
12	-0.97920E 01	0.68541E 01	0.13415E 01	-0.19691E 02
13	0.15976E 02	0.20244E 04	0.47634E 01	-0.15411E 05
14	0.47483E 01	0.71978E 01	0.61747E-01	-0.11627E 02
15	-0.86206E 01	0.70871E 01	-0.26743E-01	0.0
16	-0.10667E 02	0.73326E 01	-0.19451E 02	0.0
17	-0.64434E 01	0.15286E-01	0.12066E 02	-0.97795E 04
18	0.77512E 01	0.15290E-01	0.39719E 03	-0.13086E 05
19	0.15536E 02	-0.37396E-02	0.84479E 01	-0.12396E 05
20	-0.12634E 02	0.15352E 02	-0.93091E 04	0.77202E 05
21	-0.78122E 01	0.13988E 02	0.11813E 02	-0.10806E 05
22	0.68424E 01	0.66420E 01	-0.31409E-05	-0.20287E 05
23	0.13168E 02	0.17883E 01	-0.18899E 05	0.43392E 04
24	-0.53185E 01	0.19345E 04	-0.16096E 07	0.47532E 04
25	-0.88996E 01	0.62503E 01	-0.25007E 02	0.36932E-02
26	0.13983E 02	0.32573E 01	0.36701E 01	-0.14379E 05
27	0.12572E 02	0.39612E 01	0.76105E-02	-0.21470E 05
28	-0.38110E 02	0.57792E 01	0.24017E-02	0.26286E-01
29	0.22353E 02	0.50353E 04	0.26315E 01	-0.32829E 05
30	0.78708E 01	0.63278E 01	-0.20747E 05	0.0
31	-0.39269E 02	0.65536E 01	0.26141E-01	0.0
32	0.22114E 02	0.58931E 04	-0.34049E 05	0.0

[a]Table X, page 34, Average Creep Rate to Tertiary Creep.

the best model for the t_{ss} data. Therefore, Model 1 was taken as optimum for both the $\dot{e}_3$ and t_{ss} data as well. In particular, these models are

$$\log \dot{e}_3 = -2.6253 + \frac{3140.6}{T} \log \sigma - 44.107 \frac{U}{T} + 0.0129634\, U \log \sigma \qquad (38)$$

and

$$\log t_{ss} = 4.7303 - \frac{3331.3}{T} \log \sigma + 29.834 \frac{U}{T} - 0.0068761\, U \log \sigma\,. \qquad (39)$$

Alternatively, t_{ss} and $\dot{e}_3$ can be described by Eqns. 30 and 34 as functions of $\dot{e}_m$ and t_r, respectively. Referring to Tables XXIII, page 90, and XXVII, page 95, these equations become

$$t_{ss} = 0.752\, t_r^{0.977} \qquad (40)$$

and

$$\dot{e}_3 = 1.11\, \dot{e}_m^{0.974} \qquad (41)$$

Figures 29 and 30 illustrate the fits of these equations to available data.

Figure 31 shows the fit of Eqns. 36 and 37 to data for t_{ss} for two heats of type 304 stainless steel at 593°C, while Figure 32 shows the fit of Eqns. 35 and 38 to data for $\dot{e}_3$. Clearly, there is very little difference between the results obtained using the two prediction methods. The predictions using average values of ultimate tensile strength appear to well estimate average behavior, while predictions made using maximum and minimum (in the sense of mean ± 2SEE) values of U appear to span the scatter band of the data. Since Eqns. 37, page 88,

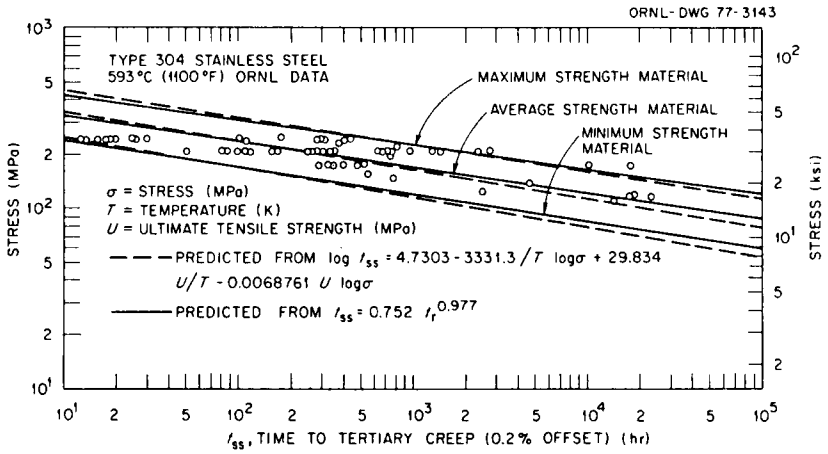

Figure 29. Comparison of Experimental ORNL Data for the Time to Tertiary Creep, t_{ss}, With Predicted Values at 593°C (1100°F). Predictions were made both by a direct fit using Model 1 (dashed lines) and by relating t_{ss} to the rupture life, t_r (solid lines). Predictions are shown for estimated average, minimum and maximum ultimate tensile strength material.

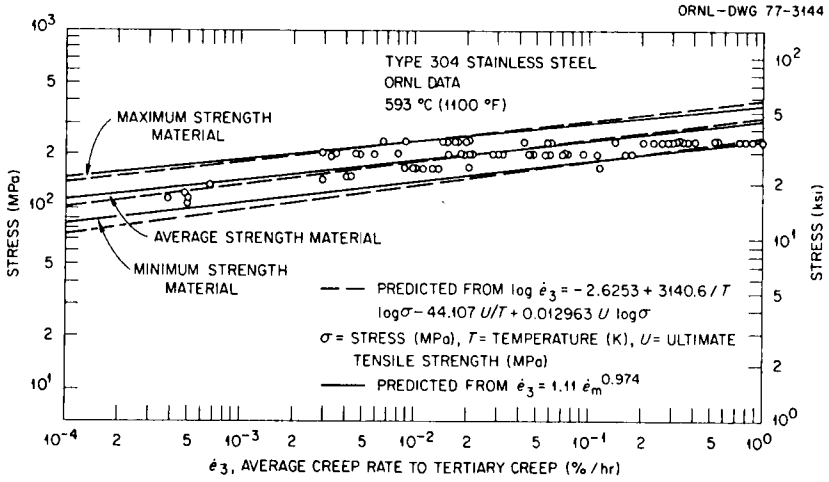

Figure 30. Comparison of Experimental ORNL Data for the Average Creep Rate to Tertiary Creep, $\dot{e}_3$, With Predicted Values at 593°C (1100°F). Predictions were made both by a direct fit using Model 1 (dashed lines) and by relating e_3 to the minimum creep rate, $\dot{e}_m$ (solid lines). Predictions are shown for estimated average, minimum, and maximum ultimate tensile strength material.

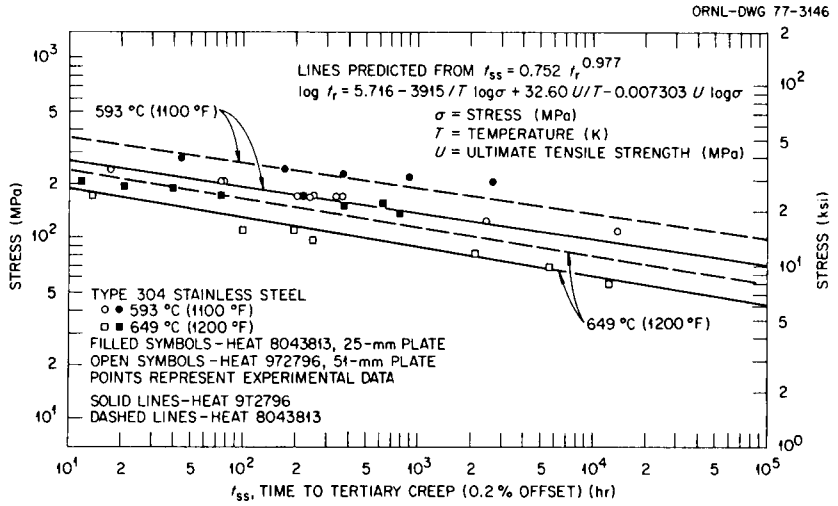

Figure 31. Comparison of Experimental Data With Predicted Values of Time to the Onset of Tertiary Creep at 593°C (1100°F) and 649°C (1200°F). Predictions are shown for heat 8043813 (a strong heat) and for heat 9T2796 (a weak heat).

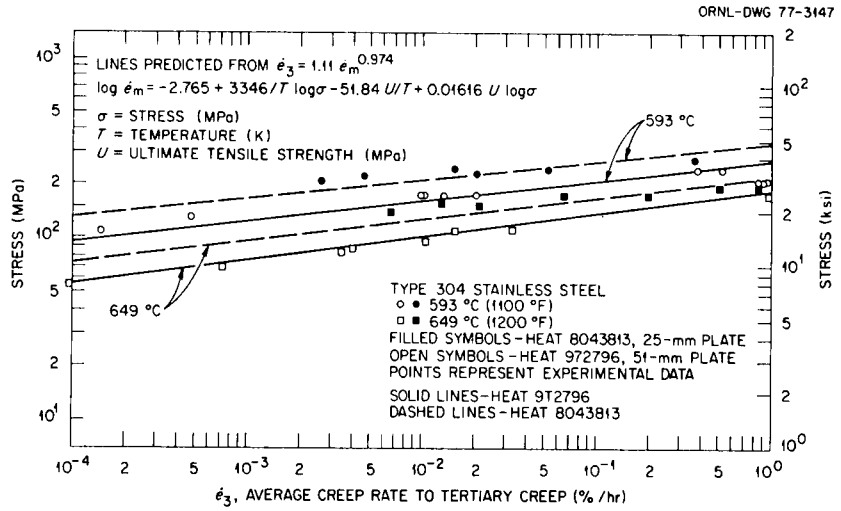

Figure 32. Comparison of Experimental Data With Predicted Values of Average Creep Rate to the Onset of Tertiary Creep at 593°C (1100°F) and 649°C (1200°F). Predictions are shown for heat 8043813 (a strong heat) and for heat 9T2796 (a weak heat).

and 38, page 101, are simpler and rely upon the more widely available data for $\dot{e}_m$ are t_r, they are preferred.

Analogous to the development of Eqn. 34, page 88, above, Eqns. 38 and 39, page 101, can be combined to yield a direct expression for e_3 as a function of U, σ, and T as

$$\log e_3 = 2.105 - \frac{190.7}{U} \log \sigma - 14.273 \frac{U}{T} + 0.0060869\, U \log \sigma \,. \qquad (42)$$

Equations 40 and 41, page 101, yield an expression of the form

$$e_3 = 0.835\ \dot{e}_m^{\,0.974}\ t_r^{\,0.977} \,. \qquad (43)$$

Figures 33 and 34 compare results obtained using Eqns. 35 and 35, page 88, and 43 to estimate e_3 with experimental data for heats 9T2796 and 8043813. As with the plasticity resource, the predictions appear to accurately reflect trends in the data, although the uncertainty is again large.

For type 304 stainless steel the analyses in Refs. [50-52] treated data for creep strain only, and did not include the instantaneous strain incurred upon loading. In many cases, however, the only available measure of ductility is the total strain (creep plus loading) to rupture, e_t. Fortunately, the quantity e_t can be treated in the same fashion as was e_r in Eqn. 33, page 87. Thus, one can write

$$\dot{e}_t = G\, t_r^{\,-\varepsilon} \,, \qquad (44)$$

where $\dot{e}_t = e_t/t_r$. Thus,

$$e_t = G\, t_r^{\,1-\varepsilon} \,. \qquad (45)$$

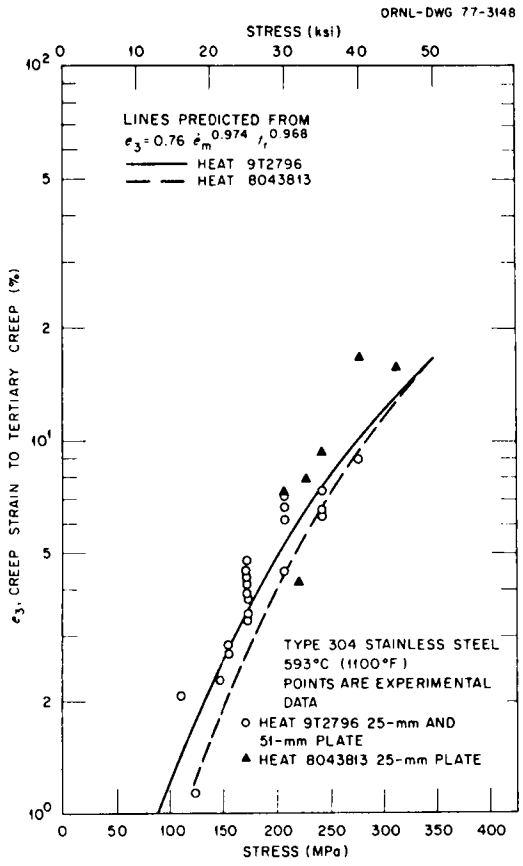

Figure 33. Comparison of Experimental Data With Predicted Values of Creep Strain to the Onset of Tertiary Creep at 593°C (1100°F). Predictions are shown for heat 8043813 (a strong heat) and for heat 9T2796 (a weak heat).

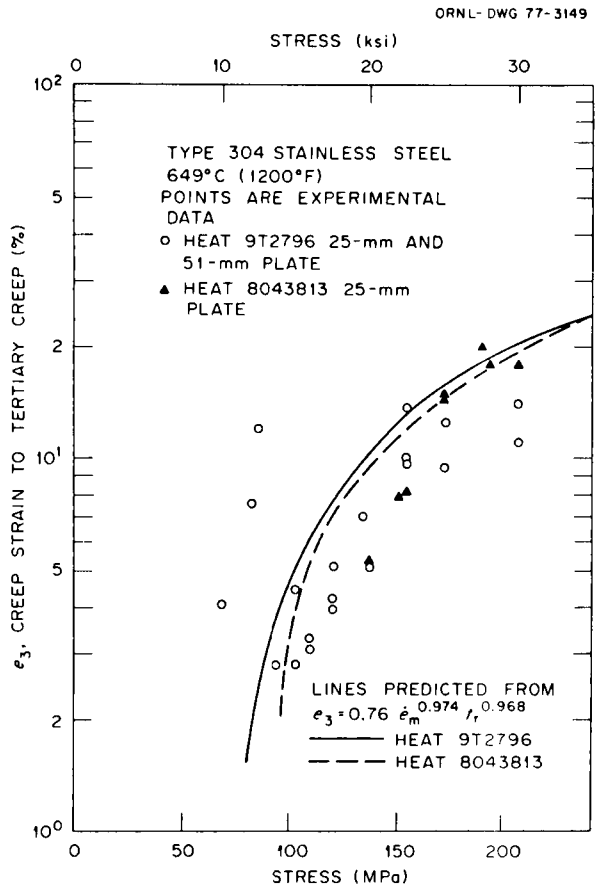

Figure 34. Comparison of Experimental Data With Predicted Values of Creep Strain to the Onset of Tertiary Creep at 649°C (1200°F). Predictions are shown for heat 8043813 (a strong heat) and for heat 9T2796 (a weak heat).

Sikka and Booker [18] have applied this method to data from the US, NRIM, and BSCC data mentioned last chapter. However, since Eqns. 44 and 45 are independent of ultimate tensile strength, all NRIM and BSCC available data were used rather than only those for which corresponding ultimate tensile strength data were available. Table XXX summarizes the results from Ref. [18] for type 304 stainless steel, including separate analyses of data for individual product forms for which a significant amount of data were available. No noticeable effects due to product form were observed. Figure 35, taken from Ref. [18], illustrates the results. The top row of plots in Figure 35 shows the results obtained by fitting Eqn. 44, page 106, to the data for $\dot{e}_t$. The solid line was determined by a least squares best fit, while the dashed lines were determined by adding or subtracting 2 × SEE (Table XXX) in log $\dot{e}_t$ from the mean values. The lower row of plots in Figure 35 shows data and predictions for e_t as a function of t_r. Solid lines and dashed lines were obtained merely by multiplying the solid and dashed lines in the upper row by t_r. The fit to the data is quite good.

Interpretation of Ductility Predictions

Although data for rupture ductility are widely available, the processes occurring during third-stage creep (grain boundary cracking, etc.) that lead to rupture are highly variable. As a result, variations in rupture data can be especially large [35,57]. If one views rupture as a kind of instability, it is reasonable to expect that the material condition at the onset of this stability is a more fundamental property than the condition after its occurrence [35]. These considerations

TABLE XXX

RELATIONSHIP BETWEEN AVERAGE STRAIN RATE TO RUPTURE AND RUPTURE LIFE[a]

Data Source	Product	Number of Data Points	Temperature (°C)	Temperature (°F)	Regression Coefficients G	Regression Coefficients -ε	SEE. ($\log e_r$)	R^2 (%)	10^4-hr Creep Total Elongation (%)
BSCC	Tube	13	600	1112	1.69	-1.11	0.144	95.74	
BSCC	Tube	23	625	1157	1.81	-1.17	0.127	98.08	
BSCC	Tube	13	650	1202	1.82	-1.11	0.186	94.98	
NRIM	Tube	32	600	1112	2.19	-1.22	0.138	96.16	
NRIM	Tube	32	650	1202	2.46	-1.30	0.126	98.54	
NRIM	Tube	40	700	1273	2.41	-1.30	0.249	95.77	
NRIM	Tube	27	750	1383	2.20	-1.25	0.274	89.24	
US	Tube	22	593	1100	1.46	-1.05	0.194	92.81	
US	Tube	53	649	1200	1.73	-1.10	0.267	90.40	
US	Tube	5	732	1350	1.03	-0.93	0.248	88.71	
BSCC	Bar	15	550	1022	1.52	-1.14	0.105	99.11	
BSCC	Bar	13	600	1112	1.47	-1.05	0.256	95.27	
BSCC	Bar	14	650	1202	1.35	-1.00	0.111	99.17	
BSCC	Bar	4	700	1293	1.62	-0.92	0.154	97.56	
US	Bar	14	538	1000	1.73	-1.22	0.060	99.60	
US	Bar	5	565	1050	1.72	-1.23	0.065	99.61	
US	Bar	16	593	1100	1.50	-1.13	0.099	99.04	
US	Bar	35	649	1200	1.57	-1.06	0.159	98.49	
US	Bar	15	704	1300	1.52	-1.07	0.226	97.05	
US	Bar	12	732	1350	1.72	-1.06	0.159	96.26	
US	Bar	9	760	1400	1.50	-1.05	0.178	98.52	
US	Bar	10	816	1500	1.42	-1.04	0.178	97.67	
BSCC	Combined	15	550	1022	1.52	-1.14	0.105	99.11	9.12
BSCC	Combined	26	600	1112	1.53	-1.08	0.202	96.13	16.22
BSCC	Combined	23	675	1157	1.81	-1.17	0.127	98.08	13.49
BSCC	Combined	27	650	1202	1.48	-1.02	0.170	97.17	25.12
BSCC	Combined	4	700	1293	1.62	-0.92	0.154	97.56	87.10
NRIM	Combined	10	550	1022	1.90	-1.16	0.087	97.54	18.20
NRIM	Combined	10	575	1067	1.74	-1.08	0.163	95.47	26.30
NRIM	Combined	41	600	1112	2.17	-1.21	0.153	94.84	21.38
NRIM	Combined	34	650	1202	2.49	-1.31	0.126	98.51	17.78
NRIM	Combined	40	700	1293	2.41	-1.30	0.249	95.77	16.22
NRIM	Combined	27	750	1383	2.20	-1.25	0.274	89.24	17.78
US	Combined	17	538	1000	1.61	-1.17	0.086	99.29	8.51
US	Combined	5	565	1050	1.72	-1.23	0.065	99.61	6.31
US	Combined	44	593	1100	1.49	-1.08	0.181	95.86	14.79
US	Combined	91	649	1200	1.60	-1.06	0.231	95.21	22.91
US	Combined	26	704	1300	1.59	-1.04	0.266	95.75	26.92
US	Combined	17	732	1350	1.35	-0.97	0.226	90.99	29.51
US	Combined	9	760	1400	1.50	-1.05	0.178	98.52	19.95

TABLE XXX (continued)

Data Source	Product	Number of Data Points	Temperature (°C)	Temperature (°F)	Regression Coefficients G	Regression Coefficients -ε	SEE (log $\dot{e}_r$)	R^2 (%)	10^4-hr Creep Total Elongation
US	Combined	21	816	1500	1.58	-1.02	0.254	95.03	31.63

[a]Average strain rate to rupture, $\dot{e}_t$, and rupture life, t_r, have been related by $\dot{e}_t = Gt_r^{-\varepsilon}$.

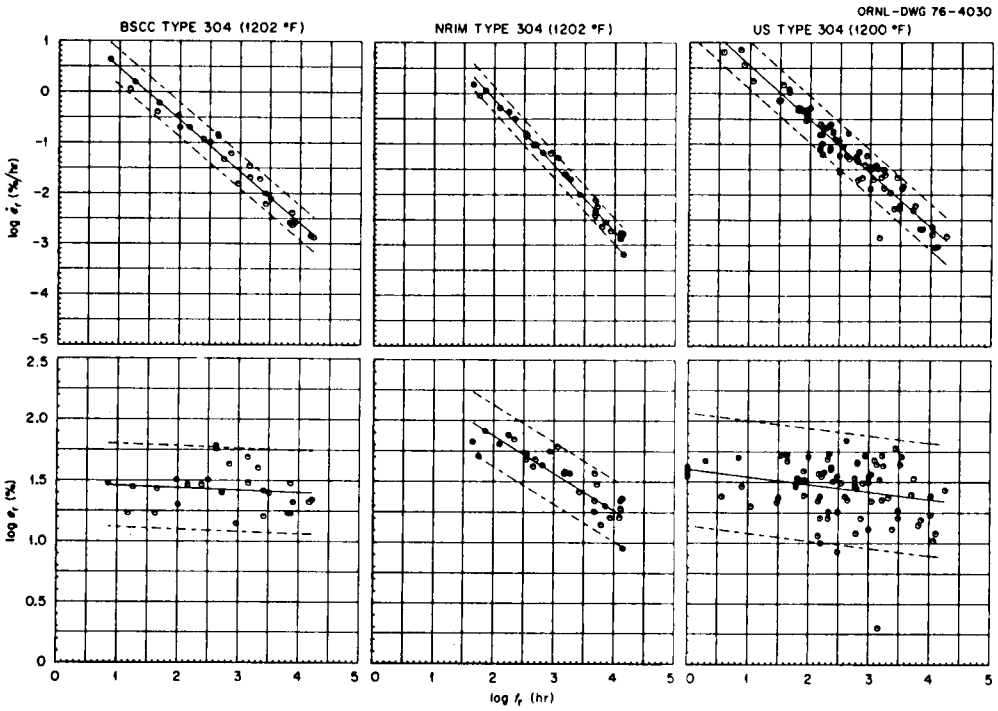

Figure 35. Plots of Average Creep Rate and Creep Total Elongation for Type 304 Stainless Steel Data Collected from US and Two Foreign Countries.

suggest the use of the strain to onset of tertiary creep, e_3, as a criterion of creep ductility.

Grant et al. [57,58] have suggested the use of e_3 as a criterion, referring to it as the "true" creep elongation. Booker and Sikka [51] have discussed the advantages of e_3 for design application. The major advantage to the use of e_3 in design is the prevention of tertiary creep and the associated cracking, void formation, and other instabilities. Also, most currently used design creep strain-time equations are valid only for the first and second stages of creep, so that e_3 represents the maximum amount of strain that can be predicted from these equations. The cutoff point for the validity of these equations for a constant load, isothermal situation could also be located simply by knowing the time to tertiary creep. However, for variable load conditions, previous results [8,9] have shown the behavior of this material to be adequately described by the hypothesis of strain hardening [12]. This hypothesis assumes that, under a given load-temperature condition, the instantaneous strain rate—and thus the instantaneous material condition—depends only on the previously accumulated strain. Booker and Sikka [51] present results which indicate that e_3 is indeed relatively insensitive to the effects of variable loads—depending only upon the instantaneous stress and temperature at the onset of tertiary creep. Therefore, the strain to tertiary creep might be a more meaningful criterion for variable load conditions than the time to tertiary creep. In the next chapter, the predicted values of e_3 will be used in the development of a creep strain-time equation for type 304 stainless steel. Thus, it is seen

that a knowledge of the quantity e_3 can be very useful in design applications—both as a measure of usable ductility and as a cutoff point for creep strain-time temperature.

The plasticity resource, e_s, was first introduced [59,60] by Soviet investigators who viewed it as an approximation to the creep strain to tertiary creep, e_3. This approximation was used to alleviate shortages in available data for the quantity e_3 itself. Goldhoff [61] has disputed the general validity of this approximation, although recent work [51] indicates that the approximation is fairly good for type 304 stainless steel. Actually, it can be shown [52] that e_s and e_3 are related by

$$e_s = \frac{t_r}{t_2}(e_3 - e_p) \tag{46}$$

where e_p is the transient creep strain (see Figure 1, page 5). The exact relationship thus depends upon t_r, t_2, and e_p.

Several investigators [62-65] have discussed the possibility that e_s is a material constant, independent of stress and temperature (and thus of rupture life and strain rate). While some theoretical work has been done [62], the conclusion that e_s is constant has been largely based on the Monkman-Grant relationship [55]. That equation, however, is essentially empirical, although similar relationships have been defended theoretically [66,67]. The current results however indicate a small but significant dependence of e_s on stress (nonunity slope in the Monkman-Grant equation), and a definite dependence upon temperature. A

temperature dependence has also been observed by other investigators [68-70]. Thus, one must conclude that e_s is not a fundamental material constant, but is in some cases a reasonable approximation to e_3.

Trends in Behavior

Figures 36 and 37 illustrate predicted trends in the value of e_3 with variations in stress, temperature, minimum creep rate, and ultimate tensile strength obtained using Eqn. 43 from page 106. For a given heat of material, e_3 increases with increasing temperature from 482°C to 704°C; while it decreases with decreasing stress or minimum creep rate. Trends in e_s with variations in ultimate tensile strength (U) are slightly more complex, although smaller. At a given stress, e_3 generally decreases as U increases up to some high stress level, when the trend is reversed. The relationship between U and e_3 over the range of creep at a constant minimum creep rate is a strong function of temperature. Predicted trends in e_s are similar, although the values are generally slightly higher than those for e_3. The above trends are clearly born out by experimental data, except for the variations with ultimate tensile strength, which are so small that they are obscured by the scatter in the data.

It will be seen in the next chapter that these predictions of trends in e_3 can be important in predicting general trends in creep deformation behavior.

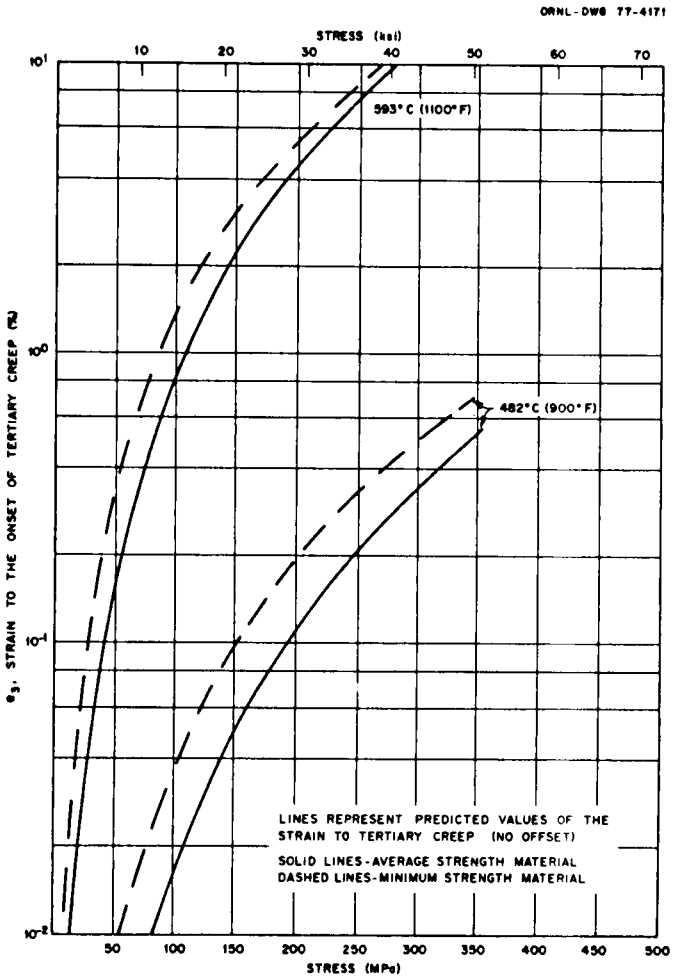

Figure 36. Predicted Trends in the Strain to the Onset of Tertiary Creep (No Offset) as a Function of Stress.

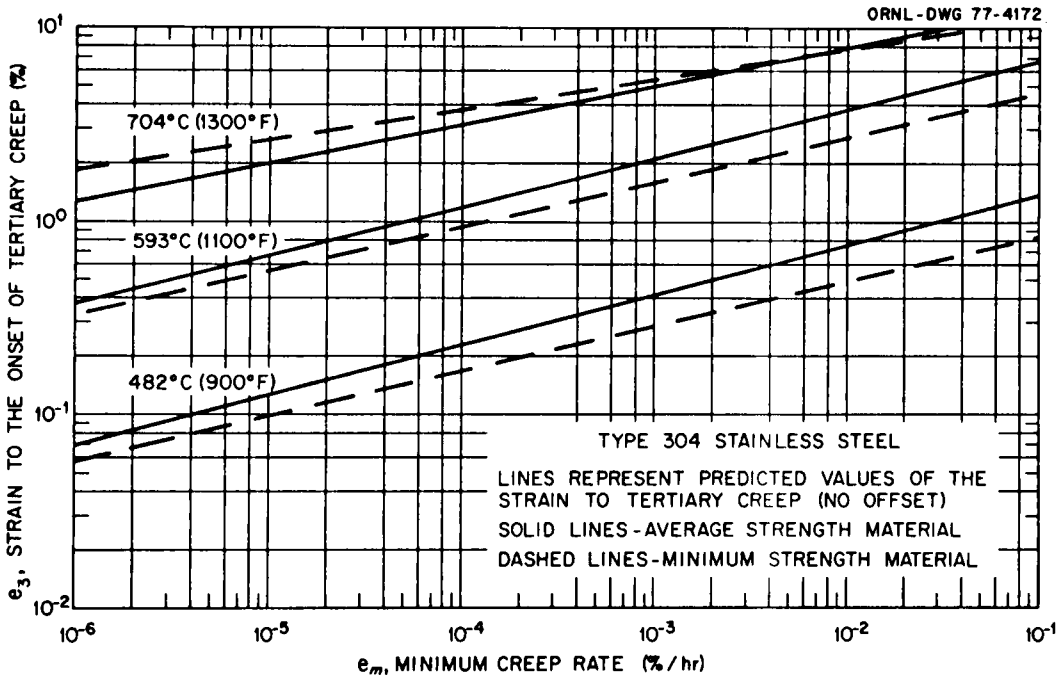

Figure 37. Predicted Trends in the Strain to the Onset of Tertiary Creep (No Offset) as a Function of Minimum Creep Rate.

CHAPTER IV

ANALYSIS OF CREEP STRAIN-TIME BEHAVIOR

As stated in the Introduction, elevated temperature inelastic design requires an expression for creep strain as a function of time (t), stress (σ), and temperature (T). Such an equation can also be used to estimate the time allowed by the ASME Code Case 1592 [49] restriction that the inelastic strain be limited to 1% and for inelastic analyses. Methods for relating creep strain to time under constant load (or stress), isothermal, uniaxial conditions, include the following:

1. The times to accumulation of given amounts of creep strain (t_x) can be analyzed by techniques similar to those commonly used for rupture life data. This method was used to describe data for Incoloy Alloy 800 (Grade 2), Inconel Alloy 625 (Grade 2), and 2 1/4 Cr-1 Mo steel by Roberts and Sterling [71]. Using a series of strain levels and interpolating between them, one can then reconstruct an entire creep curve. This method suffers from the fact that it does not yield an expression for the creep strain rate, which is required in design calculations. It can be used to generate isochronous stress-strain curves such as those given in ASME Code Case 1592 [49]. It should be noted that the particular method used by Sterling [72] for Alloy 800 and 2 1/4 Cr-1 Mo steel assumed an equation relating strain level to time and thus analytically "tied together" the various strain levels. The Sterling equation can yield an expression for creep rate as well as for creep strain.

2. A second possibility consists of using empirical relationships among creep strain-time properties and better-established properties such as rupture life or minimum creep rate. These relationships generally involve equations similar to Eqns. 29-33, page 87, and 34, page 88, except that they might relate t_x to $\dot{e}_m$ or to t_r [52]. Other investigators [73-75] have proposed stress-based correlations, relating the stress to cause x% strain in a given time to the stress to cause rupture in that time. Such relationships again do not yield estimates of creep rate.

3. A method that has found some use is the parametric approach of Rabotnov [76]. At a given level of total strain (e) (loading plus creep), this parameter is given by

$$\phi(e) = \sigma(1 + \alpha t^n) \tag{47}$$

where σ and t are again the stress and time, ϕ is the parameter, α is a constant, and n is a constant whose value is about one-third. One can use monotonic stress-strain curves (t = 0) to determine the value of ϕ at various strains, from which α can be determined from creep curves by assuming n = 1/3 and solving Eqn. 47 to yield

$$\alpha = (\frac{\phi}{\sigma} - 1)t^{-\frac{1}{3}} . \tag{48}$$

Since α is supposedly independent of σ and t, only one point from one creep curve should be required to determine α at each temperature. Alternatively, the values of ϕ, α, and n can be determined by least squares fits to creep data [77].

4. The most popular method for design applications in recent years has involved the use of creep equations, i.e. an analytical expression

for creep strain as a function of time, stress, and temperature. Since these equations can generally be differentiated to yield expressions for creep rate, they are the more useful for design purposes than the above methods. Moreover, a creep equation can be more easily related to the actual microstructural processes occurring during creep. This method is thus the most useful both for practical design applications and for fundamental studies of material behavior. Therefore, it is this method that will be adopted here.

Methods for Development of Creep Equations

In general, the creep strain, e_c, is given by $e_c(\sigma, t, T)$. Two basic methods for evaluation of this function have been proposed. The first method, discussed by Penny and Marriott [35], assumes that the functional dependence of e_c upon σ, t, and T is separable such that

$$e_c = f_1(\sigma) f_2(t) f_3(T) \quad . \tag{49}$$

Such a separation simplifies analysis procedures, but it may place an undue restriction upon the flexibility of the equation to describe material behavior.

The method that has recently been applied with some success [29,38,78] involves first describing individual creep curves by a strain-time equation. The parameters in this equation are then themselves expressed as functions of stress and temperature. This approach allows considerable flexibility and will be used here; however, a new method for evaluating the stress and temperature dependence of the equation parameters is proposed which alleviates

certain shortcomings in previous [29,38,78] evaluations. In particular, the analyses for t_r, $\dot{e}_m$, t_3, and e_3 reported above are utilized in the development of the creep equation. The resulting creep equation thus allows a prediction of heat-to-heat variations in creep strain-time behavior as it is reflected by ultimate tensile strength (U).

Choice of Strain-Time Equation Form

For the purposes of a design equation, it is necessary that the creep equation be valid only through primary and secondary creep, since design rules [49] preclude the onset of tertiary creep in service. Fortunately, type 304 stainless steel exhibits almost exclusively classical creep curves (as shown in Figure 1, page 5), further simplifying the choice of strain-time equation form. A large number of equation forms have been proposed as reviewed in Refs. [79-82]. Of these, the most widely popular are listed in Table XXXI, following the listing of Garofalo [80]. The most commonly used forms for austenitic stainless steels have been the so-called single and double exponential equations, given by

$$e_c = e_t[1 - \exp(-rt)] + \dot{e}_m t \tag{50}$$

and

$$e_c = e_x[1 - \exp(-st) + e_t[1 - \exp(-rt)] + \dot{e}_m t \ . \tag{51}$$

Equation 50, first introduced empirically by McVetty [83] gained acceptance for type 316 stainless steel through the work of Garofalo et al. [84]. Subsequent investigators have applied Eqn. 50 to a variety

TABLE XXXI

SOME COMMON CREEP STRAIN-TIME RELATIONS

Equation Name	Equation Form	T/T_m	Materials
Logarithmic	$e = \alpha \ln t + c$	0.05-0.3	Al,Ag, Au,Cd,Cu,Mg, Ti-Steel, Al-10% Cu, and Cu-3% Ag
Power Law	$e = e_o + \beta t^m$ or $e = e_o + \beta t^m + kt$	0.2-0.7	Al,Ag,Brass,Cd, Cu, Iron and Steel, Mg, Mg-2% Al, Ni, Pb, Pt, Sn, and Zn
Exponential	$e = e_o + e_t(1 - e^{-rt}) + \dot{e}_s t$ or $e = e_o + e_t(1 - e^{-rt}) + e_x(1 - e^{-st}) + \dot{e}_s t$	0.4-0.6	Ferritic and Stainless Steel
Linear	$e = e_o + \dot{e}_s t$	0.96-0.99	Al,Au,Cu, and δ-Fe

of materials, and considerable attention has been given to the meanings of and interrelationships among the parameters e_t, r, and $\dot{e}_m$ [85-95]. In fact, some investigators [90,92-94] have extended the validity of the equation through tertiary creep by the addition of a positive exponential term. Although Eqn. 50, page 121, has been widely applied, it often underestimates the creep rate in the initial part of the creep curve [29,89-95]. Blackburn [29] proposed Eqn. 51, page 121, where the second exponential term (the so-called "fast transient" term) was added to increase the accuracy of the equation in the initial stages. It should be noted, however, that Wilshire and co-workers [89-94] fit Eqn. 50 to experimental data in the form

$$e = e_L + e_t[1 - \exp(-rt)] + \dot{e}_m t \qquad (52)$$

where e_L is the instantaneous strain incurred upon loading and thus corresponds to the strain at zero time. In fitting this equation, e_L was generally overestimated, resulting in the situation shown schematically in Figure 38. The curve fitting procedure used by Blackburn [29] suffers from a similar shortcoming. On the other hand, if one subtracts the loading strain and fits creep strain only using Eqn. 51, the equation form itself forces a better fit in the initial stages, since e_c is always zero at $t = 0$. Thus, the problems incurred with fitting the single exponential equation were probably due as much to the particular curve-fitting procedures employed as to shortcomings in the equation form. For design applications, any additional precision obtained by adding the second exponential term is probably not justified by the increase in the complexity of the model.

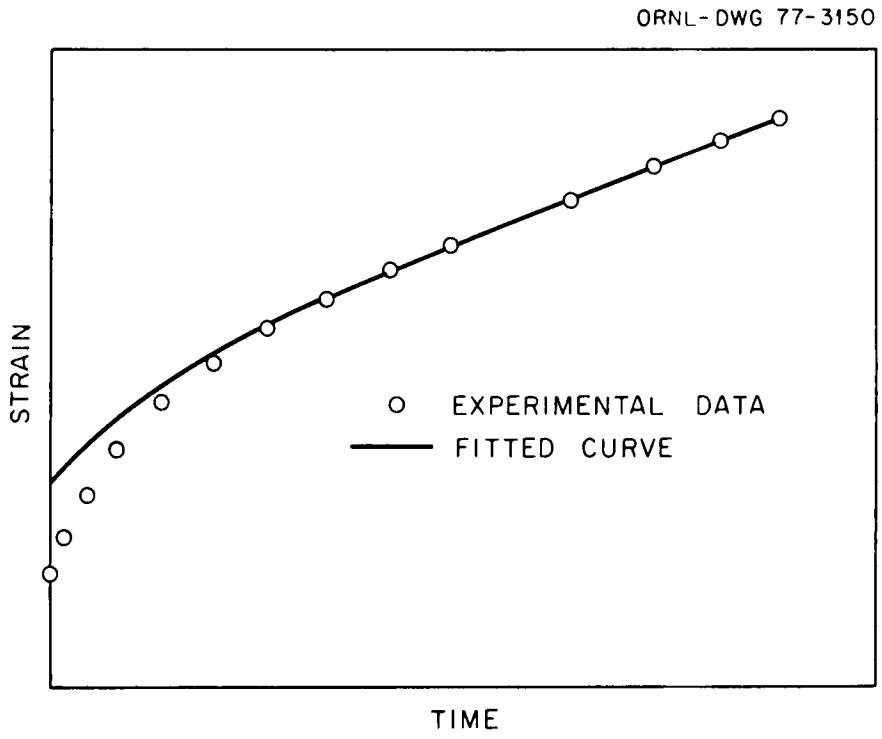

Figure 38. Schematic Diagram Showing Results of Fitting Eqn. 49 Directly to an Experimental Creep Curve.

It should be noted the "double exponential" equations developed by Blackburn [29] for types 304 and 316 stainless were used to develop the isochronous stress-strain curves in ASME Code Case 1592 [51]. These equations have several shortcomings which are alleviated by the current results, as will be shown below.

Recent results for 2 1/4 Cr-1 Mo steel [38] indicate the applicability of a rational polynomial equation, which can be written as

$$e_c = \frac{Cpt}{1 + pt} + \dot{e}_m t \tag{53}$$

where e_c is again the creep strain, t the time, $\dot{e}_m$ the minimum creep rate, and C the limiting value of the transient primary creep strain. The parameter p is related to the sharpness of the curvature of the primary creep region. Preliminary results in the current analysis indicated that Eqn. 53 could also be used to describe individual creep curves for type 304 stainless steel. Subsequently, an analysis for type 316 stainless steel [78] found the rational polynomial equation to be superior to the exponential equations. Significantly, although both single and double primary term exponential equations and single and double term rational polynomial equations were studied, it was found in Ref. [78] that the single rational polynomial equation was preferable due to its inherent simplicity. At any rate, it appears justified to examine both the exponential and rational polynomial equations in detail.

The Exponential Creep Equation

The exponential creep equation form was first introduced [83,84,89-94] on an empirical basis merely because its mathematical properties resemble

those of primary and secondary creep curves. Differentiating Eqn. 50, page 121, one obtains an estimate of the creep rate, $\dot{e}_c$, as

$$\dot{e}_c = e_t r e^{-rt} + \dot{e}_m \ . \tag{54}$$

Thus, the initial creep rate, $\dot{e}_o$ is given by

$$\dot{e}_o = e_t r + \dot{e}_m \ , \tag{55}$$

but $\dot{e}_c$ decreases exponentially and asymptotically approaches the minimum creep rate. The contribution of the primary term approaches a maximum value of e_t. The parameter r, often called the time constant, controls the rate of decay of the transient contribution and thus is related to the sharpness of curvature of the primary region of the creep curve. It can easily be seen that these same basic comments apply to the double exponential form of the equation.

Recently, this same equation has been derived by several investigators on a phenomenological basis. Webster et al. [95] begin by assuming that primary and secondary creep obey first-order kinetics,

$$\frac{d\dot{e}_c}{dt} = - (\dot{e}_c - \dot{e}_m) r \ . \tag{56}$$

Integrating this expression twice yields Eqn. 50. Equation 51, page 121, can be derived upon the assumption that two separate mechanisms operate independently, each obeying its own first-order kinetics.

Mejia et al. [96] recently presented a similar phenomenological approach through which a variety of equation forms can be derived.

Their basic equation was

$$\frac{d\dot{e}_c}{dt} = -g(\dot{e})(\dot{e}_c - \dot{e}_m) \quad . \tag{57}$$

It should be noted that Eqn. 56 is merely a form of Eqn. 57 with $g(\dot{e}) = r$.

Soviet investigators [87,88] have also derived a relationship from an independent phenomenological approach. They assumed that a material contains randomly distributed sources of deformation, each of which requires a certain stress for activation. Once activated, a source produces a mean amount of deformation $\bar{\delta}$ in a mean time of $\bar{t}$. Each source then ceases to act due to the buildup of internal stresses or work hardening. At high enough temperatures, the source can recover in a mean time $\bar{\tau}$, after which it can be reactivated. Next, it was assumed that both source activation and source recovery obey first-order reaction kinetics, so that

$$\frac{dN}{dt} = -vN + w(N_o - N) \tag{58}$$

where $v = 1/\bar{t}$, $w = 1/\bar{\tau}$, N_o is the number of sources initially present and N is the number of sources available for activation at a given time.

Equation 58 can be integrated with $N = N_o$ for $t = 0$ to give

$$N = N_o \frac{w}{v + w} [1 - e^{-(v+w)t}] + N_o e^{-(v+w)t} \quad . \tag{59}$$

The total number of sources actually activated in a time, t, is then given by

$$N_a = \int_o^t r \, N dt \quad . \tag{60}$$

Noting that the total creep strain, e_c, occurring in time, t, is given by δN_a, Eqn. 59 can be integrated to yield

$$e_c = e_1\left[\frac{vw}{v+w}\,t + \frac{v^2}{(v+w)^2}\,(1 - e^{-(v+w)t})\right] \tag{61}$$

where e_1 is the maximum strain that could be incurred in the absence of any recovery (i.e. $e_1 = \overline{\delta N}_o$). Equation 61 is clearly of the same form as Eqn. 50, page 121, except that the equation parameters are now explicitly defined in terms of e_1, v, and w.

The Rational Polynomial Creep Equation

The properties of the rational polynomial creep equation given in Eqn. 53, page 125, are reviewed in detail in a recent report by Hobson and Booker [97], but will be briefly described here for completeness. While not as widely used through the years as the exponential equations, the rational polynomial equation is not new. In fact, an equation equivalent to Eqn. 53 but without the linear secondary term was used by Freudenthal more than forty years ago [98]. The equation was introduced in its present form by Oding more than twenty years ago [99]. The current popularity of the equation began with the analysis reported in Ref. [38] for 2 1/4 Cr-1 Mo steel.

Clearly, the parameter C in the national polynomial equation is analogous to e_t in the single exponential equation, while $\dot{e}_m$ is the minimum creep rate in both cases. Differentiating Eqn. 53 one expresses the creep rate, $\dot{e}_c$, as

$$\dot{e}_c = \frac{Cpt}{(1+pt)^2} + \dot{e}_m\,, \tag{62}$$

while the initial creep rate is given by

$$\dot{e}_o = Cp + \dot{e}_m \ . \tag{63}$$

The parameter p is related to the rate of approach of the creep rate from $\dot{e}_o$ to $\dot{e}_m$. Figure 39 summarizes the properties of the rational polynomial equation.

Equations 50, page 121, and 53, page 125, being of different form, cannot be made identically equal, but they can be made to approximate one another within the accuracy of engineering creep data. To do so, one first lets $\dot{e}_m$ be the same in each equation, and then lets $c = e_t$. Then, the two equations can be set equal at any point along the curve to determine the relationship between p and r. A logical choice of this point is the point at which half the transient strain has been exhausted. Calling the time at this point t*, it can easily be verified from Eqn. 53 that $t^* = \frac{1}{p}$. Equating Eqns. 50 and 53 at $t = t^*$ yields

$$p = 1.44r \ . \tag{64}$$

Thus, the single exponential and rational polynomial equations can be used almost interchangeably. Interestingly, Eqns. 63 and 64 imply that the rational polynomial equation yields a slightly higher initial creep rate than the exponential equation, other things remaining the same.

The rational polynomial creep equation is probably best viewed as a simple, flexible means of empirically representing experimental creep data. However, it too has been derived from various formulations of creep behavior. Oding [81,99] derived the equation form based on a self-diffusion theory of creep. The equation was also derived [81] on a phenomenological basis, as follows.

ORNL-DWG 76-3985R

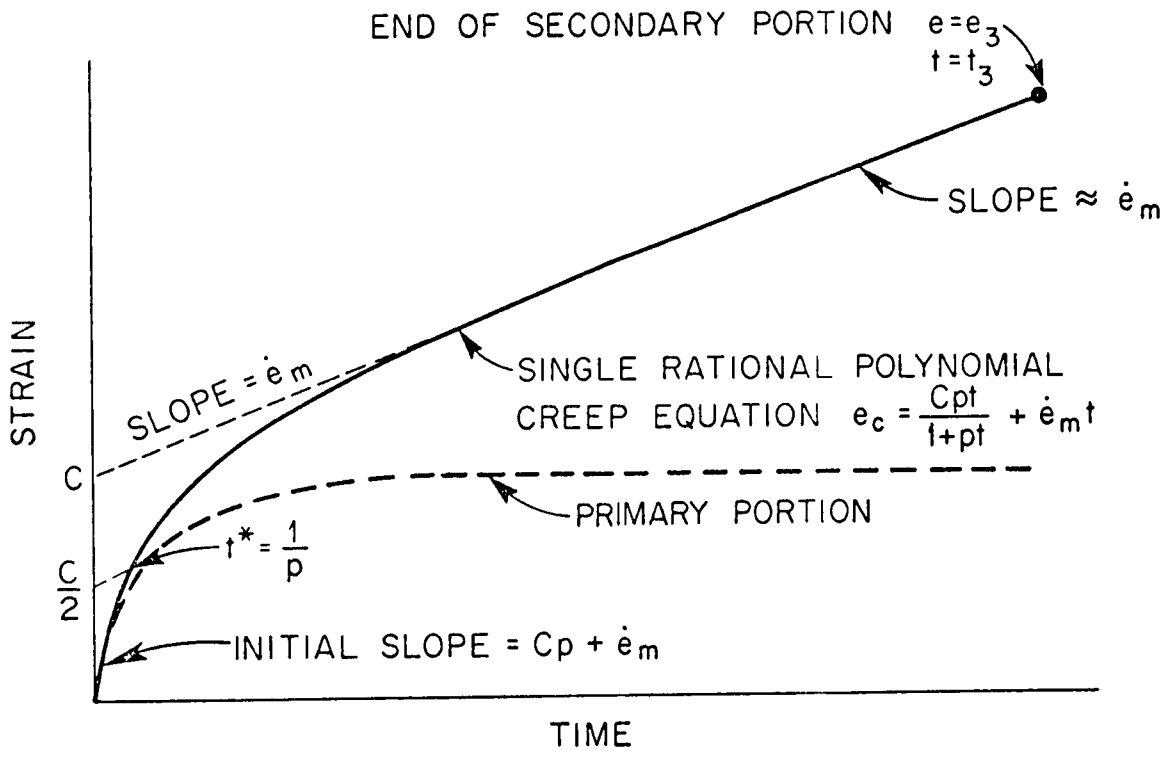

Figure 39. Schematic Illustration of the Properties of the Rational Polynomial Creep Equation.

The creep rate was assumed to be proportional to the number of mobile dislocations, W(t), so that

$$\frac{de_c}{dt} = AW(t) \quad . \tag{65}$$

Then, a simple but general form of the time dependence of W was chosen, yielding

$$\frac{de_c}{dt} = AW_o(1 + \alpha t)^m \tag{66}$$

where W_o is the initial number of mobile dislocations, and α and m are constants which may depend upon material, stress, temperature, and possibly other factors. If m = -2, integration of Eqn. 69 yields Eqn. 53, page 125, where now $C = AW_o/\alpha$ and $p = \alpha$. The similarity of the rational polynomial and exponential equations also means that interpretations involving the parameters in the exponential equation, e.g. the work of Morchan et al. [97,98], can also be applied to the rational polynomial equation.

Equation 53 can be solved explicitly for time, yielding

$$t = \frac{e_c p - Cp - \dot{e}_m + \sqrt{(Cp + \dot{e}_m - e_c p)^2 + 4e_c p\dot{e}_m}}{2p\dot{e}_m} \tag{67}$$

Thus, the equation can be easily applied to variable stress situations involving strain hardening analyses.

The analytical flexibility and simplicity of the rational polynomial equation give it a definite advantage over the exponential equation. Moreover, the equation is much more economical to apply in terms of computer time used in performing design calculations. Our analyses showed that the equation does very good job of fitting experimental creep data. Therefore, the rational polynomial form was chosen as the basic strain-time equation to use in developing a creep equation for type 304 stainless steel.

Fits to Experimental Curves

The rational polynomial equation can be fitted to experimental curves by various least-squares and graphical techniques, as described elsewhere [97]. In general, the least-squares techniques will yield the most objective fit. However, in the current analysis, many low-stress and low-temperature tests were used in which the amount of strain incurred was so small compared to the accuracy of the strain-measuring equipment employed that a great deal of scatter occurred in the data. In order to avoid drawing wrong conclusions from least-squares fits due to this scatter, the semigraphical approach described by Bunatyan [81,100] was employed.

Bunatyan [100] showed that if one chooses three points (t_1,e_1), (t_2,e_2), (t_3,e_3) from an experimental creep curve, the values of p and $\dot{e}_m$ can be found by

$$p = \frac{\frac{t_1 - t_2}{t_3 - t_2}\left(\frac{e_3}{t_3} - \frac{e_2}{t_2}\right) + \left(\frac{e_2}{t_2} - \frac{e_1}{t_1}\right)}{\frac{t_1 - t_2}{t_3 - t_2}(e_2 - e_3) + e_1 - e_2} \tag{68}$$

and

$$\dot{e}_m = \frac{1}{(t_1 - t_2)} \left(\frac{e_1}{pt_1} - \frac{e_2}{pt_2} + e_1 - e_2 \right) \quad . \tag{69}$$

The value of C can then be determined by setting the prediction of Eqn. 53, page 125, equal to the experimental strain at any point on the curve. In the current analyses, we determined C at each of the above three points and then averaged those values, although they did not vary greatly. Figures 40-44 illustrate fits to experimental curves obtained using this method.

Stress and Temperature Dependence of Equation Parameters

In other analyses [29,38,78] the stress and temperature dependence of the creep equation parameters were evaluated as follows. First, available experimental creep curves are individually fit using the chosen equation form to yield a set of parameter values for each test. Then, the individual equation parameters are themselves directly expressed as functions of stress and temperature. Although this method has met with some success, it suffers from several shortcomings, enumerated below, and hereafter referred to as Objections 1-4.

1. The number of available creep curves is often quite small in comparison to rupture and other data. The number of creep data can be too small to adequately identify the dependence of the equation parameters upon stress and temperature.

2. Experimental variations and complex interrelationships among equation parameters can cause considerable scatter in the values of these parameters. As a result, the correlations between these parameters

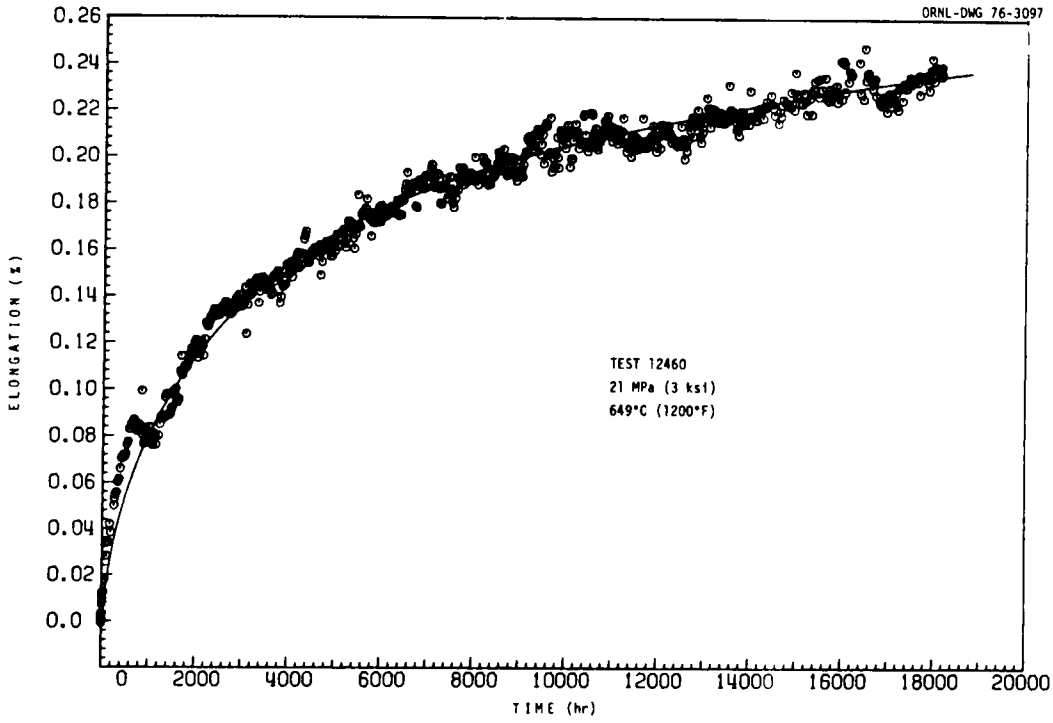

Figure 40. Fit of the Rational Polynomial Creep Equation to an Experimental Curve at 649°C (1200°F).

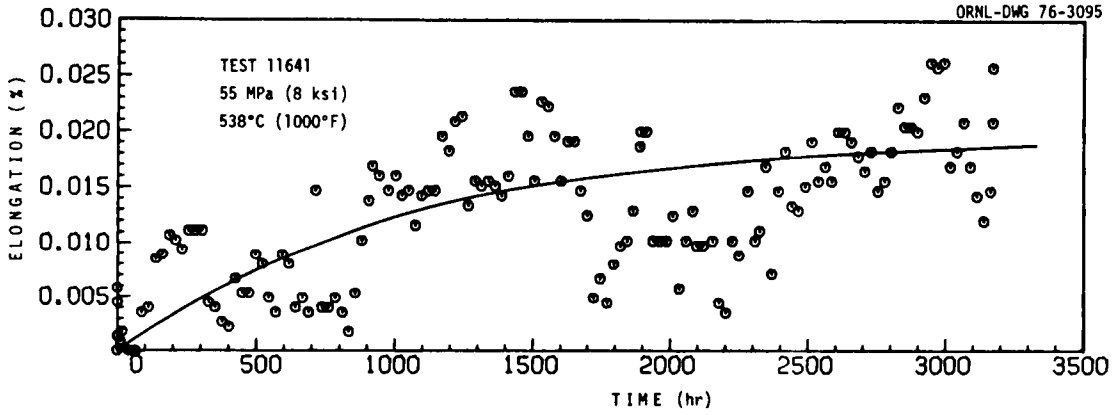

Figure 41. Fit of the Rational Polynomial Creep Equation to an Experimental Curve at 538°C (1000°F).

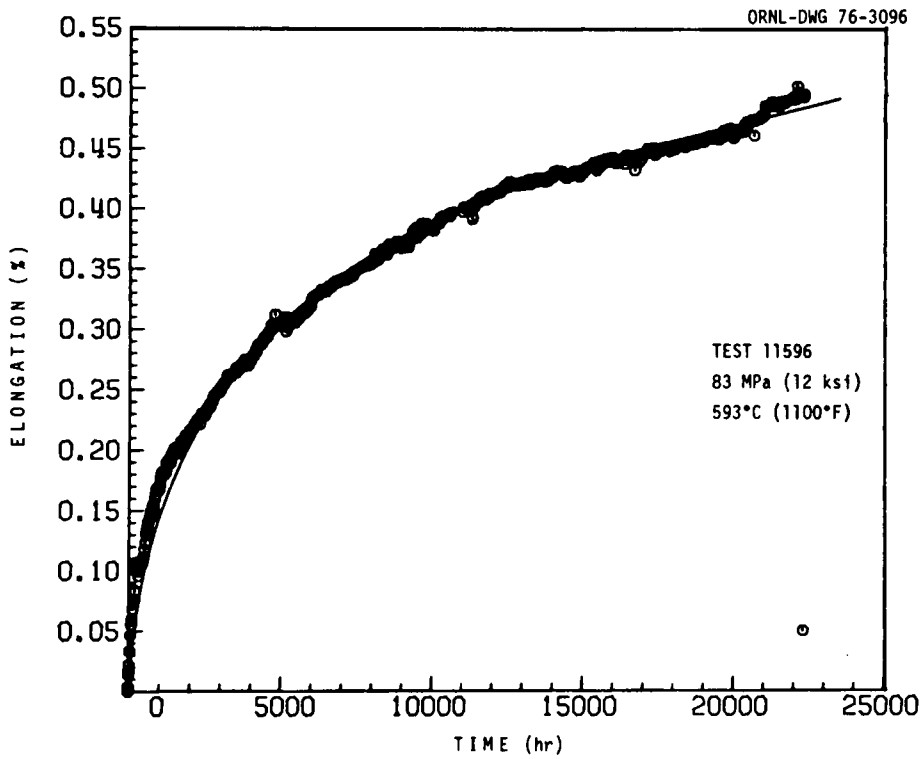

Figure 42. Fit of the Rational Polynomial Creep Equation to an Experimental Curve at 593°C (1100°F).

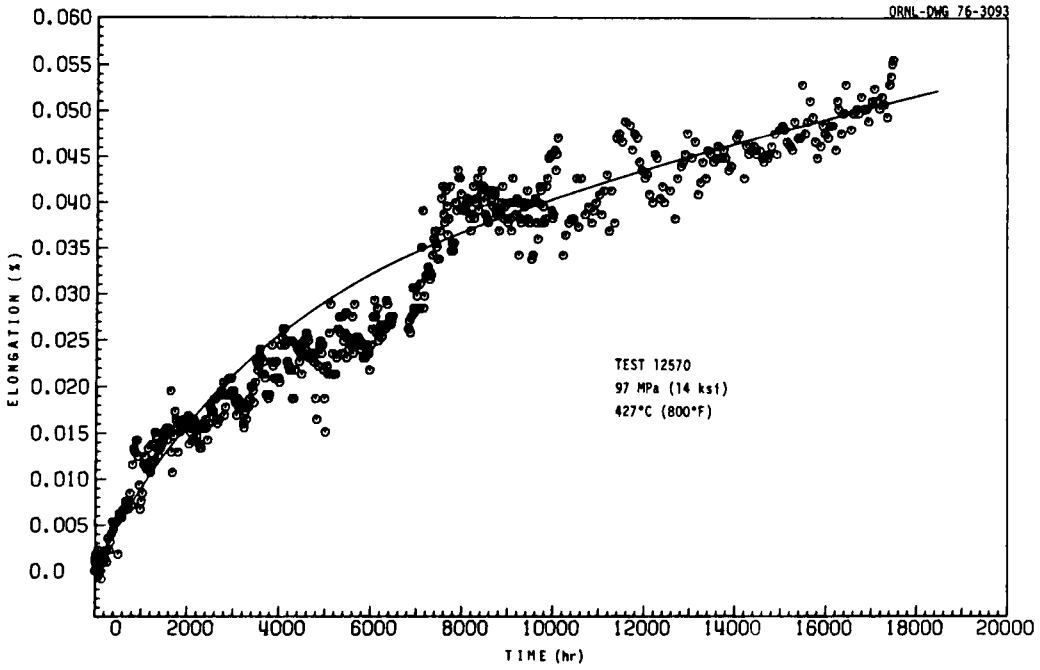

Figure 43. Fit of the Rational Polynomial Creep Equation to an Experimental Curve at 427°C (800°F).

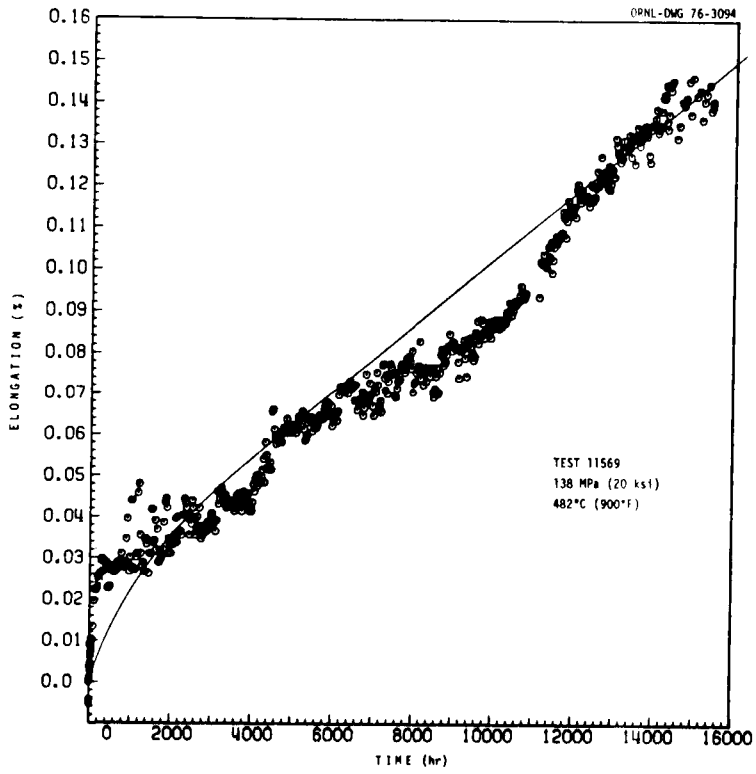

Figure 44. Fit of the Rational Polynomial Creep Equation to an Experimental Curve at 482°C (900°F).

and the test conditions (σ, T) can be very poor. This problem becomes particularly large when extrapolation in one or more of the independent variables is necessary.

3. Separate analysis of the equation parameters as functions of stress and temperature can cause problems when the parameters are recombined into a unified equation, since they are actually strongly interrelated.

4. It is extremely difficult to account for heat-to-heat variations using this method.

In the present investigation, an alternate method has been devised to help overcome the above objections. One of the advantages of the current equation form is the explicit minimum creep rate term. While analytical fits of Eqn. 53, page 125, to experimental curves will in general yield slightly different values of $\dot{e}_m$ than will graphical measurements, this difference is insignificant in comparison to the overall uncertainty in creep strain-time predictions. The approach used here has been to use the analyses of minimum creep rate data from Chapter III of this report to express $\dot{e}_m$ as a function of stress and temperature. Since the creep curves were primarily from the ORNL data (Table VII, page 13), the ORNL equation for $\dot{e}_m$ was used. Reiterating the results of Chapter III, this equation is

$$\log \dot{e}_m = -2.765 + \frac{3346}{T}\log \sigma - \frac{51.84U}{T} + 0.01616U \log \sigma \qquad (70)$$

where $\dot{e}_m$ is the minimum creep rate (%/hr), T the temperature (K), σ the stress (MPa), and U the ultimate tensile strength (MPa) at temperature for a given heat of material at a tensile strain rate of 6.7×10^{-4} sec^{-1}.

From Figure 39, page 130, it can easily be verified that the value of C is given by

$$C = e_3 - \dot{e}_m t_3 \ , \tag{71}$$

where e_3 and t_3 are the strain and time to the onset of tertiary creep (first deviation from linear secondary creep). Again reiterating results previously mentioned in this report, t_3 and e_3 can be found from

$$t_3 = 0.685\ t_r^{0.968} \tag{72}$$

and

$$\dot{e}_3 = e_3/t_3 = 1.11\ \dot{e}_m^{0.974} \ , \tag{73}$$

where

$$\log t_r = 5.716 - \frac{3915}{T} \log \sigma + \frac{32.60U}{T} - 0.007303U \log \sigma \tag{74}$$

with t_r = rupture life and σ, T, and U as in Eqn. 70. Equations 71-74 in turn yield

$$e_3 = \dot{e}_3 t_3 = 0.760\ \dot{e}_m^{0.974}\ t_r^{0.968} \tag{75}$$

and

$$C = 0.685\ t_r^{0.968}\ (1.11\dot{e}_m^{0.974} - \dot{e}_m) \ . \tag{76}$$

Many previous investigators [84-87, 89-96], using the single exponential creep equation, found the initial creep rate, $\dot{e}_o$, to be a constant multiple of $\dot{e}_m$ for a variety of materials. The time

constant, r, was also found to be a constant multiple of $\dot{e}_m$ except at low stresses in iron [95] and type 316 stainless steel [84]. Several such relationships were examined in the current analysis, the one chosen as optimum being

$$\dot{e}_o = 3.43\ \dot{e}_m^{0.80}, \tag{77}$$

as illustrated in Figure 45. Since $\dot{e}_o$ is given by $Cp + \dot{e}_m$, the parameter $p(hr^{-1})$ is given by

$$p = \frac{\dot{e}_o - \dot{e}_m}{C}. \tag{78}$$

With the aid of Eqns. 70, page 137, 76-78, it is possible to evaluate the entire creep equation from a knowledge of $\dot{e}_m$ and t_r for a given material.

Predictions of Creep Behavior

The method described above allows an evaluation of the dependence of the parameters C, p, and $\dot{e}_m$ upon stress, temperature, and relative strength of a given heat of material (as reflected by the ultimate tensile strength). Figure 46 illustrates the predicted behavior of these parameters for the 51-mm thick plate of heat 9T2796 [25], a weak heat. The predictions were made using values of ultimate tensile for these heats of material from Refs. [25] and [27] respectively. The experimental points represent values obtained by fitting individual creep curves using the method described above.

Several points are apparent from Figures 46. First, the scatter in the data is large (thus the second objection above to previous evaluation procedures). Second, although the current equations were

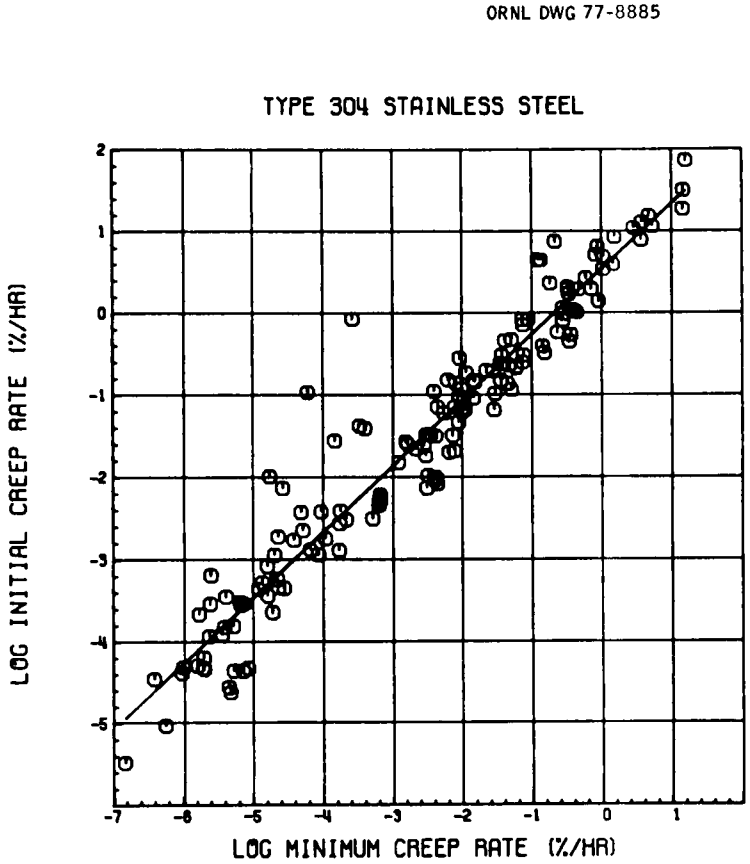

Figure 45. Relationship Between Minimum Creep Rate and Initial Creep Rate for Type 304 Stainless Steel.

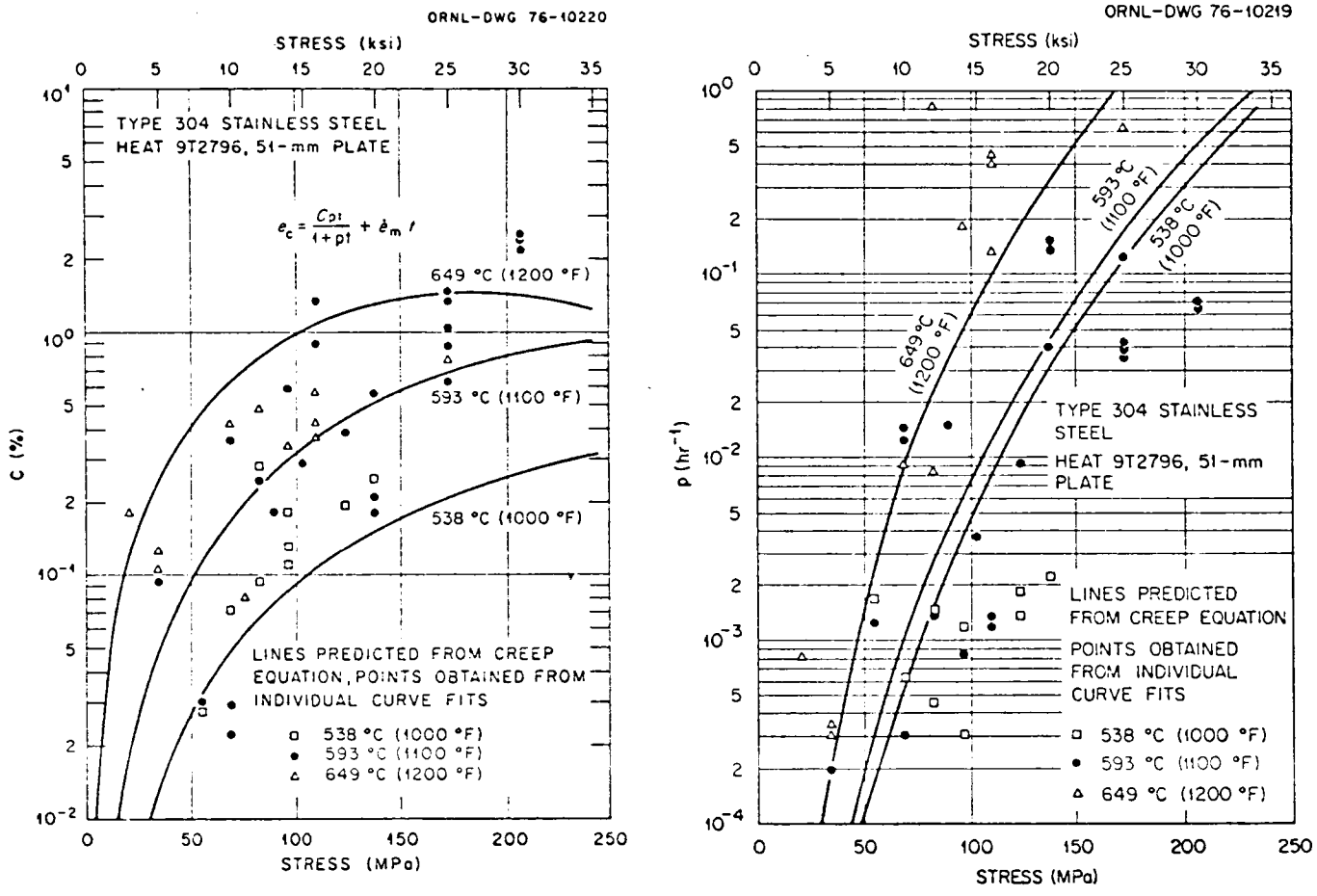

(a) (b)

Figure 46. Variation of the Rational Polynomial Creep Equation Parameters With Stress at Three Temperatures for Heat 9T2796, 51-mm Plate of Type 304 Stainless Steel. (a) Experimental data for the parameter C, with predictions from the creep equation; (b) experimental data and predictions for the parameter p.

developed from a large multiheat data base, the predictions still appear to capture the trends in the behavior for a given heat and thus to reflect to some degree the effect of heat-to-heat variations. The data shown in Figure 46 are primarily from long-term, low-stress creep tests which had not entered the tertiary creep region. Thus, in the current method, the data from most of these tests were not actually used in determining C or $\dot{e}_m$. The comparisons in Figure 46 are primarily extrapolations. Considering this fact, the comparison is quite good. Predictions for $\dot{e}_m$ and t_r are described in Chapter III of this report, while predictions for e_3 and t_3 are described in Chapter IV.

It is obvious that the current models cannot yield precise fits to every individual heat of material. Moreover, the scatter and lack of reproducibility in creep data are such that no one curve even for a single heat can be predicted precisely by any technique. The method employed here is an attempt to reduce the uncertainty in such predictions as much as possible for engineering applications. Still, the most meaningful criterion for judging a creep equation is its ability to predict reasonable values for creep strain for a given heat of material under a given loading condition.

Figures 47 and 48 illustrate predictions of individual creep curves for heats 9T2796 (51-mm plate) and 8043813 from the current equation. Also shown are predictions from the equation developed by Blackburn [29]. Clearly, the current equation more accurately depicts the strain-time behavior of these heats, mainly because it does

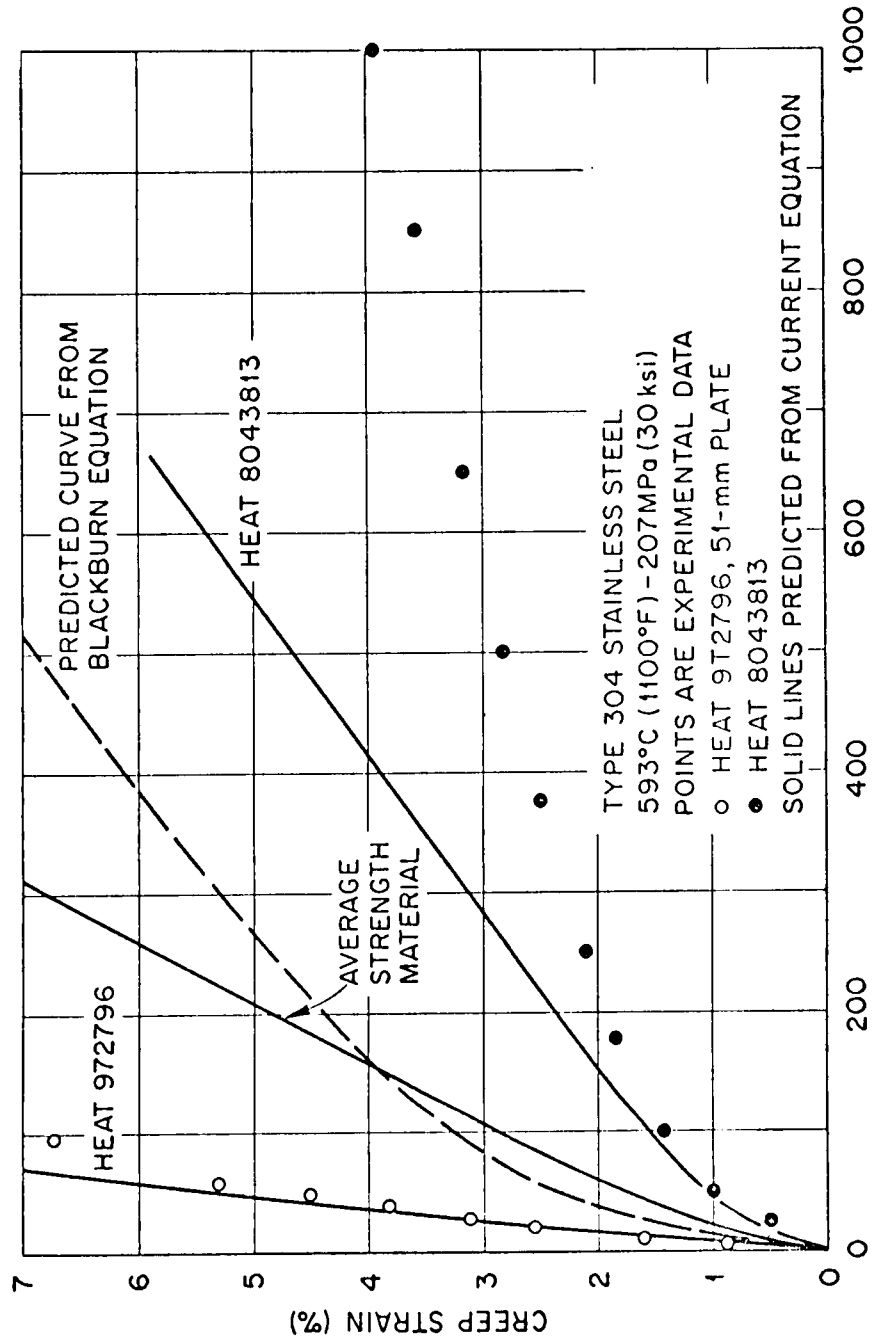

Figure 47. Comparison of Predictions With Experimental Creep Curves for Type 304 Stainless Steel, Including Predictions of Average Behavior from the Current Equation and from the Blackburn Equation. The testing conditions were temperature = 593°C, stress = 207 MPa.

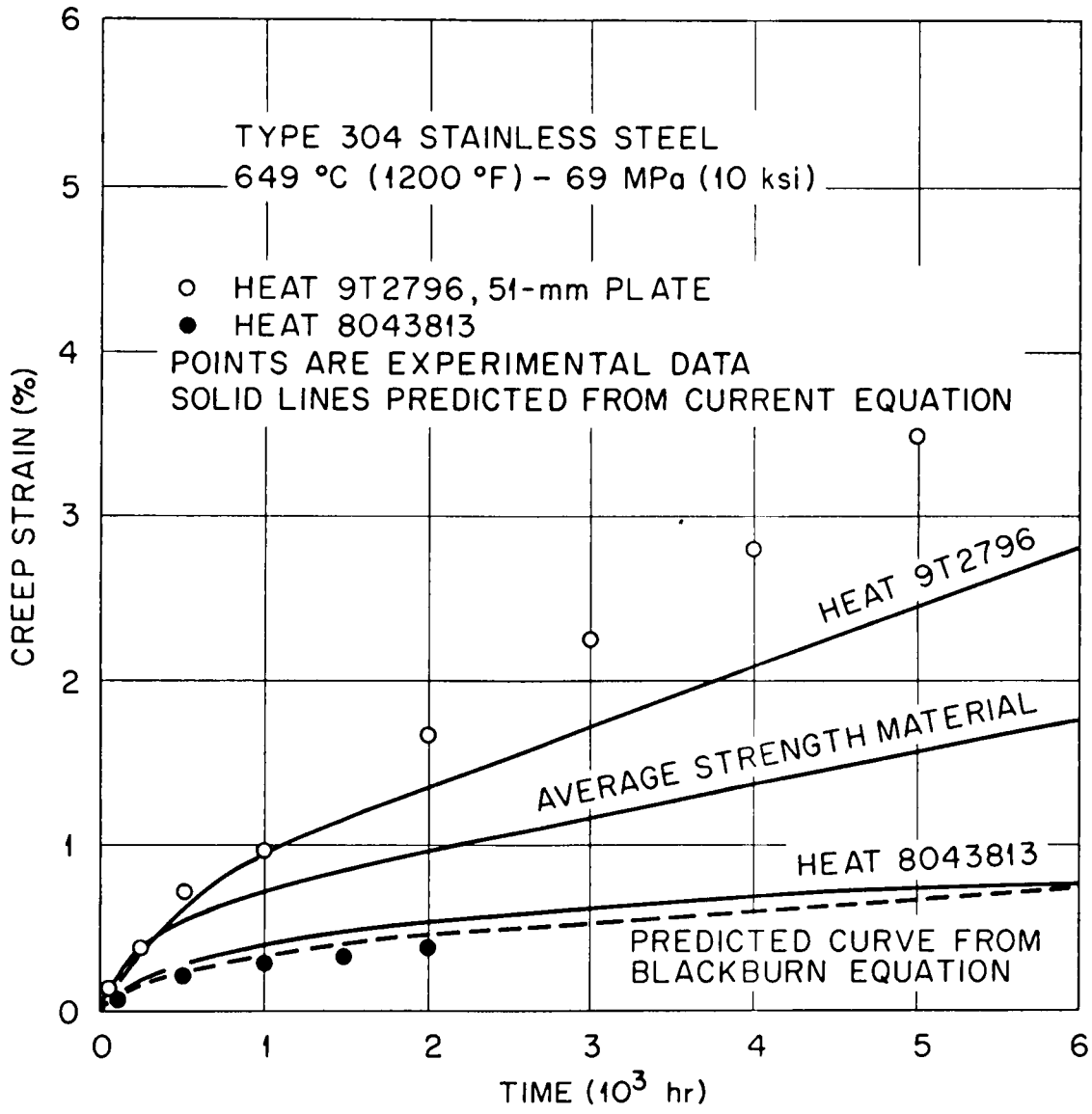

Figure 48. Comparison of Predictions With Experimental Creep Curves for Type 304 Stainless Steel, Including Predictions of Average Behavior from the Current Equation and from the Blackburn Equation With the Testing Conditions: Temperature = 649°C, Stress = 69 MPa.

reflect heat-to-heat variation whereas the Blackburn equation does not. Figure 49 illustrates the ability of the current equation to predict the range in creep behavior for this material.

Finally, the data used in establishing the current predictions were almost exclusively from tests conducted at temperatures of 538°C (1000°F) and above. However, creep in this material has been recognized as important in design [49] at temperatures down to 427°C (800°). The predictions must therefore be extrapolated downward in temperature. Creep data at such low temperatures are primarily from heat 9T2796. Comparisons between the predictions and data at 482°C (900°F) for this heat yielded generally good results at high stresses, with the equation tending to underpredict the amount of creep strain as the stresses were lowered. At 427°C (800°F) only relatively low stress data were available. The creep strain occurring under these conditions is significantly underpredicted by the current equation. In fact, at these low stresses and temperatures the dependence of creep strain on temperature appears to be markedly reduced. As shown in Figure 50, this material can creep as much or more at 427°C than at 482°C for the same stress. A close look at Figure 17, page 70, indicates a possible trend toward a downward break in the log σ - log $\dot{e}_m$ isothermals (less stress dependence in $\dot{e}_m$) at low stress even at 593°C and 649°C. These trends toward decreased stress and temperature dependence at low stresses and temperatures may be indicative of changes in creep deformation mechanism. This possibility will be addressed in the next chapter.

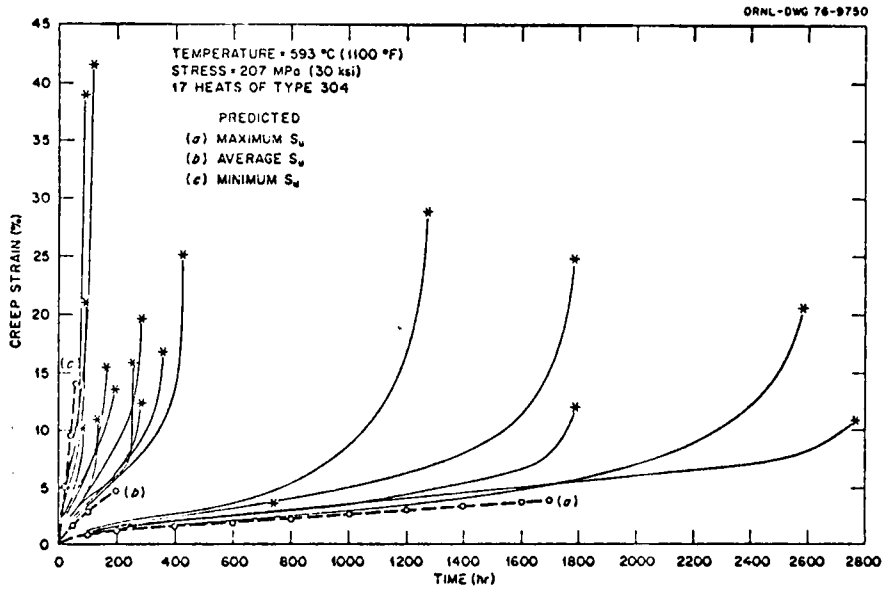

(a)

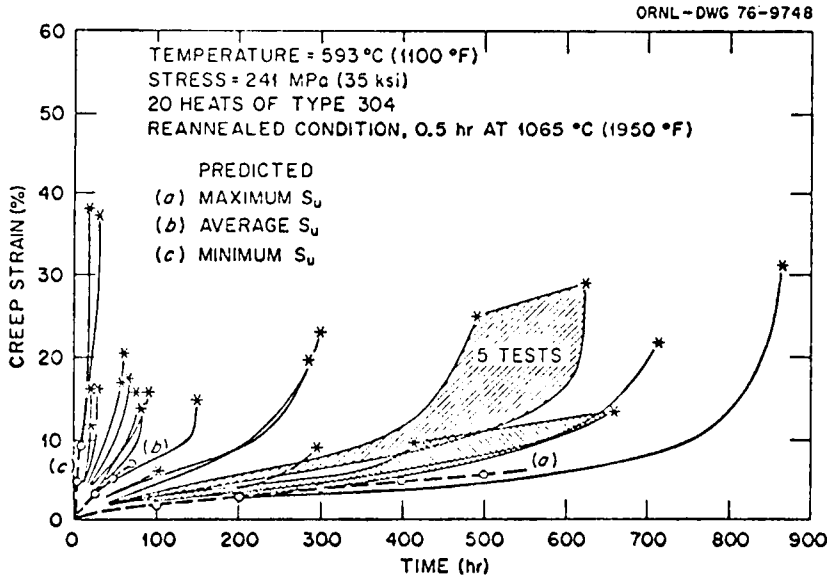

(b)

Figure 49. Heat-to-Heat Variations in Creep Curves of Several Reannealed Heats of Type 304 Stainless Steel. (a) Creep tests at 241 MPa (35 ksi) and 593°C (1100°F). (b) Creep tests at 207 MPa (30 ksi) and 593°C (1100°F).

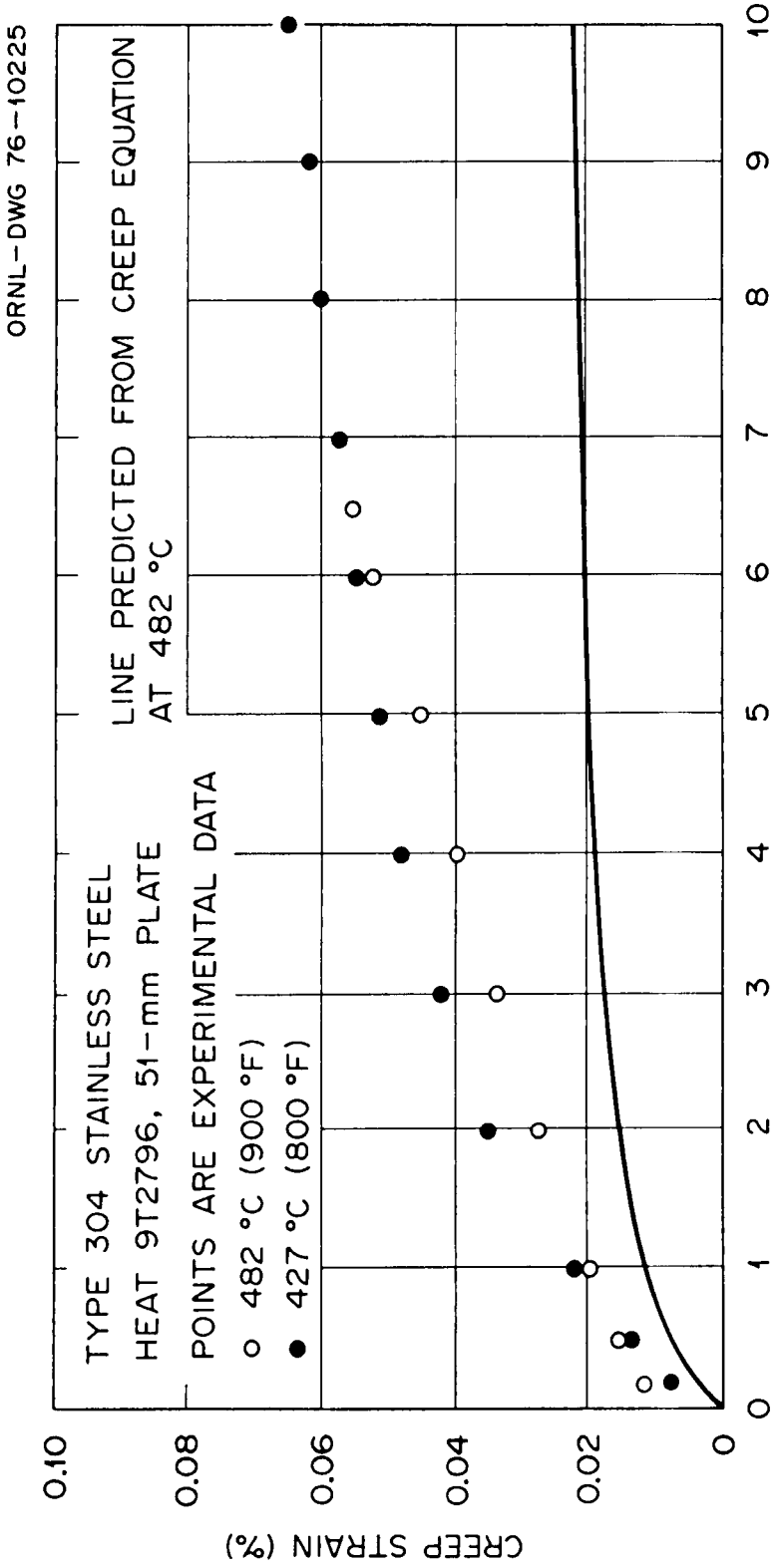

Figure 50. Illustrative Comparison Among Creep Data at 482°C (900°F) and 427°C (800°F) and Predicted Behavior at 482°C.

Variable Load and Relaxation Behavior

Actual design applications will seldom involve simple constant-load situations. Various system transients and other effects will result in repeated changes of stress or temperature or both. Also, many loading situations involve constant strain stress relaxation rather than constant load creep straining. To be of full use, a creep equation must provide some means of accounting for such situations. Little study has been done of variable temperature behavior, but some data from variable load tests are available.

It is beyond the scope of this investigation to undertake a study of schemes for treating variable load creep behavior in this material. Currently used constitutive relationships [8,9] suggest that the hypothesis of strain hardening [12] be used to describe the variable stress creep behavior of type 304 stainless. This hypothesis assumes that the instantaneous strain rate at any stress and temperature is given uniquely as a function of the stress, temperature, and accumulated strain. Current rules [8,9] specify that this accumulated strain includes creep strain only. Since the rational polynomial equation can be solved explicitly for time as a function of strain [Eqn. 67, page 131], it is a simple matter to apply the strain hardening approach. Knowing the accumulated creep strain, one can solve the equation for time at the given stress and temperature, thus locating a point on the predicted creep curve for that stress and temperature. Creep then proceeds along that curve until the stress or temperature changes again. Figure 51 illustrates a prediction made from the current equation for a variable load creep test for heat 8043813 [27], while Figure 52

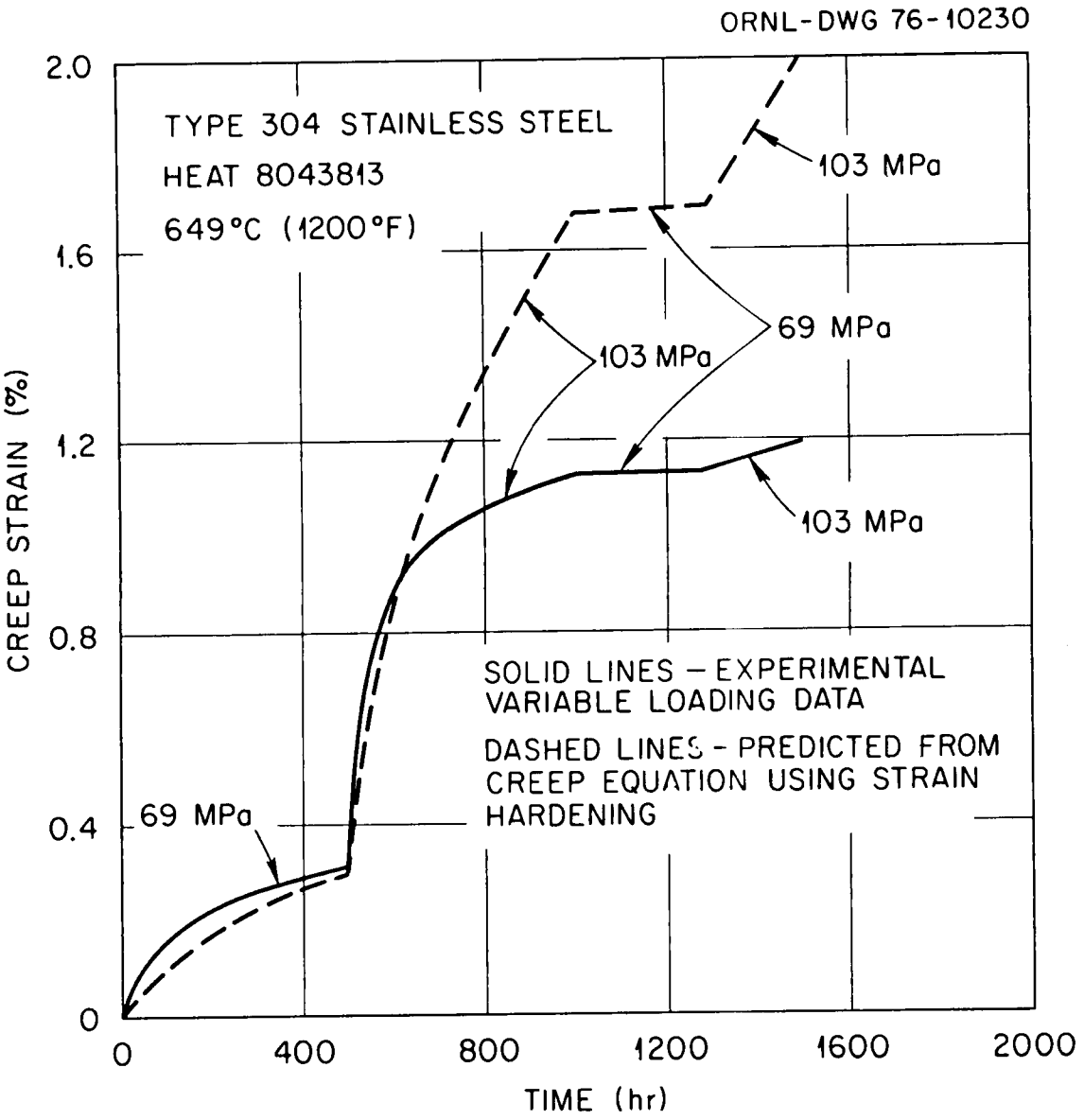

Figure 51. Comparison Between an Experimental Variable Load Creep Test for Heat 8043813 With Predicted Behavior Using the Current Creep Equation and the Hypothesis of Strain Hardening.

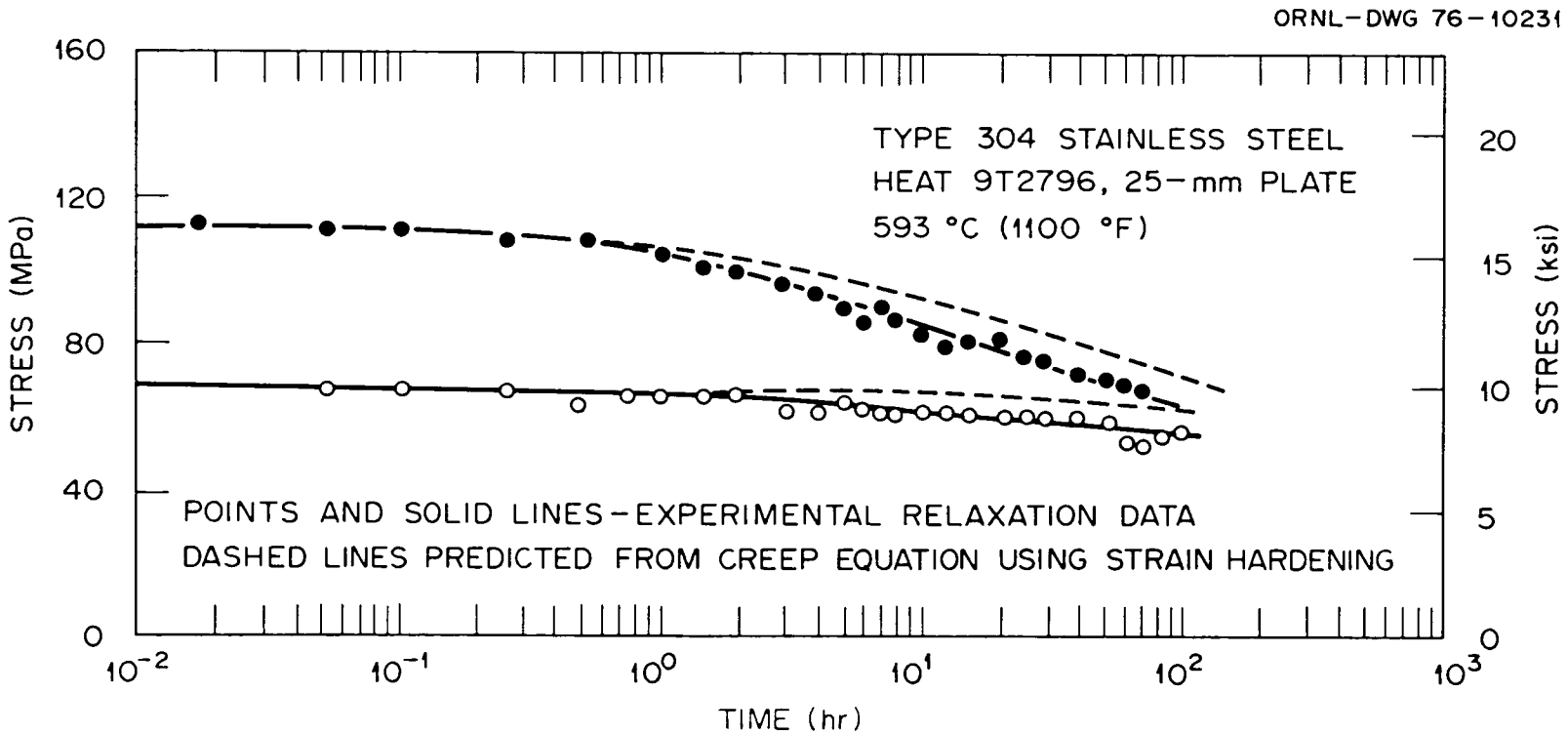

Figure 52. Comparison of Two Experimental Relaxation Curves for Heat 9T2796 at 593°C With Predicted Behavior Using the Current Creep Equation and the Hypothesis of Strain Hardening.

illustrates results obtained in predicting relaxation behavior for the 25-mm plate of heat 9T2796 [101]. The predictions show good agreement with the experimental data.

Isochronous Stress-Strain Curves

One of the most useful forms of displaying creep strain-time behavior is the isochronous stress-strain curve. Various methods exist for the construction of such curves, such as that summarized in Ref. [71].

Equation 50, page 121, with the constants $\dot{e}_m$, C, and p defined by Eqns. 70, page 137, 76, page 138, and 78, page 139, respectively, can be used to calculate the creep strain accumulated in a given time at a given stress and temperature. Thus, from an estimate of the instantaneous strain incurred upon loading, one can develop isochronous stress-strain curves from the equation. This loading strain can be determined from monotonic tensile stress-strain curves.

The monotonic tensile stress-strain behavior of this material can be described by:

$$(\sigma - \sigma_0) = \frac{C' p' \varepsilon_p}{1 + p' \varepsilon_p} + \dot{h}_m \varepsilon_p , \qquad (79)$$

where σ is the stress (MPa), ε_p the plastic strain (cm/cm), and σ_0 corresponds to the proportional limit. The value of σ_0 can be well estimated as $0.5\,\sigma_y$, where σ_y is the 0.002 strain offset yield strength. The constant $\dot{h}_m$ is approximately equal to 2586 MPa, while p is given by $500\,C'$. The value of C' is determined by the criterion that $\sigma = \sigma_y$ for $\varepsilon_p = 0.002$. Interestingly, Eqn. 79 is of the same form as Eqn. 53, page 125,

reflecting the great flexibility of this equation. Since a knowledge of stress and Young's modulus yields the magnitude of the elastic strain, Eqn. 79 can be used to calculate the total strain corresponding to a given stress. A full description of our analysis of stress-strain behavior is given elsewhere [102].

Equations 53, page 125, and 79 were combined to calculate isochronous stress-strain curves as shown in Figure 53. Average, maximum, and minimum creep strength curves were calculated by using the corresponding values of tensile strength from Eqn. 22, page 71, for the ORNL data. For all cases shown in Figure 53, the loading strains were calculated using average yield strengths from Ref. [16] for as-received material, to allow comparison with the results of Ref. [29]. Thus, all variations shown are due to the effects of creep strength only.

Figure 53 shows that there are considerable differences between the current results and those of Ref. [29]. Since the current method allows one to calculate a series of isochronous curves for different heats of material, it is generally expected to be more accurate for a given heat of material. At 538°C (1000°F) and below, the results of Ref. [29] sometimes fall even below the current minimum predictions. However, based on available low temperature data (427-538°C), our results are the more realistic of the two.

Finally, for comparison purposes, two alternate methods were used to construct isochronous curves for the heat 9T2796 51-mm plate. First, the times to accumulation of given amounts of creep strain were analyzed by parametric techniques similar to those commonly used for rupture data. This method is similar to the one described in

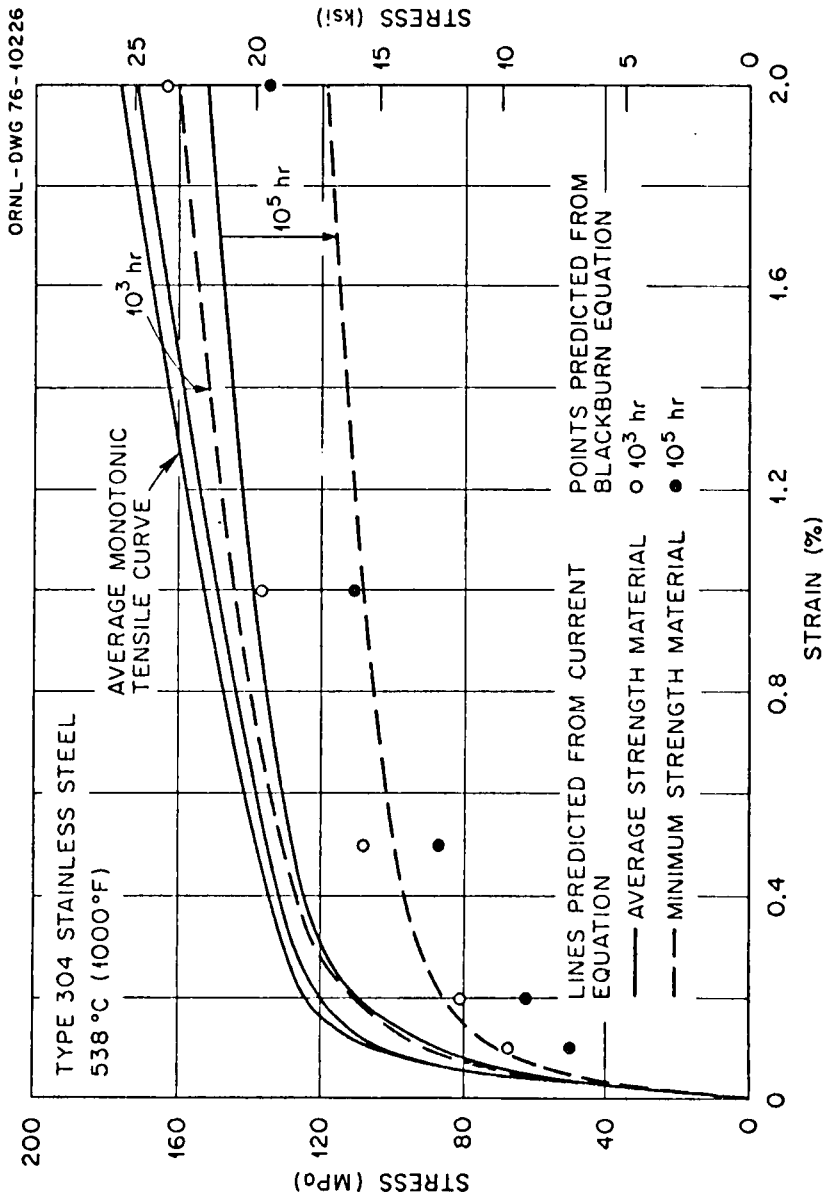

(a)

Figure 53. Predicted Isochronous Stress-Strain Curves at 10^3- and 10^5-hr from the Creep Equation and the Rational Polynomial Equation for Average Stress-Strain Behavior. Shown are predictions for estimated average, minimum, and maximum ultimate tensile strength levels. Also shown are values from isochronous curves constructed from the Blackburn equation. (a) 538°C (1000°F); (b) 593°C (1100°F); (c) 649°C (1200°F).

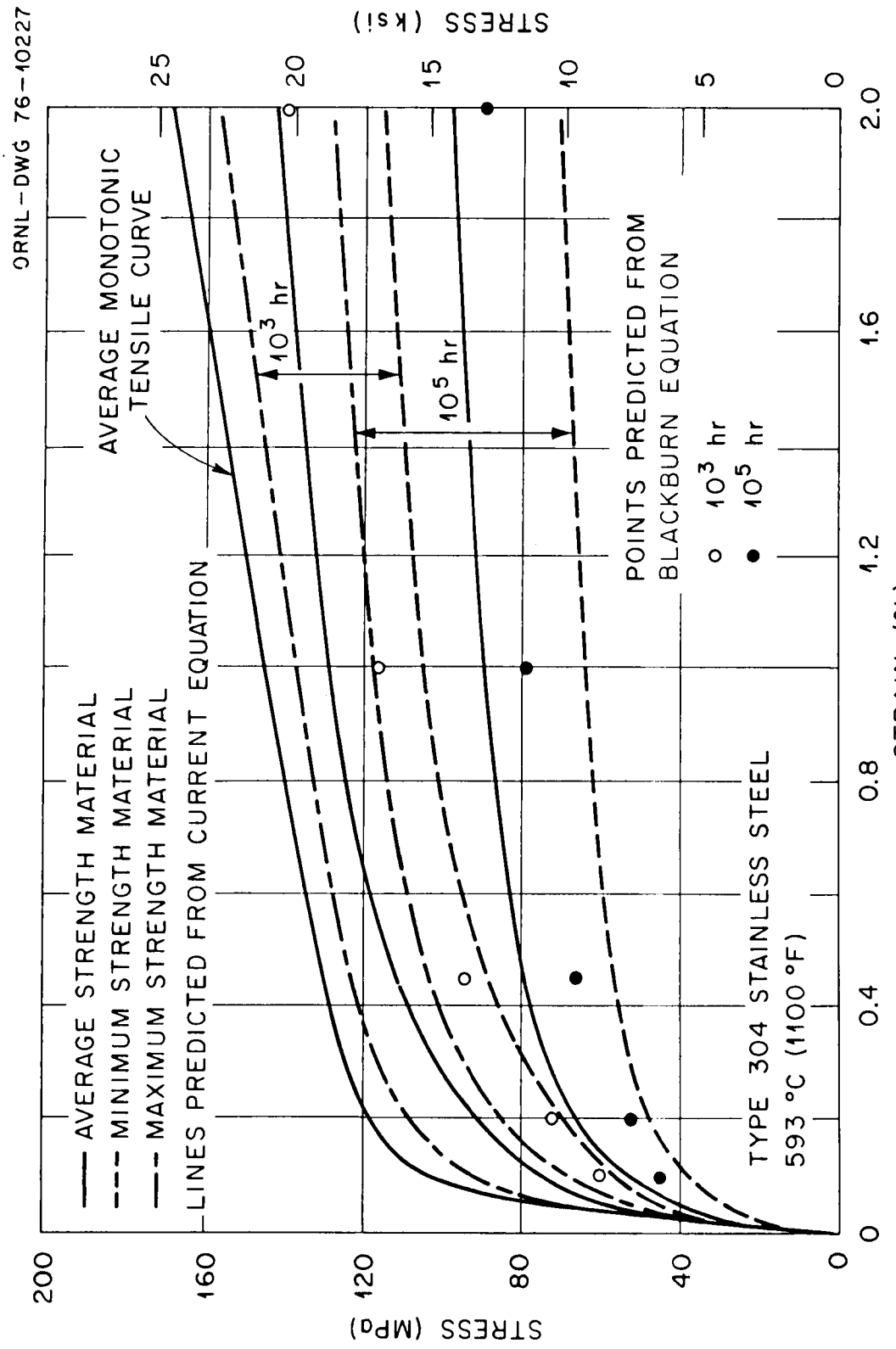

(b)

Figure 53 (continued)

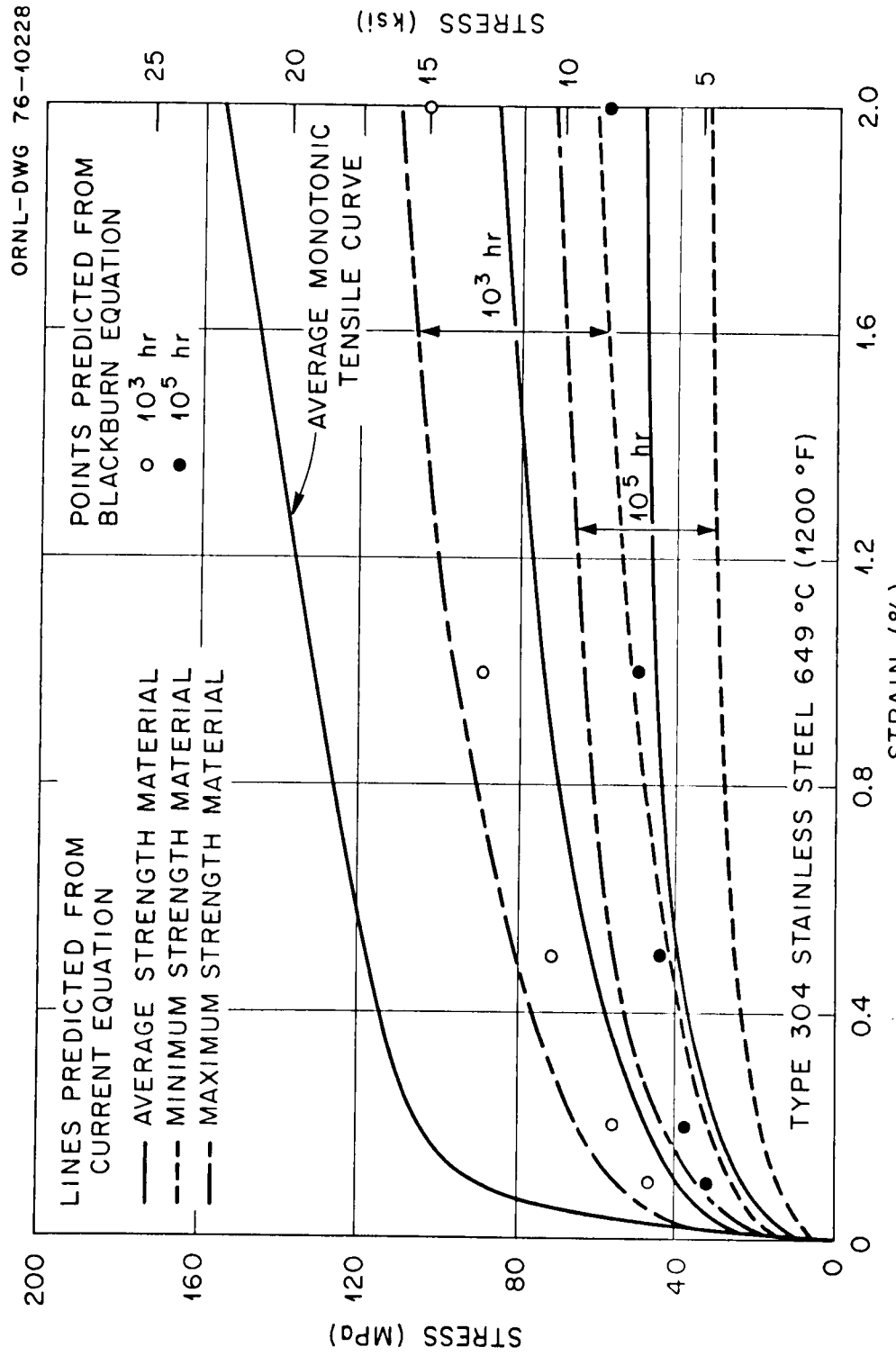

(c)

Figure 53 (continued)

Ref. [71]. No extensive modeling was attempted, although we did fit several standard time-temperature parameters to data for 0.1, 0.25, 0.5, 1, 1.5, and 2% creep strain. The best results were obtained by a simple Larson-Miller [45] parameter of the form

$$\log t_x = \alpha_0 + \frac{\alpha_1 \log \sigma}{T} + \frac{\alpha_2}{T} , \tag{80}$$

where α_0, α_1, and α_2 were estimated by least squares methods at each of the above levels of creep strain. Equation 80 allows one to calculate the stress that will cause a given amount of creep strain at a given time and temperature. Using this stress, one can then use Eqn. 79, page 151, and Young's modulus to calculate isochronous stress-strain curves.

Finally, isochronous curves at 593°C (1100°F) were constructed using a form of the Rabotnov parameter [76]. At a given level of strain (loading plus creep), this parameter is given by

$$\phi(\varepsilon) = \sigma(1 + \alpha t^{1/3}) , \tag{81}$$

where σ and t are again the stress and time, ϕ is the parameter and α is a constant. We used stress values obtained from the above-mentioned monotonic tensile stress-strain curves for ϕ, and assumed a time exponent of 1/3. Attempts at determining ϕ and the exponent by least squares methods, such as was done in Ref. [77], yielded poor results due to insufficient data. Once the values for ϕ and the time exponent were determined, the value of α for a given stress was calculated from

$$\alpha = \left(\frac{\phi}{\sigma} - 1\right)^{1/3} . \tag{82}$$

Applying this equation at various points along the experimental creep curves showed that α varied both with stress and strain, rather than being constant. We used an approximate average value of $\alpha = 0.01$ for use in our calculations.

Figure 54 compares the results obtained by each of these three methods at 593°C (1100°F) for this heat of material. The monotonic tensile curve used to construct the isochronous curves in Figure 54 was based on Eqn. 79 using the yield strength for reannealed material from this heat. Reannealing generally lowers the yield strength of type 304 stainless steel by about 35 MPa from that in the as-received condition, although the tensile strength and creep strength are not greatly affected [15,16]. Reannealed tensile properties were used in Figure 54 since the Rabotnov parameter always involves total strain, not separate analysis of creep and loading strain. For this reason, the tensile and creep properties should be obtained from the same material condition. The three methods illustrated in Figure 54 yield similar results, although the creep equation is preferred since it has a wider range of uses than the other methods.

Analytical Limitations

The design lifetimes of operating systems are typically of the order of 30 years, making it necessary to make many design calculations based on extrapolations beyond the time-stress-temperature regime where experimental data are available. Such extrapolations must be made with caution, however. Specific analytical limitations on the applicability of the creep equation presented here are:

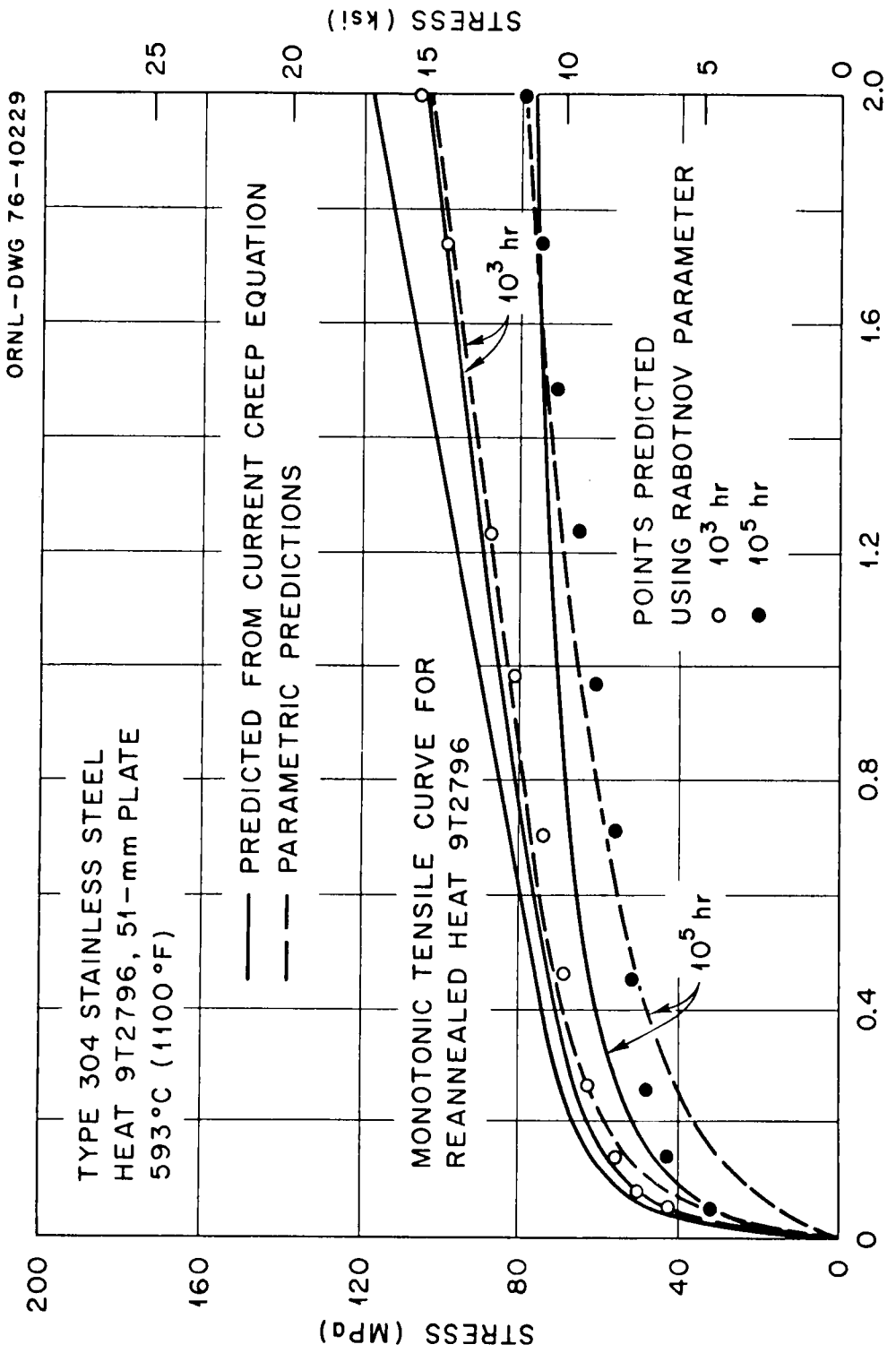

Figure 54. Isochronous Stress-Strain Curves at 593°C (1100°F) for Heat 9T2796, 51-mm Plate Predicted by Three Methods.

1. time < the time to the onset of tertiary creep;
2. temperature in the range 427°C(800°F)-704°C(1300°F);
3. ultimate tensile strength within 42.8 MPa of the average strength at temperature defined by Eqn. 22 on page 71.

Figure 46a, page 141, shows that the parameter C exhibits a maximum with stress; the stress at the maximum (σ_c) is smaller for weaker heats or at higher temperatures. This behavior is consistent with previous results for both type 304 [27] and 316 [78,84] stainless steels. To avoid any possible analytical difficulties, the value of σ_c can be taken as the maximum applicable stress. Table XXXII gives the values of σ_c at various temperatures. The ranges shown are for minimum (lower values) to maximum strength material in terms of ultimate tensile strength, with the value of σ_c increasing with material strength. Otherwise, the ultimate tensile strength of a given heat is the maximum applicable stress for that heat. Equation 73, page 138, predicts $\dot{e}_m > \dot{e}_3$ for values of $e_m > 55.36\%/hr$. However, this anomaly occurs at stresses higher than those cited above and does not affect the stated limits. The creep equation is analytically valid to zero stress as the lower limit. "Analytical" validity unfortunately does not necessarily imply physical validity. Implications of extrapolating the current equations are given in the next chapter.

Advantages

The creep equation presented herein has several important advantages for design applications. First, the rational polynomial equation from

TABLE XXXII

STRESS VALUES CORRESPONDING TO MAXIMUM VALUES OF THE PARAMETER C

Temperature (°C)	Stress, σ_c (MPa) (Minimum Strength to Maximum Strength)
427	>414
482	>414
538	365 to >414
593	241 to 407
649	138 to 255
704	41 to 124

itself has distinct advantages over other popular forms. These advantages were mentioned briefly above and are described in more detail elsewhere [97].

The analysis of stress and temperature dependence used here clearly alleviates the first objection to previous methods, since the results depend largely upon rupture life and minimum creep rate data. Creep curves are still needed, of course, to supply data for e_3, t_3, and $\dot{e}_o$, and for verification of results. However, the current technique allows utilization of all available information, rather than using available creep curves only.

The empirical relationships [Eqns. 72-73, page 138, and 77, page 139, used in developing the current equation are simple and describe well the experimental data. Therefore, fewer data are required to evaluate these relationships than to develop direct expression for the parameters C and p as functions of stress and temperature. The fact that the relationships appear to closely reflect trends in the data lessens the chance of obtaining misleading results, especially in the extrapolated region, and avoids Objection 2.

The method used here inherently involves interrelationships among the various equation parameters. Thus, the third objection is eliminated.

Perhaps the most unusual and potentially useful feature of the current equation is its ability to account for heat-to-heat variations, alleviating Objection 4. It is not possible to predict the behavior of every individual heat precisely. Still, an ability to reflect the

variation in strength from heat-to-heat can greatly decrease the uncertainty involved in modeling elevated temperature mechanical behavior. At the very least, the current approach gives a clear idea of minimum and maximum strength, indicating the expected range of behavior.

The method presented here is extremely flexible, and many variations are possible. For instance t_3 may be modeled directly, as were rupture life and minimum creep rate. Various methods for predicting e_3, including that used here, are presented in Ref. [51]. For instance, in some cases it may be possible to approximate e_3 by the plasticity resource, $\dot{e}_m t_r$. In that case, there would be even less reliance on actual creep curves than in the approach given here. An alternate method for predicting heat-to-heat variations might be to model t_r and $\dot{e}_m$ for given individual heats, which are known beforehand to be strong, weak, medium, etc.

It is recognized that the current method also has some disadvantages. These are primarily (1) that the predictions are largely indirect, and (2) that the data bases used in different steps may be different, yielding possible inconsistencies. The second problem could easily be solved by using data from the same tests in every step, but this approach limits the analysis to those tests for which all data are available. The empirical relationships used are really normalization procedures, so any inconsistencies should be small. In short, we feel that the great advantages of the current approach far outweigh any disadvantages.

CHAPTER V

EXTRAPOLATION OF RESULTS

An unavoidable problem incurred in the development of creep models for design applications is the necessity to extrapolate results to regions of time, stress, and perhaps temperature beyond the range of experimental data. For example, a typical power plant operating life is of the order of 300,000 hours (about 30 years), whereas the longest experimental rupture life available in this investigation was 65,000 hours. Operating stresses and temperatures are chosen such that the actual rupture life would be longer than the plant service life in order to prevent component failures. Two specific examples illustrate this situation.

First, a common problem in elevated temperature components is that of "creep-fatigue," or cyclic deformation interspersed with periods of monotonic creep or relaxation. Elevated temperature design rules [49] specify a life fraction approach to the prevention of creep-fatigue failures, based on the analysis proposed by Campbell [103]. This method suggests that creep-fatigue failure be prevented by specifying that

$$\sum_{j=1}^{P} (n/N_D)_j + \sum_{k=1}^{Q} (t/T_d)_k \leq D^* \ , \tag{83}$$

where

D^* = a specified "damage factor,"

n = the number of cycles applied under loading condition j,

N_D = the number of design allowable cycles under loading condition j,

t = time duration of loading condition k,

T_D = allowable time under loading condition k.

T_D is calculated as the lower limit time to rupture at the temperature of interest under a stress given by the stress from load k divided by a factor K', which is defined as 0.9 for type 304 and 316 austenitic stainless steels and for Incoloy Alloy 800H.

Since the quantity T_D is a lower limit estimate of rupture life, design conditions are generally such that the evaluation of Eqn. 83 requires predictions of rupture lives to perhaps 10^7 or 10^8 hrs.

Second, a creep strain-time formulation is used to estimate the magnitude of time-dependent (i.e. creep and relaxation) deformation incurred in components during service. For example, it is expected [104] that type 304 stainless steel will be used extensively as a structural material in the reactor vessels and the intermediate heat exchanger pressure boundaries for the Liquid Metal Fast Breeder Reactor (LMFBR)[105]. Design conditions vary with the particular application, but the maximum expected operating temperature for this material in LMFBR service will be about 538°C (1000°F)[104]. In such an application, the stresses on the material will be somewhere below the allowable stress levels given in ASME Code Case 1592 [49]. Figure 55 compares this limited region of stress-temperature operating conditions (for an operating life of 3×10^5 hours) with the region of

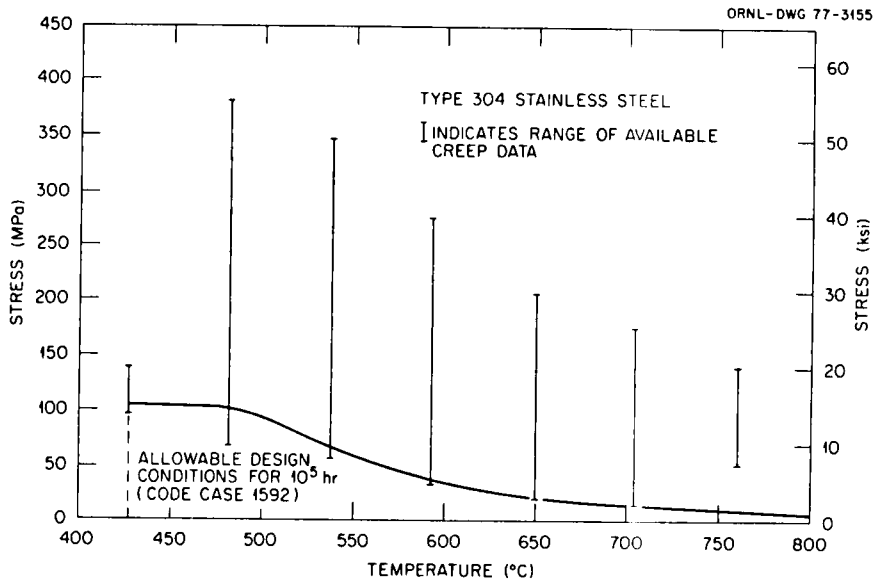

Figure 55. Comparison of Stress-Temperature Operating Conditions Allowed by ASME Code Case 1592 With the Range of Available Experimental Creep Data for Type 304 Stainless Steel.

the experimental creep tests used in the current evaluation. Estimation of behavior for these operating conditions again can require extrapolation to regions of stress and temperature well outside those available experimentally.

A large number of data for type 304 stainless steel are available over a large range of stress-temperature conditions. The material appears well-behaved in this range, and its behavior can be adequately described by simple empirical models. The problem with extrapolating the results beyond the range of the data has two facets. First, there is the possibility of long-term metallurgical instabilities such as the formation of embrittling phases. Second, there is the possibility that deformation and fracture mechanisms may be different in the extrapolated stress-temperature region than in the region where data were available. Otherwise, the amount of available data is sufficient to warrant considerable extrapolation, and all of the models proposed herein behave well analytically when extrapolated. Thus, it is desirable to consider these two possibilities in more detail.

While there have been some indications [106] of sigma-phase formation in long-term tests on type 304 stainless steel, available data indicate that metallurgical stability is not a significant problem for most practical applications [1]. The only change in fracture mode appears to be the transition from transgranular to intergranular fracture which occurs at short rupture times. Since most data reflect this latter intergranular fracture mode, no problems should be incurred in this respect as far as extrapolation is concerned.

The remaining uncertainty in extrapolating the current equations beyond the range of data concerns possible changes in deformation mechanism. A few low stress-low temperature tests which are still in progress at ORNL indicate that such changes may occur. A detailed fundamental investigation of creep deformation mechanisms is beyond the scope of this report; however implications of mechanism changes on predictive equations will be considered in the next section.

Possible Effects of Changes in Deformation Mechanism

Creep deformation can occur by a variety of mechanisms within the same material at different stresses and temperatures. A convenient form for presenting the deformation mechanisms that occur for a given material is through the use of "deformation maps," recently devised by Ashby [107,108]. These maps are plots on axes of stress versus temperature, which show the areas in σ-T space where different creep mechanisms are dominant. (Actually Frost and Ashby plotted normalized shear stress σ_s/μ vs T/T_m where μ is the shear modulus and T_m the melting temperature. This choice was mainly to reduce variations among materials and is not mandatory.)

Due to the many approximations and simplifications used by Frost and Ashby in constructing their maps, the maps probably cannot be used for quantitative design calculations. Nevertheless, the construction contains useful qualitative information that can be helpful in defining possible areas of uncertainty in predictions and in identifying areas where more data are needed.

At high stress values, the dominant creep mechanism should involve flow by dislocation glide. These stresses are higher than most of those seen in the current data and are certainly higher than those of interest in design applications. Therefore, this mode of deformation will not be discussed here.

Virtually all of the currently available creep data fall in the region where deformation is expected to be controlled by dislocation creep (with the possible exception of a few of the ORNL low stress creep tests that are still in progress). Creep in this region occurs primarily through the motion of dislocations by both glide and climb. Theoretical considerations [109] dictate that the steady-state creep rate in this region should be given by

$$\dot{e}_m = AD_v \frac{Gb}{kT} \left(\frac{\sigma}{G}\right)^n \tag{84}$$

where A and n are material constants ($n \approx 4$), G is the shear modulus, b is the burgers vector and k is Boltzmann's constant. D_v is the bulk diffusion coefficient, given by $D_v = D_o e^{-Q/RT}$. Equation 84 suggests that a log $\dot{e}_m$ – log σ plot should be linear, which is born out by the current results. However, the current data show a slope of this curve which decreases with temperature but is considerably larger than 4; also the observed activation energy appears to be somewhat larger than that for vacancy self-diffusion in this material. Both of these observations are common for creep-resistant engineering alloys. Many investigators, for example Refs. [94,110-116], have attributed these

effects to the existence of an internal stress, σ^*, which opposes the effects of the applied stress. Thus the creep rate is determined by the magnitude of $(\sigma - \sigma^*)^4$ rather than by σ^4.

At lower stresses, the dominant creep mechanism becomes that of vacancy diffusion through a crystal or around the grain boundaries. Following Raj and Ashby [117], Gittus [118] gives the steady-state creep rate due to diffusion as

$$\dot{e}_m = 14 \frac{\sigma\Omega}{KT} \cdot \frac{1}{d^2} D_v \left(1 + \frac{\pi\delta}{d} \frac{D_B}{D_v}\right) \tag{85}$$

where Ω is the atomic volume, d the grain size, D_v the bulk diffusion coefficient, and δ the effective cross section of a grain boundary for diffusion. Thus, the creep rate is projected to vary linearly with stress. Equation 85 neglects the effects of grain boundary precipitates, which can be important [119]. Roughly, such precipitates introduce a threshold stress, σ_o, below which no diffusion creep occurs. The term $(\sigma - \sigma_o)$ then replaces σ in Eqn. 85, and may make the slope of a log $\dot{e}_m$ – log σ plot greater than unity, analogous to the effects of σ^* on dislocation creep.

Note that the above changes in deformation mechanisms imply an accompanying change in the slope of a log σ – log $\dot{e}_m$ plot. The existence of "breaks" in plots of log $\dot{e}_m$ vs. log σ has been observed for a number of materials, including some niobium-stabilized austenitic steels [120]. Unfortunately, the present data for type 304 stainless steel are not sufficient to define a quantitative estimate of the exact

point where the break occurs, or of the sharpness of the break. The data merely indicate the possible existence of such a break. The current minimum creep rate model (and thus the creep equation) will significantly overestimate the creep strength of this material in the low stress region if such a break does occur. Thus, it is important to consider the possible implications of such a change in slope even though a detailed quantitative analysis awaits additional data.

One cause of such breaks could be the occurrence of a metallurgical instability, but this explanation does not appear likely in the case of type 304 stainless steel. Thus, a change in deformation mechanism appears to be a likely cause.

Figure 56 displays the minimum creep rate data from ORNL for heat 9T2796, estimated through fits of the rational polynomial creep equation by the method of Bunatyan [100]. Many of these tests are still in progress, and the values of $\dot{e}_m$ in Figure 56 are approximate (thus the large amount of scatter). At low stresses, there appears to be a possible break in the plots of log $\dot{e}_m$ vs. log σ indicating a decrease in the value of n (the slope of these curves). In Figure 56, the slope below the break has arbitrarily been chosen as 4, but appears to be consistent with the data.

The data do not permit a detailed analysis of the break in Figure 56. However, two possible explanations can be given. First, the break may indicate a transition from dislocation creep to diffusion creep. The slope of 4 is perhaps too high for diffusion creep, although this inconsistency may merely indicate that the transition is not yet complete.

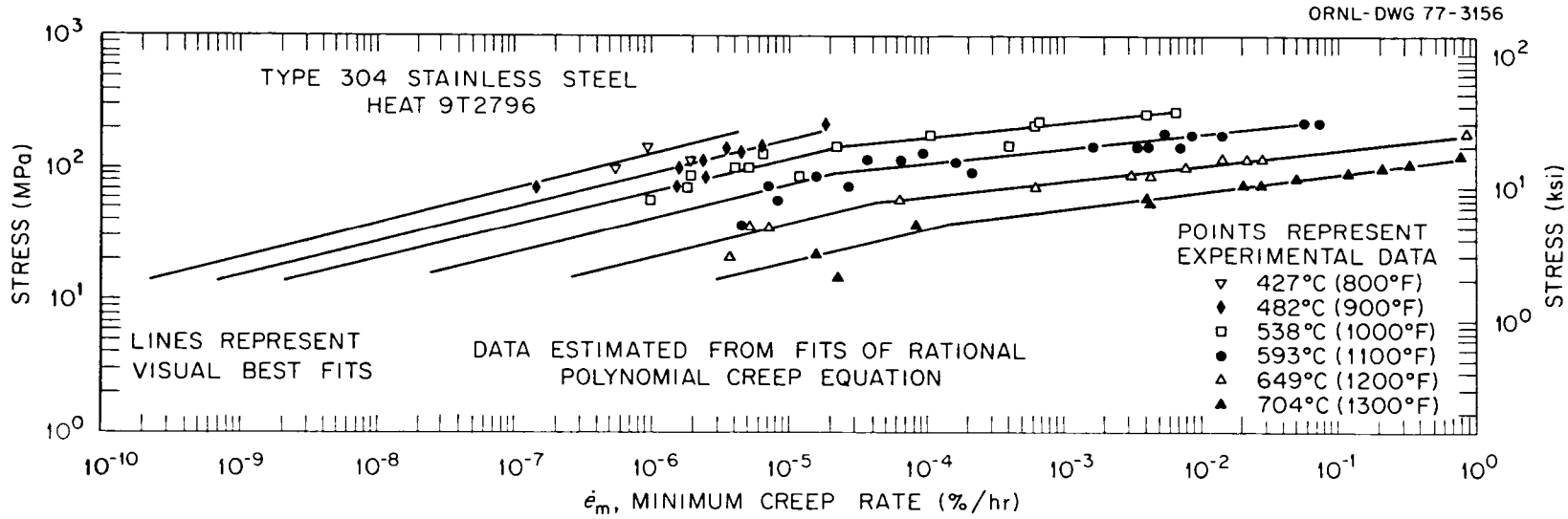

Figure 56. Minimum Creep Rate Data for Heat 9T2796 51-mm Plate of Type 304 Stainless Steel. Data shown include estimated values for low stress tests currently in progress. The data indicate a possible downward break in the log $\dot{e}_m$ – log σ isothermals at low stresses.

A second explanation is that of Lagneborg and Bergman [116], who based the following analysis of such breaks on the internal stress. Their analysis was strictly applicable to classical precipitation-hardened alloys, where a uniform dispersion of particles is precipitated within the matrix. The case of an austenitic stainless steel, where precipitation occurs preferentially on dislocations and at grain boundaries, is more complicated, but analogies can be drawn. According to Lagneborg and Bergman, the stress dependence of the creep rate should be proportional to $(\sigma - \sigma_p)^4$, where σ_p is the internal stress due to the resistance to dislocation motion caused by the precipitates within the matrix. Above the break point, σ_p is a constant whose value strongly depends upon the size, shape, and spacing of the precipitate particles. In this region, dislocations move past the particles either by cutting through them or by the Orowan mechanism. The net effect is to make the slope of a log σ vs. log $\dot{e}_m$ plot somewhat larger than 4. Below the break, Lagneborg and Bergman propose that dislocations surmount the particles by a climb mechanism. In this region, they predict that σ_p should be proportional to σ. Thus, the creep rate is proportional to $(\sigma - K\sigma)^4 = (1 - K)^4\sigma^4$, again yielding a slope of 4 in a log σ – log $\dot{e}_m$ plot. Incidentally, σ_p in this region is almost independent of the size, shape, and spacing of the precipitate particles. Available data do not permit a clear identification of the cause of the breaks shown in Figure 56, and the fact that the slope below the break has been drawn as 4 in that figure does not indicate a preference for the Lagneborg-Bergman explanation on the part of the author. If the

Lagneborg-Bergman explanation is correct, another break may occur at still lower stresses indicating a change to diffusional creep.

There is sound physical basis for believing that the break shown in Figure 56, page 171, might be real. Consideration of a numerical example points out the importance of a further study of these slope changes. First, assume that the break is drawn in the proper place in Figure 56. Now choose a possible design condition for temperature and stress, say 593°C (1100°F) and 20 MPa (2.9 Ksi). The current analysis of minimum creep rate data Eqn. 36, page 88, yields (for heat 9T2796) an estimated value of $\dot{e}_m = 5.7 \times 10^{-11}$ %/hr. Assuming a slope of 4 below the break in Figure 56 yields a value of $\dot{e}_m = 3 \times 10^{-7}$ %/hr. Assuming that the break is due to a change to diffusion creep and taking the slope below the break to be 2 requires a slight alteration of the placement of the break point in Figure 56 to remain as consistent as possible with the data. This reconstruction yielded a value of $\dot{e}_m = 10^{-6}$ %/hr. Thus, such breaks can cause underestimates of the value of $\dot{e}_m$ by Eqn. 36 by a factor of over 10^4! (On the other hand, the net deviation in 10^5 hr would only be perhaps 0.1% strain.)

A second point that can be noted from Figure 56 is the decreased temperature dependence of the minimum creep rate at lower temperatures (< 538°C). This decrease could have several causes. First, at these temperatures there appear to be very few carbides precipitated within the grains or at the grain boundaries. Thus, the strengthening effect of these particles is lost at these low temperatures. A second possible cause involves the often observed phenomenon, e.g. Ref. [121], of a lower activation energy for creep at lower temperatures. Robinson and

Sherby [122] have attributed such a decrease to the increasing dominance of dislocation core diffusion as a deformation mechanism at these low temperatures.

Finally, Figure 56, page 171, presents the data for the minimum creep rate only since that is one of the few quantities analyzed in the current report that can be estimated from the continuing ORNL long-time creep tests. The other quantity that can be estimated is initial creep rate, $\dot{e}_o$. In fact, these long-time data were used in developing Eqn. 77 (page 139). There is no definite indication of a break in the relationship of log $\dot{e}_m$ with log $\dot{e}_o$. However, Eqn. 77 does indicate an increase in the ratio of $\dot{e}_o$ to $\dot{e}_m$ as $\dot{e}_m$ (and thus σ) decreases. For example, if $\dot{e}_m$ is 10^{-2} %/hr, $\dot{e}_o/\dot{e}_m$ would be predicted to be 8.6. If $\dot{e}_m$ is 10^{-6} %/hr, $\dot{e}_o/\dot{e}_m$ would be predicted to be about 54.4. There is some evidence that grain boundary sliding contributes more to the creep strain in the earlier stages of creep [123], due to the development of ledges or other obstacles to sliding as deformation proceeds. Since grain boundary sliding is an especially prominent feature of diffusional creep [117], the increase in $\dot{e}_o/\dot{e}_m$ with lower stress could indicate a relative increase in the importance of diffusional creep as a deformation mechanism. However, a full explanation of this phenomenon awaits further study.

CHAPTER VI

DISCUSSION OF RESULTS

Many of the results presented in this report require no further explanation. Others have been discussed as they were presented. This chapter presents a further discussion of some of the more important points made in the report.

Regression Analysis of Creep and Rupture Data

Regression analysis is a standard, widely used technique, and the usefulness of the method in a large variety of situations is indisputable. The advantages of a regression approach for the analysis of creep data will be discussed below, with specific comparison being made with the common time-temperature parameter approach.

References [32-35] present comprehensive reviews of parametric analysis techniques, especially with application to creep rupture data. The use of such parameters is primarily based on two factors. First, the technique collapses data at different temperatures onto a single master curve to simplify the analysis. Second, high temperature low-stress data can be used to estimate lower temperature (and thus longer time) data at these same stresses.

Unfortunately, neither of these supposed advantages of parametric analysis is real unless the parameter chosen is correct, i.e. unless the true $\sigma - T - t$ relationship is at least approximately that implied by the parameter. The choice of the "correct" or "best" parameter can

be somewhat complicated. Dozens of distinct parameters have been proposed. When the various possible stress dependences are considered, the total number of parameters climbs into the hundreds.

It must be realized that even though a given parameter fits the available data, that same parameter may not yield accurate extrapolations. The last chapter indicated some of the problems that can occur in the extrapolation of creep data. Parametric prediction of low-stress, low-temperature data by higher temperature data at those stresses represents an extrapolation and should only be done with extreme caution. Figure 57 illustrates this situation schematically. Thus, even though a point may lie within the range of the "master curve," it can still represent an extrapolation and should be treated accordingly.

Another problem incurred with time-temperature parameters is their lack of flexibility. Larke and Inglis [124] presented an analysis of the restrictions imposed by various commonly used parameters. Also, variables other than stress and temperature may be important (such as ultimate tensile strength). Within the form of a given parameter, the flexibility with which new variables can be added is severely restricted.

Finally, it is often difficult to estimate the constants in the parametric equations with accuracy except by the use of regression techniques, especially for large multiple-heat data sets. Many of the common parameter forms can be rewritten as linear regression models with $\log \dot{e}_m$ or $\log t_r$ as the dependent variable, although some become nonlinear models when written in this way. Thus, if one is essentially reduced to using regression analysis anyway, it is a logical extension

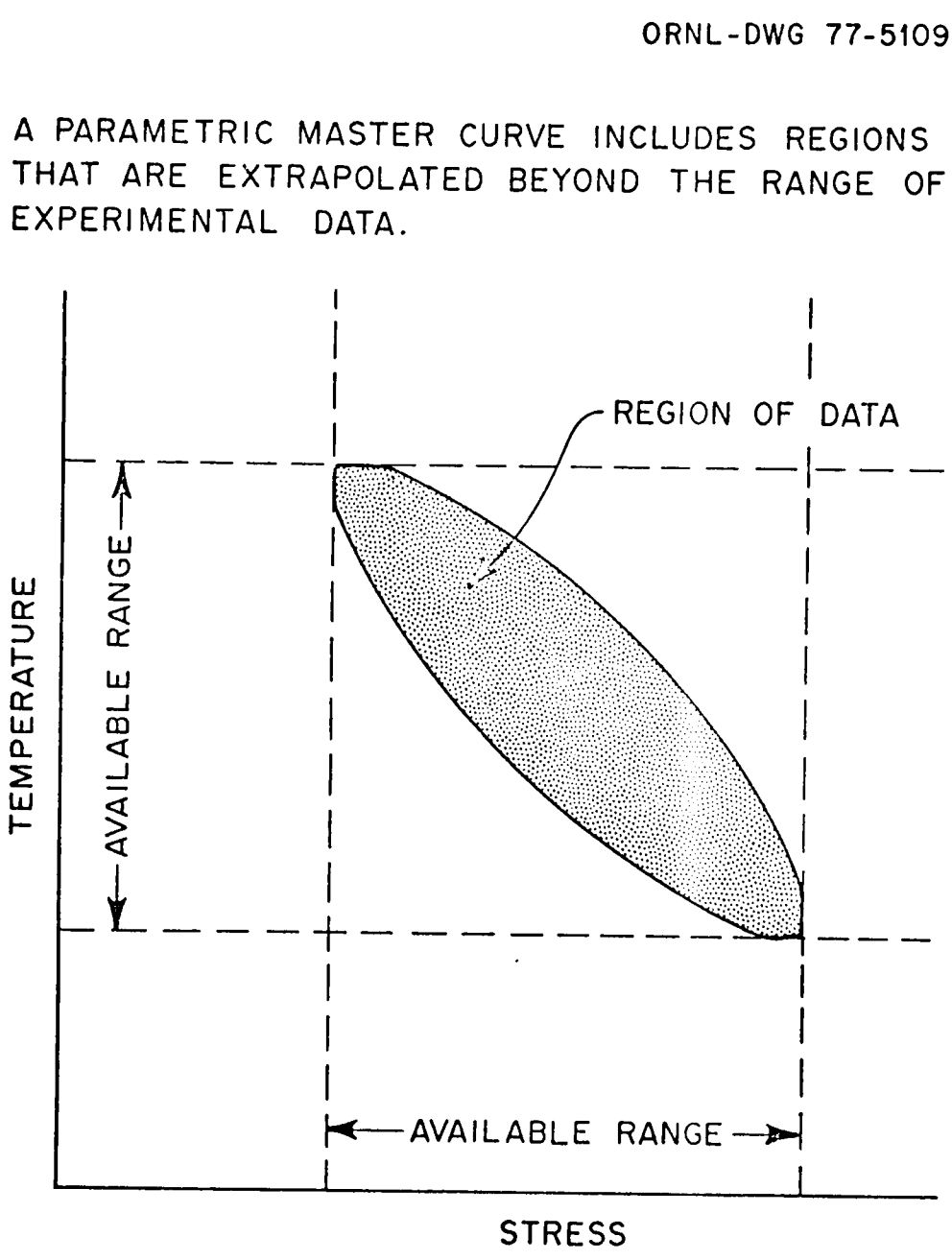

Figure 57. Schematic Illustration of the Region of Interpolation Versus Extrapolation for Creep Data. Any point within the boxed region lies within the parametric "master curve," while only points within the shaded region lie within the range of experimental data.

to consider a generalized set of models rather than restricting the analysis to a small subset which also happen to correspond to time-temperature parameters. Regression will in general yield a single well-behaved mathematical model with clear statistical implications. Thus, such a technique is particularly useful for analyses whose results are intended for design applications.

Once regression analysis has been selected as the technique to use, a variety of options still remain. In particular, the final "optimum" model can be selected by a number of techniques. In the case of creep data, the method used here has the advantage that several candidate models are output from the statistical selection procedure so that some physical judgment can be applied in the choice of a final model. If one merely wishes to represent a set of data and is not interested in extrapolation, it would be sufficient to use a procedure (such as stepwise regression) which might yield only one optimum model based solely on statistical considerations.

No representation is made that the current technique is the best possible. This technique is, however, very useful and easily applied. It allows considerably more flexibility than a parametric analysis, and the results are easily applied to design. Perhaps the most controversial aspect of the particular results given here is the use of ultimate tensile strength as an indicator of heat-to-heat variations in creep strength.

Relationship Between Ultimate Tensile Strength and Creep Properties

One of the more powerful features of the current formulation is the ability to predict heat-to-heat variations in creep behavior from a knowledge of the ultimate tensile strength of a given heat of material. The models presented herein also embody a much sought after relationship between short-term tensile properties and long-term creep properties. Therefore, it is desirable to examine the validity of this relationship in more detail.

The use of U to aid in predicting creep behavior is not a totally novel approach. For instance, Conrad [125] proposed an equation of the form

$$t_r = D \exp\left(\frac{\Delta H}{RT}\right) \exp\left[-\frac{\sigma}{\sigma_o(T)}\right] \tag{86}$$

where D is a constant, H the activation energy of self-diffusion, R the gas constant, and σ_o is some measure of variation of strength with temperature. Our use of ultimate tensile strength is a similar concept. Various American [126-129] and Soviet [130-132] investigators have related either hot-hardness or ultimate tensile strength at temperature to creep and creep rupture strength. These investigations are summarized in Ref. [20].

Analytically, the ultimate tensile strength, U, can be considered as the stress corresponding to a rupture life of the duration of a tensile test or to a minimum creep rate of the tensile strain rate.

Therefore, the ultimate tensile strength for a given heat of material at a given temperature effectively determines the location of the short time/high rate end of the stress-rupture or stress-minimum creep rate isotherm for that heat at that temperature.

Sikka et al. [20] have discussed the metallurgical factors involved in relating ultimate tensile strength to creep behavior. For completeness, their arguments will be reproduced here. Perhaps the main objection to the use of ultimate tensile strength to predict creep behavior is the possibility that metallurgical changes which occur during long-term creep may sufficiently alter material behavior so as to destroy any correlation between ultimate tensile strength and long-term creep or creep rupture strength. For type 304 stainless steel, the metallurgical changes are limited primarily to precipitation of carbides at grain boundaries and in the matrix. ORNL data for test times approaching 40,000 hr show the weak or strong character of a heat to be retained during a long-term test, which indicates that metallurgical changes have comparatively little influence on factors controlling the relative creep strength of various heats. There is evidence [1] that thermal aging for a period of 100,000 hr (11.4 yr) at 565°C (1050°F) causes essentially no changes in the creep properties of type 304 stainless steel. The apparent linearity in log σ vs. log t_r and log σ vs. log $\dot{e}_m$ isotherms for the current data extends to test times of 65,000 hr, indicating thereby the absence of any significant metallurgical changes in this period of time [133].

Another question which should be addressed concerns possible effects of differences between creep and tensile modes of deformation.

However, several substructural studies [134-137] on tensile and creep tested specimens of types 304 and 316 stainless steel have shown that the dislocation structures were independent of deformation mode. Dislocation cell formation occurs at temperatures below which the deformation is primarily glide controlled, whereas subgrains form when the deformation is climb controlled. The cell or subgrain size is related simply to the true creep stress or true ultimate tensile strength by [137].

$$\lambda_{cell} \propto b(\sigma_T/E)^{-2} \tag{87}$$

and

$$\lambda_{subgrain} \propto b(\sigma_T/E)^{-1} \tag{88}$$

where b is the burgers vector (about 2.54×10^{-4} μm), σ_T is the true creep stress or true ultimate tensile strength, and E is Young's modulus.

Gittus [138] described a statistical theory of creep in which the mean stress required to overcome obstacles to creep deformation could be related to ultimate tensile strength, providing further support for the current techniques.

Finally, the fracture mode for type 304 stainless steel is generally transgranular for short-term tensile tests, while creep fractures are primarily intergranular. Therefore, a relationship between ultimate tensile strength and creep rupture strength tends to imply that the factors which control intragranular strength also at least partially determine the grain boundary strength. Manjoire [139], in describing

flow and fracture, suggested that the same factors influence the relative strengths of both the grain matrix and the grain boundary. There is much evidence that grain boundary sliding and intragranular deformation during creep are related [139]. Additional support for this contention can be found in the work of Rhines and Wray [140] and Sikka et al. [141], who have studied the minima in tensile ductility with temperature exhibited by austenitic stainless steels. Figure 58 shows the tensile reduction of area as a function of test temperature for the weakest and strongest (in terms of ultimate tensile strength) heats in the ORNL testing program for types 304 and 316 stainless steel. As noted in Ref. [141], the weak heats show a drop in ductility at temperatures which are in the creep range. Rhines and Wray [140] offered an explanation for such ductility minima. At the lower temperatures, failure occurs by a transgranular crack propagation mechanism, and ductility is high. As temperatures approach the temperature of the minimum in ductility, some deformation occurs by grain-boundary shear, resulting in rapid growth of intergranular voids formed at triple points, causing a drastic loss in ductility. As the temperatures become still higher, recrystallization occurs along with the intergranular void formation, continuously breaking up the intergranular fracture path and causing the ductility to again increase.

Figure 58 indicates that the ductility minimum associated with intergranular cracking occurs in the weak heat of type 304, but is either absent or postponed to higher temperatures in the strong heat. This effect can be explained in terms of the increased grain boundary strength of these strong heats. Since these same heats have high

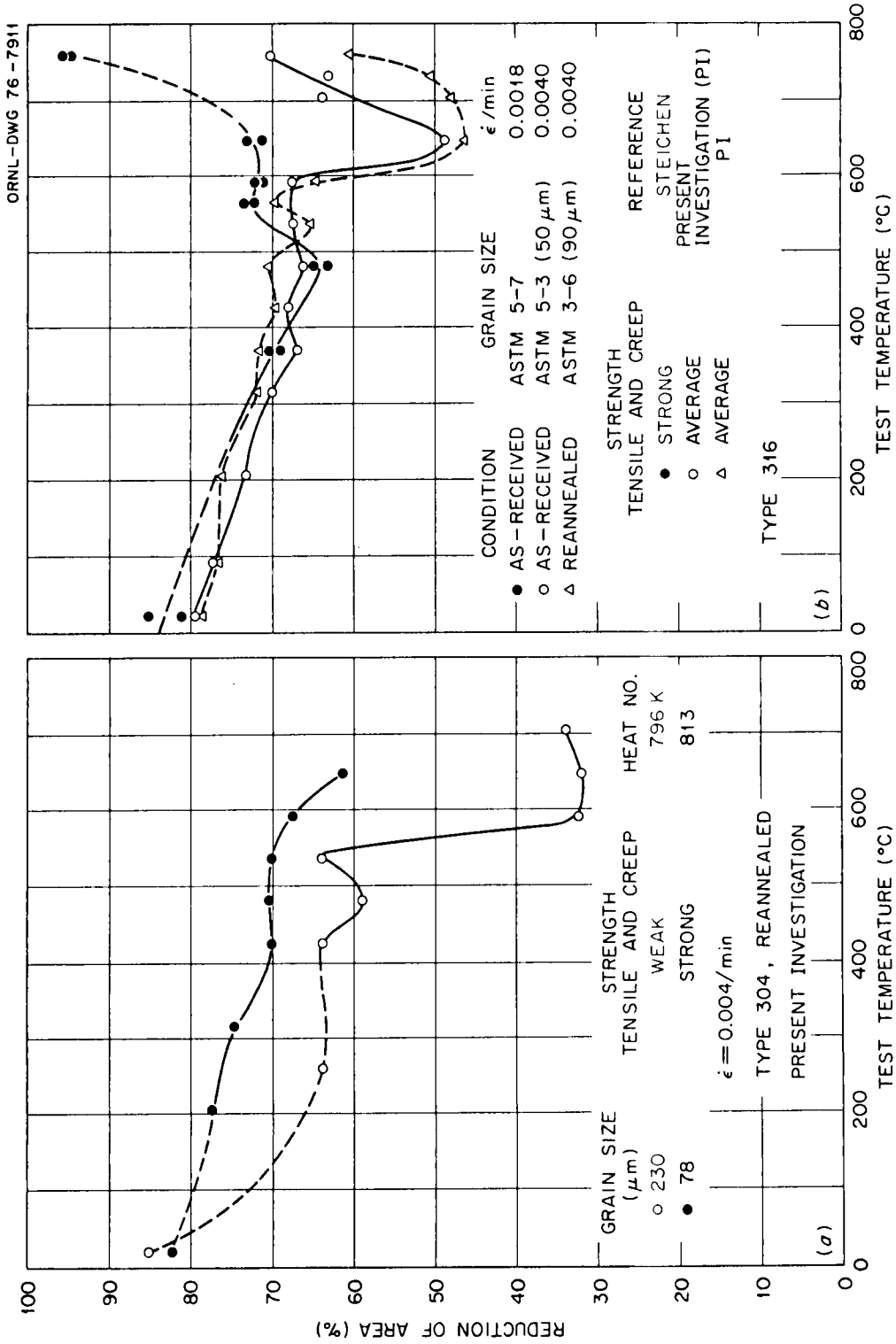

Figure 58. Trends in the Tensile Reduction of Area With Temperature for Weak and Strong Heats of Types 304 and 316 Stainless Steel.

values of U, their matrix strength is also relatively high. These observations support the proposition that inter- and intragranular strengths are related and are perhaps controlled by similar factors.

The use of ultimate tensile strength in predicting creep and creep-rupture strength for type 304 stainless steel is justified both by an empirical, statistically based modeling procedure and by more fundamental metallurgical considerations. An alternative might be to use some direct measure of the property being modeled as an indicator of the strength of a given heat. For instance, the stress to cause rupture in 10^2 hours at the temperature of interest or the stress to cause a minimum creep rate of 10^{-2} %/hr might be used as variables rather than ultimate tensile strength. However, the use of ultimate tensile strength appears adequate and is easier to apply.

Predicted Trends in Ductility Data

Although these analyses were done primarily on an empirical basis, the results appear consistent with those that would be expected from a physical model. The predictions of the variations in creep ductility in Chapter III illustrate this point. It is generally accepted that the observed creep strain consists of the strain occurring within individual grains (e_g) and the deformation occurring by grain boundary sliding (e_b). Thus,

$$e_3 = e_g + e_b \ , \tag{89}$$

where the values of e_g and e_b depend on the relative strengths of grain

matrix and grain boundaries. Since the annealing treatment in the type 304 stainless steel does not cause the formation of strengthening phases, applied creep stress can produce deformation both in the matrix and at grain boundaries. The matrix deformation causes the formation of a subgrain or dislocation cell structure; meanwhile, the grain boundary deformation causes stress concentrations. For test temperatures below about 649°C, carbide precipitates deposited at the grain boundaries during testing are continuous and thus inhibit [142] both grain boundary sliding and migration. As a result, the stress concentrations generated at triple points can nucleate cracks [143] causing onset of tertiary creep after only small strains at low temperatures. Precipitates at higher temperatures are larger and make possible both grain boundary sliding and migration. Grain boundary migration can relax stresses, thus allowing a greater intergranular deformation before the initiation of enough cracks to cause onset of tertiary creep. There is a great deal of evidence that an increase in stress results in a decrease of the contribution of grain boundary sliding to the total strain [123]. Thus, the amount of matrix deformation incurred before the occurrence of intergranular cracks increases as stress increases. The effect of strain rate is similar. Equation 40, page 101, predicts a decrease in the ratio of t_3 or t_r within increasing time (decreasing strain rate), due to the larger contribution of grain boundary deformation and faster cracking under these conditions.

The predicted variations in creep ductility due to ultimate tensile strength can also be explained. A given applied stress is effectively lower for a strong heat than for a weak heat. Thus, the isostress

effect of increasing strength (U) is similar to the effect of decreasing stress, i.e., a decrease in ductility. However, at very high stresses, the increased strength of strong heats begins to dominate and stronger heats can withstand more deformation before cracking and the onset of tertiary creep. At a constant strain rate, the increased grain boundary strength of stronger heats results in an increased contribution of intragranular deformation to the total strain. Therefore, more strain occurs before grain boundary deformation is sufficient to cause extensive cracking and the onset of tertiary creep. At a constant strain rate, e_3 is thus generally larger for stronger heats. In short, all of the trends predicted by the current empirical calculations are consistent with the metallurgical features of this material.

Comparison With ASME Code Case 1592 Allowable Stress Levels

The current results can be directly compared with the results given in ASME Code Case 1592 [49] in terms of the time dependent allowable stress levels, S_t, for elevated temperature applications. The value of S_t is defined as the lowest of the three following criteria:

1. 2/3 of S_r, the minimum stress to cause rupture in time t;
2. 80% of S_3, the minimum stress to cause onset of tertiary creep in time t;
3. $S_{1\%}$, the minimum stress to cause 1% total strain in time t.

Values of S_r and S_t are tabulated directly in ASME Code Case 1592 [49]. For the current results S_r, S_3, $S_{1\%}$, and S_t were calculated at

times of 10^3 hours and 10^5 hours. Values of $S_{1\%}$ were taken directly from the minimum strength isochronous stress-strain curves from Figure 53, pages 153-155). Values of S_r were determined using Eqn. 35, page 88, and evaluating at minimum values of ultimate tensile strength (mean minus two standard errors). Values of S_3 were calculated similarly, using Eqn. 40, page 101, to estimate t_3 from t_r.

Table XXXIII compares the current results with those of the code case. Considering the large differences in data bases and analytical techniques, the two sets of values correspond quite closely. The current minimum values are in general slightly lower than those of the code case, perhaps reflecting the large variations in strength displayed by the current ORNL data. As explained above, many uncertainties remain in the extrapolated regions. The current results do not in themselves indicate any alarming problems in the results of ASME Code Case 1592 [49].

TABLE XXXIII

COMPARISON BETWEEN ESTIMATED TIME-DEPENDENT ALLOWABLE STRESS LEVELS CALCULATED FROM THE CURRENT RESULTS AND THOSE GIVEN IN ASME CODE CASE 1592[a]

Temperature (°C)	$S_{1\%}$ Minimum Stress to 1% Strain		S_3, Minimum Stress to Tertiary Creep		S_r, Minimum Stress to Rupture		S_t,[c] Allowable Time-Dependent Stress	
	10^3 hr	10^5 hr	10^3 hr	10^5 hr	10^3 hr	10^5 hr	10^3 hr	10^5 hr
				Current Results				
538	144	108	156(125)	81(65)	166(111)	88(59)	111	59
593	105	65	115(92)	57(46)	123(82)	62(42)	82	42
649	51	30	74(59)	34(27)	79(53)	37(25)	51	25
				ASME Code Case 1592				
538					213(143)	114(77)	143	77
593					140(94)	70(47)	94	47
649					92(62)	43(29)	62	29

[a]All stress values are given in MPa.

[b]Values in parenthesis represent adjustment by standard safety factors of 0.8 on S_3 and of 2/3 on S_r.

[c]S_t is the lowest of $S_{1\%}$, $0.8S_3$, and 2/3 S_r.

CHAPTER VII

CONCLUSIONS

A large base of creep and creep-rupture data for type 304 austenitic stainless steel has been subjected to an analytical treatment in order to develop a mathematical representation of the properties of this material for design applications. Specific conclusions of the current analysis are:

1. Standard techniques of linear regression analysis can be applied to develop analytical models for rupture life (t_r) and minimum creep rate ($\dot{e}_m$). These models fit the data well, including the prediction of heat-to-heat variations in properties through the inclusion in the models of terms involving the ultimate tensile strength of a given heat of material at the temperature of interest. However, extrapolation of these models is only valid so long as no significant metallurgical changes (instabilities or deformation mechanism changes) occur. The final equations used were:

$$\log t_r = 5.716 - \frac{3915}{T} \log \sigma + \frac{36.60U}{T} - 0.007303\, U \log \sigma \qquad (90)$$

$$\log \dot{e}_m = -2.765 + \frac{3346}{T} \log \sigma - \frac{51.84U}{T} + 0.01616\, U \log \sigma \ . \qquad (91)$$

2. The use of variations in ultimate tensile strength to estimate variations in creep and rupture strength is consistent with available data and appears to be reasonable based on metallurgical considerations.

3. Simple empirical relationships can be used to estimate the time to tertiary creep, t_3, from the time to rupture. The average creep rate to tertiary creep, $\dot{e}_3 = e_3/t_3$ (e_3 is the creep strain at the onset of tertiary creep), can be estimated from the minimum creep rate. These relationships are:

$$t_3 = 0.686\ t_r^{0.968} \tag{92}$$

and

$$\dot{e}_3 = 1.11\ \dot{e}_m^{0.974} . \tag{93}$$

Thus, the creep strain to tertiary creep, e_3, can be estimated by

$$e_3 = 0.761\ t_r^{0.968}\ \dot{e}_m^{0.974} . \tag{94}$$

Alternatively, $\dot{e}_3$ and t_3 can each be separately modeled by regression analysis and then multiplied to yield e_3. Other creep ductility criteria (e.g., the strain to rupture) can be similarly estimated. Predicted trends in creep ductility appear consistent with the metallurgical characteristics of type 304 stainless steel.

4. Type 304 stainless steel generally exhibits classicial three stage creep. The shape of the strain-time creep curves in the primary and secondary stages can be adequately modeled by the single rational polynomial creep equation,

$$e_c = \frac{Cpt}{1 + pt} + \dot{e}_m t , \tag{95}$$

where e_c is the creep strain, t the time, and C, p, and $\dot{e}_m$ are equation parameters ($\dot{e}_m$ = minimum creep rate).

5. The parameter C corresponds to the total amplitude of the primary term in the rational polynomial creep equation. It can be shown that $C = t_3(\dot{e}_3 - \dot{e}_m)$, so that the equations given in conclusion (3) above yield

$$C = 0.686\ t_r^{0.968}(1.11\ \dot{e}_m^{0.974} - \dot{e}_m)\ . \tag{96}$$

The initial creep rate, $\dot{e}_o = Cpt\dot{e}_m$, can be estimated by

$$\dot{e}_o = 3.43\ \dot{e}_m^{0.80}, \tag{97}$$

so that the parameter p can be estimated by

$$p = \frac{(\dot{e}_o - \dot{e}_m)}{C}\ . \tag{98}$$

Thus, the entire creep equation can be estimated from a knowledge of $\dot{e}_m$ and t_r alone. The above models (Eqns. 90 and 91, page 189) thus yield a prediction of the strain-time behavior which reflects heat-to-heat variations in creep strength through variations in ultimate tensile strength. (Equations 92-94, 96, and 97 appear to be relatively insensitive to heat-to-heat variations, since they are normalization procedures.)

6. The occurrence of metallurgical instabilities does not appear to be a significant problem for type 304 stainless steel. However, available low-stress creep tests from Oak Ridge National Laboratory (many of which are still in progress) appear to indicate a change in

deformation mechanism at low stresses. As a result, the above equations would be valid only to the point where this change occurs. The data do not permit an exact determination of the nature of this change, but metallurgical considerations show that it is reasonable to expect such a change. A quantitative analysis of behavior below the break requires more data than are currently available. In particular, there is no information about heat-to-heat variations in properties below the break. The creep process appears to display a lower activation energy at lower temperatures.

7. By using an estimated minimum value of ultimate tensile strength in the predictive equations, the behavior of minimum strength material can be estimated. These results can be compared with the allowable stress levels for this material given in ASME Code Case 1592.

REFERENCES

REFERENCES

1. W. E. Ray et al., "Selection of Steam Generator Tubing Material for the Westinghouse LMFBR Demonstration Plant," Nuclear Technology, Vol. 11, June 1971, pp. 222-231.

2. R. A. Moen et al., "Specifying and Manufacturing Piping for the Fast Flux Test Facility," in Elevated Temperature Properties of Austenitic Stainless Steels, A. O. Schaefer, ed., The American Society of Mechanical Engineers, New York, 1974, pp. 141-155.

3. R. Stickler and A. Vinckier, "Morphology of Grain-Boundary Carbides and Its Influence on Intergranular Corrosion of 304 Stainless Steel," Transactions of the American Society for Metals, Vol. 54, 1961, pp. 362-380.

4. B. Weiss and R. Stickler, "Phase Instabilities During High Temperature Exposure of 316 Austenitic Stainless Steel," Metallurgical Transactions, Vol. 3, 1972, pp. 851-866.

5. J. E. Spruiell et al., "Microstructural Stability of Thermal-Mechanically Pretreated Type 316 Stainless Steel," Met. Trans., Vol. 4, 1973, pp. 1533-1544.

6. C. F. Etienne, W. Dortland, and H. B. Zeedijk, "On the Capability of Austenitic Steel to Withstand Cyclic Deformation During Service at Elevated Temperature," paper presented at International Conference on Creep and Fatigue in Elevated Temperature Applications, Philadelphia, September 1973, and Sheffield, UK, April 1974.

7. V. K. Sikka, C. R. Brinkman, and H. E. McCoy, Jr., "Effect of Thermal Aging on Tensile and Creep Properties of Types 304 and 316 Stainless Steels," in Structural Materials for Service at Elevated Temperatures in Nuclear Power Generation, MPC-1 A. O. Schaefer, ed., American Society of Mechanical Engineers, New York, 1975, pp. 316-350.

8. C. E. Pugh et al., Currently Recommended Constitutive Equations for Inelastic Design Analysis of FFTF Components, ORNL-TM-3602 (September 1972).

9. J. M. Corum et al., Interim Guidelines for Detailed Inelastic Analysis of High-Temperature Reactor System Components, ORNL-5014 (December 1974).

10. C. E. Pugh et al., Background Information for Interim Methods of Inelastic Analysis for High-Temperature Reactor Components of 2 1/4 Cr-1 Mo Steel, ORNL-TM-5226 (May 1976).

11. C. E. Pugh, "Constitutive Equations for Creep Analysis of LMFBR Components," in Advances in Design for Elevated Temperature Environment, S. Y. Zamrik and R. I. Jetter, eds., The American Society of Mechanical Engineers, New York, 1975, pp. 1-15.

12. C. C. Davenport, "Correlation of Creep and Relaxation Properties of Copper," J. Appl. Mech., Vol. 60, 1938, p. A-55.

13. V. K. Sikka, H. E. McCoy, Jr., M. K. Booker, and C. R. Brinkman, "Heat-to-Heat Variations in Creep Properties of Types 304 and 316 Stainless Steels," J. Pressure Vessel Technology, Vol. 93, No. 4, Nov. 1975, pp. 243-251.

14. Interpretations of the ASME Boiler and Pressure Vessel Code, Case 1592, American Society of Mechanical Engineers, New York, 1974.

15. V. K. Sikka, R. W. Swindeman, C. R. Brinkman, and M. K. Booker, Residual Cold Work and Its Influence on Tensile and Creep Properties of Types 304 and 316 Stainless Steel, ORNL-TM-5192 (January 1976), also published in Nuclear Technology, Vol. 31, Oct. 1976, pp. 96-114.

16. V. K. Sikka, T. L. Hebble, M. K. Booker, and C. R. Brinkman, Influence of Laboratory Annealing on Tensile Properties and Time-Independent Design Stress Intensity Limits for Type 304 Stainless Steel, ORNL-5175 (December 1976).

17. V. K. Sikka, Oak Ridge National Laboratory, Private communication (June 1976).

18. V. K. Sikka and M. K. Booker, "Assessment of Tensile and Creep Data for Types 304 and 316 Stainless Steels," presented at International Joint Pressure Vessels and Piping and Petroleum Mechanical Engineering Conference, Mexico City, Mexico, September 19-24, 1976. To be published in Journal of Pressure Vessel Technology.

19. V. K. Sikka and C. R. Brinkman, "Relation Between Short- and Long-Term Elevated-Temperature Properties of Several Stainless Steels," Scripta Met., Vol. 10, 1976, pp. 25-28.

20. V. K. Sikka and M. K. Booker, "Use of Ultimate Tensile Strength to Correlate and Predict Creep and Creep Rupture Behavior of Types 304 and 316 Stainless Steel," report in preparation.

21. BSCC High-Temperature Data, Published for the British Steelmakers Creep Committee by the Iron and Steel Institute, 1973.

22. "NRIM Creep Data Sheets: Elevated-Temperature Materials Manufactured in Japan, 1973," National Research Institute for Metals, Tokyo 153, Japan.

23. W. F. Simmons and H. C. Cross, Report on the Elevated-Temperature Properties of Stainless Steels, ASTM Special Technical Publication 124, American Society for Testing and Materials, Philadelphia, 1952.

24. W. F. Simmons and J. A. Van Echo, Report on the Elevated-Temperature Properties of Stainless Steels, ASTM Data Series Publication DS5-S1, American Society for Testing and Materials, Philadelphia, 1955.

25. H. E. McCoy, Interim Report of Tensile and Creep Data for Type 304 Stainless Steel Plate (Reference Heat 9T2796, 2 in. Thick), ORNL-TM-4627 (October 1974).

26. H. E. McCoy, Tensile and Creep Properties of Several Heats of Type 304 Stainless Steel, ORNL-TM-4709 (November 1974).

27. R. W. Swindeman and C. E. Pugh, Creep Studies on Type 304 Stainless Steel (Heat 8043813) Under Constant and Varying Loads, ORNL-TM-4427 (June 1974).

28. R. W. Swindeman, "Creep-Rupture Correlations for Type 304 Stainless Steel Heat 9T2796," in Structural Materials for Service at Elevated Temperatures in Nuclear Power Generation, MPC-1, A. O. Schaefer, ed., American Society of Mechanical Engineers, New York, 1975, pp. 1-29.

29. L. D. Blackburn, "Isochronous Stress-Strain Curves for Austenitic Stainless Steels," in The Generation of Isochronous Stress-Strain Curves, A. O. Schaefer, ed., American Society of Mechanical Engineers, New York, 1972, pp. 15-48.

30. ASTM Designation: A 240-71, "Standard Specification for Stainless and Heat-Resisting Chromium and Chromium-Nickel Steel Plate, Sheet and Strip for Fusion Welded Unfired Pressure Vessles," Annual Book of ASTM Standards, Part 3, American Society for Testing and Materials, Philadelphia (April 1972).

31. ASTM Designation: A 479-71, "Standard Specification for Stainless Steel and Heat-Resisting Steel Bars and Shapes for Use in Boilers and Other Pressure Vessels," Annual Book of ASTM Standards, Part 3, American Society for Testing and Materials, Philadelphia (April 1972).

32. J. B. Conway, Stress-Rupture Parameters: Origin, Calculation and Use, Gordon and Breach, New York, 1969.

33. S. S. Manson, "Time-Temperature Parameters—A Re-Evaluation and Some New Approaches," Time-Temperature Parameters for Creep-Rupture Analysis, ASM Publication D8-100, American Society for Metals, Metals Park, Ohio, 1968, pp. 1-114.

34. H. P. Van Leeuwen, Predicting Material Behavior Under Load, Time, and Temperature Conditions, Report 513, North Atlantic Treaty Organization Advisory Group for Aerospace Research and Development (June 1965).

35. R. K. Penny and D. L. Marriott, Design for Creep, McGraw-Hill, London, 1971, pp. 192-238.

36. S. S. Manson, "Design Considerations for Long Life at Elevated Temperatures," James Clayton Lecture Presented at Joint International Conference on Creep, London, 1963. Inst. Mech. Eng. Proc., Vol. 178, No. 3A, 1963-64, pp. 1045-1071.

37. A. Mendelson and S. S. Manson, "The Extrapolation of Families of Curves by Recurrence Relations, With Application to Creep Rupture Data," Trans. ASME, J. Basic Eng., Vol. 82, 1960, pp. 839-847.

38. M. K. Booker, T. L. Hebble, D. O. Hobson, and C. R. Brinkman, Mechanical Property Correlations for 2 1/4 Cr-1 Mo Steel in Support of Nuclear Reactor Systems Design, ORNL-TM-5329 (June 1976). To be published in International Journal of Pressure Vessels and Piping.

39. D. R. Rummler, "Stress-Rupture Data Correlation-Generalized Regression Analysis, An Alternative to Parametric Methods," presented at ASTM Symposium on Reproducibility and Accuracy of Mechanical Tests, St. Louis, Missouri, May 5, 1976.

40. N. R. Draper and H. Smith, Applied Regression Analysis, John Wiley and Sons, New York (1966).

41. C. Daniel and F. S. Wood, Fitting Equations to Data, John Wiley and Sons, New York (1971).

42. R. R. Hocking and R. N. Leslie, "Selection of the Best Subset in Regression Analysis, Technometrics, Vol. 9, 1967, pp. 531-540.

43. L. R. LaMotte and R. R. Hocking, "Computational Efficiency in the Selection of Regression Variables," Technometrics, Vol. 12, 1970, pp. 83-93.

44. M. K. Booker, Regression Analysis of Creep-Rupture Data: A Practical Approach, report in preparation.

45. F. R. Larson and J. Miller, "A Time-Temperature Relationship for Rupture and Creep Stresses," Trans. ASME, Vol. 74, 1952, pp. 765-771.

46. S. S. Manson and G. Succop, "Stress-Rupture Properties of Inconel 700 and Correlation on the Basis of Several Time-Temperature Parameters," Symposium on Metallic Materials for Service Above 1600°F, ASTM STP 174, American Society for Testing and Materials, Philadelphia, 1956, pp. 40-46.

47. R. L. Orr, O. D. Sherby, and J. E. Dorn, "Correlation of Rupture Data for Metals at Elevated Temperatures," Trans. ASM, Vol. 46, 1954, pp. 113-128.

48. G. T. Leiberman and R. G. Miller, Jr., "Simultaneous Tolerance Intervals in Regression," Biometrika, Vol. 50, 1963, pp. 165-181.

49. Interpretations of the ASME Boiler and Pressure Vessel Code, Case 1592, American Society of Mechanical Engineers, New York, 1974.

50. M. K. Booker, C. R. Brinkman, and V. K. Sikka, "Correlation and Extrapolation of Creep Ductility Data for Four Elevated-Temperature Structural Materials," in Structural Materials for Service at Elevated Temperatures in Nuclear Power Generation, A. O. Schaefer, ed., American Society of Mechanical Engineers, New York, 1975, pp. 108-145.

51. M. K. Booker and V. K. Sikka, Predicting the Strain to Tertiary Creep for Elevated-Temperature Structural Materials, ORNL-TM-5403 (July 1976).

52. M. K. Booker and V. K. Sikka, Empirical Relationships Among Creep Properties of Four Elevated-Temperature Structural Materials, ORNL-TM-5399 (June 1976).

53. G. V. Smith, Properties of Metals at Elevated Temperatures, McGraw-Hill, New York, 1950, p. 151.

54. R. M. Goldhoff, "A Method for Extrapolating Rupture Ductility," Elevated Temperature Testing Problem Areas, ASTM STP 488, American Society for Testing and Materials, Philadelphia, 1971, pp. 82-94.

55. F. C. Monkman and N. J. Grant, "An Empirical Relationship Between Rupture Life and Minimum Creep Rate in Creep-Rupture Tests," Proc. ASTM, Vol. 56, 1956, pp. 593-605.

56. M. K. Booker and V. K. Sikka, "Interrelationships Between Creep Life Criteria for Four Nuclear Structural Materials," Nuclear Technology, Vol. 30, July 1976, pp. 52-64.

57. N. J. Grant and A. G. Bucklin, "On the Extrapolation of Short-Time Stress-Rupture Data," Trans. ASM, Vol. 42, 1950, pp. 720-751.

58. N. J. Grant, "Stress Rupture Testing," High Temperature Properties of Metals, American Society for Metals, Cleveland, 1951, pp. 41-72.

59. V. S. Ivanova, "Creep Ductility Criterion for Metals," Zavodskaya Laboratoria, Vol. 21, No. 2, 1955, pp. 212-216; Brutcher Translation No. 4210.

60. I. A. Oding and V. S. Ivanova, "Analysis and Application of Certain Creep Criteria," Vestnik Mashinostroeniya, Vol. 35, No. 5, 1955, pp. 62-66; Brutcher Translation No. 4211.

61. R. M. Goldhoff, "Some Observations on the Extrapolation of High-Temperature Ferritic Steel Data," J. Basic Eng., Vol. 82, No. 4, Dec. 1960, pp. 848-853.

62. P. W. Davies and B. Wilshire, "An Interpretation of the Relationship Between Creep and Fracture," Structural Processes in Creep, Iron and Steel Institute, London, 1961, pp. 34-43.

63. F. Garofalo, Fundamentals of Creep and Creep Rupture, Macmillan, New York, 1965, p. 204.

64. R. Viswanathan, "Strength and Ductility of 2 1/4 Cr-1 Mo Steels in Creep at Elevated Temperatures," Metals Technology, Vol. 1, June 1974, pp. 284-294.

65. I. S. Servi and N. J. Grant, "Creep and Stress Rupture Behavior of Aluminum As a Function of Purity," Trans. AIME, Vol. 191, 1951, pp. 909-916.

66. E. S. Machlin, "Creep-Rupture by Vacancy Condensation," Trans. AIME, Vol. 206, 1956, pp. 106-111.

67. P. Feltham and J. D. Meakin, "Creep in Face-Centered Cubic Metals With Special Reference to Copper," Acta Met., Vol. 7, 1959, pp. 614-627.

68. R. L. Klueh, "The Relationship Between Rupture Life and Creep Properties of 2 1/4 Cr-1 Mo Steel," Nuclear Technology, Vol. 26, 1975, pp. 287-296.

69. R. F. Gill and R. M. Goldhoff, "Analysis of Long Time Creep Data for Determining Long Term Strength," Met. Eng. Q., Vol. 10, 1970, pp. 30-39.

70. E. E. Underwood, "Interrelationships Among High-Temperature Strength and Ductility Criteria," Joint International Conference on Creep, Institute of Mechanical Engineers, London, 1963, Section 6, pp. 49-57.

71. D. I. Roberts and S. A. Sterling, "A Parametric Method for the Development of Isochronous Stress-Strain Curves," in The Generation of Isochronous Stress-Strain Curves, A. O. Schaefer, ed., The American Society of Mechanical Engineers, New York, 1972, pp. 1-14.

72. S. A. Sterling, A Temperature-Dependent Power Law for Monotonic Creep, GA-A13027 (Rev.), June 1974, Revised March 1976.

73. R. F. Gill and R. M. Goldhoff, "Analysis of Long Time Creep Data for Determining Long Term Strength," Met. Eng. Q., Vol. 10, 1970, pp. 30-39.

74. M. C. Murphy, "Rating the Creep Behavior of Heat-Resistant Steels for Steam Power Plant," Met. Eng. Q., Vol. 13, 1973, pp. 41-50.

75. R. M. Goldhoff and R. F. Gill, "A Method for Predicting Creep Data for Commercial Alloys on a Correlation Between Creep Strength and Rupture Strength," J. Basic Eng., Vol. 94, 1972, pp. 1-6.

76. Y. N. Rabotnov, "Some Problems on the Theory of Creep," Vestnik Moskovskoyo Universiteta, No. 10, 1948. Available in English as NACA Technical Memorandum 1353.

77. R. M. Goldhoff, "The Application of Rabotnov's Creep Parameter," Proc. ASTM, Vol. 61, 1961, pp. 908-919.

78. W. E. Stillman, M. K. Booker, and V. K. Sikka, "Mathematical Description of the Creep Strain-Time Behavior of Type 316 Stainless Steel," Proceedings of the Second International Conference on Mechanical Behavior of Materials, Boston, Aug. 16-20, 1976, pp. 424-428.

79. J. B. Conway, Numerical Methods for Creep and Rupture Analyses, Gordon and Breach, New York, 1967.

80. F. Garofalo, Fundamentals of Creep and Creep-Rupture in Metals, Macmillan, New York, 1965, pp. 10-20.

81. I. A. Oding et al., Creep and Stress Relaxation in Metals translated by E. Bishop, English editor A. J. Kennedy, Oliver and Boyd, Edinburgh, 1965.

82. A. J. Kennedy, Processes of Creep and Fatigue in Metals, Oliver and Boyd, Edinburgh, 1962.

83. P. G. McVetty, "Factors Affecting Choice of Working Stresses for High-Temperature Service," Mech. Eng., Vol. 55, 1933, pp. 99-104.

84. F. Garofalo, C. Richmond, W. F. Domis, and F. von Gemmingen, "Strain-Time, Rate-Stress, and Rate-Temperature Relations During Large Deformations in Creep," Joint International Conference on Creep, The Institution of Mechanical Engineers, London, 1963, Section 1, pp. 31-39.

85. A. Ahmadieh and A. K. Mukherjee, "Stress-Temperature-Time Correlation for High Temperature Creep Curves," Mat. Sci. and Eng., Vol. 21, 1975, pp. 115-124.

86. A. Ahmadieh and A. K. Mukherjee, "Transient and Steady-State Creep Curves in Ni-Fe Alloy System," Scripta Met., Vol. 9, 1975, pp. 1299-1304.

87. B. A. Movchan, L. M. Nerodenko, O. G. Kasatkin, and E. V. Dabizha, "A Phenomenological Structural Approach to High-Temperature Creep," Strength of Materials, Vol. 6, 1974, pp. 1041-1046. Translated from Problemy Prochnosti.

88. B. A. Movchan and E. V. Dabizha, "A Phenomenological Model for High-Temperature Creep in Pure Nickel," Strength of Materials, Vol. 7, 1975, pp. 278-283. Translated from Problemy Prochnosti.

89. D. Sidey and B. Wilshire, "Mechanisms of Creep and Recovery in Nimonic 80A," Metal Sci. J., Vol. 3, 1969, pp. 56-60.

90. B. Wilshire, "Some Grain Size Effects in Creep and Fracture," Scripta Met., Vol. 4, 1970, pp. 361-366.

91. W. J. Evans and B. Wilshire, "Transient and Steady-State Creep Behavior of a Copper-15 at. % Aluminum Alloy," Metal Sci. J., Vol. 4, 1970, pp. 89-94.

92. P. W. Davies, W. J. Evans, K. R. Williams, and B. Wilshire, "An Equation to Represent Strain/Time Relationships During High Temperature Creep," Scripta Met., Vol. 3, 1969, pp. 671-674.

93. W. J. Evans and B. Wilshire, "The High Temperature Creep and Fracture Behavior of 70-30 Alpha-Brass," Met. Trans., Vol. 1, 1970, pp. 2133-2139.

94. P. L. Threadgill and B. Wilshire, "Mechanisms of Transient and Steady-State in a γ'-Hardened Austenitic Steel," in Creep Strength in Steel and High-Temperature Alloys, The Metals Society, London, 1974, pp. 8-14.

95. G. A. Webster, A. P. D. Cox, and J. E. Dorn, "A Relationship Between Transient and Steady-State Creep at Elevated Temperatures, Metal Sci. J., 1969, pp. 221-225.

96. M. Mejia, R. Gomez-Ramirez, and M. A. Martinez, "The Phenomenological Theory of Creep," Scripta Met., Vol. 10, 1976, pp. 589-591.

97. D. O. Hobson and M. K. Booker, Materials Applications and Mathematical Properties of the Rational Polynomial Creep Equation, ORNL-5202 (December 1976).

98. A. M. Freudenthal, "Theory of Wide-Span Arches in Concrete and Reinforced Concrete," International Association Bridge and Structural Engineers, Vol. 4, 1936, p. 249, as cited in Ref. 79.

99. I. A. Oding, Izvestiya Akad. Nauk SSSR, OTN, 1948, as cited in Ref. 81.

100. L. A. Bunatyan, Proceedings of a Seminar on the Strength of Engineering Components, Izd. Akad. Nauk SSSR, Vol. 1, 1953, as cited in Ref. 81.

101. R. W. Swindeman, Oak Ridge National Laboratory, private communication, June 1976.

102. V. K. Sikka, M. K. Booker, and J. P. Hammond, Rational Polynomial Tensile Stress-Strain Equation for Low Strain Behavior of Types 304 and 316 Stainless Steels, report in preparation.

103. R. D. Campbell, "Creep/Fatigue Interaction Correlation for 304 Stainless Steel Subjected to Strain-Controlled Cycling With Hold Times at Peak Strain," J. Eng. for Industry, Vol. 93, Nov. 1971, pp. 887-892.

104. R. T. King et al., "Alternate Structural Materials for Liquid Metal Fast Breeder Reactors," in Structural Materials for Service at Elevated Temperatures in Nuclear Power Generation, MPC-1, A. O. Schaefer, ed., American Society of Mechanical Engineers, New York, 1975, pp. 365-390.

105. F. L. Culler, Jr., and W. O. Harms, "Energy from Breeder Reactors," Phys. Today, Vol. 25, No. 5, May 1972, pp. 28-39.

106. V. Biss, D. L. Sponseller, and M. Semchyshen, "Metallographic Examination of Type 304 Stainless Steel Creep Rupture Specimens," Journal of Materials, Vol. 7, No. 1, March 1972, pp. 88-94.

107. M. F. Ashby, "A First Report on Deformation Mechanism Maps," Acta Met., Vol. 20, 1972, pp. 887-897.

108. H. J. Frost and M. F. Ashby, "Deformation-Mechanism Maps for Pure Iron, Two Austenitic Stainless Steels, and a Low-Alloy Ferritic Steel," unpublished private communication, July 1975.

109. J. Weertman, "Theory of Steady-State Creep Based on Dislocation Climb," J. Applied Physics, Vol. 26, No. 10, Oct. 1955, pp. 1213-1217.

110. C. N. Ahlquist, R. Gasca-Neri, and W. D. Nix, "A Phenomenological Theory of Steady State Creep Based on Average Internal and Effective Stresses," Acta Met., Vol. 18, June 1970, pp. 663-671.

111. R. Gasca-Neri, C. N. Ahlquist, and W. D. Nix, "A Phenomenological Theory of Transient Creep," Acta Met., Vol. 18, June 1970, pp. 655-661.

112. P. W. Davies, G. Nelmes, K. R. Williams, and B. Wilshire, "Stress-Charge Experiments During High-Temperature Creep of Copper, Iron, and Zinc," Metal Sci. J., Vol. 7, 1973, pp. 87-92.

113. T. Hasegawa and H. Oikawa, "Internal Stress in Creep Deformation," Nippon Kinzoku Gakkaishi Kaiho, Vol. 11, No. 3, 1972, pp. 192-202. Translated by H. Kubota, ORNL-tr-2818.

114. J. J. Jonas, "The Back Stress in High Temperature Deformation," Acta Met., Vol. 17, April 1969, pp. 397-405.

115. R. Lagneborg, "A Modified Recovery-Creep Model and Its Evaluation," Metal Sci. J., Vol. 6, July 1972, pp. 127-133.

116. R. Lagneborg and B. Bergman, "The Stress/Creep Rate Behavior of Precipitation-Hardened Alloys," Metal Sci. J., Vol. 10, Jan. 1976, pp. 20-28.

117. R. Raj and M. F. Ashby, "On Grain Boundary Sliding and Diffusional Creep," Met. Trans., Vol. 2, April 1971, pp. 1113-1127.

118. J. H. Gittus, Creep Viscoelasticity and Creep Fracture in Solids, John Wiley and Sons, New York, 1975, p. 6.

119. M. F. Ashby, "On Interface-Reaction Control of Nabarro-Herring Creep and Sintering," Scripta Met., Vol. 3, 1969, pp. 837-842.

120. B. Russell, R. K. Ham, J. M. Silcock, and G. Willoughby, "Creep Mechanisms in Niobium-Stabilized Austenitic Steels," Metal Sci. J., Vol. 2, 1968, pp. 201-209.

121. O. D. Sherby and P. M. Burke, "Mechanical Behavior of Crystalline Solids at Elevated Temperature," Progress in Materials Science, Vol. 13, No. 7, 1967, pp. 325-389.

122. S. L. Robinson and O. D. Sherby, "Mechanical Behavior of Polycrystalline Tungsten at Elevated Temperature," Acta Met., Vol. 17, Feb. 1969, pp. 109-125.

123. F. Garofalo, Fundamentals of Creep and Creep-Rupture in Metals, Macmillan, New York, 1965, pp. 139-142.

124. E. C. Larke and N. P. Inglis, "A Critical Examination of Some Methods of Analyzing and Extrapolating Stress-Rupture Data," Joint International Conference on Creep, The Institution of Mechanical Engineers, London, 1963, Section 4, pp. 6-33.

125. H. Conrad, "Correlation of High Temperature Creep and Rupture Data," Trans. ASME, J. Basic Eng., Vol. 81, 1959, pp. 617-626.

126. E. P. Bens, "Hardness Testing of Metals and Alloys at Elevated Temperatures," Trans. ASM, Vol. 38, 1947, pp. 505-516.

127. F. Garofalo, P. R. Malenock, and G. V. Smith, "Hardness of Various Steels at Elevated Temperatures," Trans. ASM, Vol. 45, 1953, pp. 377-396.

128. E. E. Underwood, "Creep Properties from Short Time Tests," Mater. Methods, Vol. 45, 1957, pp. 127-129.

129. O. D. Sherby and J. E. Dorn, "Creep Correlations in Alpha Solid Solutions of Aluminum," Trans. AIME, Journal of Metals, Vol. 192, 1952, pp. 959-964.

130. "High Temperature Hardness Testing, Some Recent Russian Work," Metallurgia, Sept. 1950, pp. 207-208.

131. F. S. Novik and A. A. Klypin, "Correlations Between the Properties of Certain Heat-Resisting Alloys," Strength of Materials (Translated from Problemy Prochnosti), Vol. 4, 1972, pp. 1119-1124.

132. V. V. Krivenyuk, "Relationship Between Short-Time Mechanical Characteristics and Long-Term Strength," Strength of Materials (Translated from Problemy Prochnosti), Vol. 6, 1974, pp. 295-299.

133. D. J. Wilson, "The Influence of Simulated Service Exposure on the Rupture Strengths of Grade 11, Grade 22, and Type 304 Steels," J. Engineering Materials and Technology, Vol. 96, No. 1, Jan. 1974, pp. 10-21.

134. K. D. Challenger and J. Moteff, "Quantitative Characterization of the Substructure of AISI 316 Stainless Steel Resulting from Creep," Met. Trans., Vol. 4, March 1973, pp. 749-755.

135. D. J. Michel, J. Moteff, and A. J. Lovell, "Substructure of Type 316 Stainless Steel Deformed in Slow Tension at Temperatures Between 21°C and 816°C," Acta Met., Vol. 21, Sept. 1973, pp. 1269-1277.

136. V. K. Sikka, H. Nahm, and J. Moteff, "Some Aspects of Subboundary and Mobile Dislocations During High Temperature Creep of AISI 316 and 304 Stainless Steels," Mat. Sci. and Eng., Vol. 20, 1975, pp. 55-62.

137. R. K. Bhargava, J. Moteff, and R. W. Swindeman, "Correlation of the Microstructure with the Creep and Tensile Properties of AISI 304 Stainless Steel," in Structural Materials for Service at Elevated Temperatures in Nuclear Power Generation, A. O. Schaefer, ed., American Society of Mechanical Engineers, New York, 1975, pp. 31-54.

138. J. H. Gittus, "A Statistical Theory of Steady-State Creep and Its Application to Type 316 Stainless Steel, Zinc, Magnox AL80 and Nickel, J. Mech. Phys. Solids, Vol. 13, 1965, pp. 69-75.

139. M. J. Manjoine, "Basic Creep-Rupture Testing at 1100°F (593°C) of Uniaxially Loaded Specimens with Uniform Sections of Type 304 Stainless Steel," WARD-HT-3045-9 (July 1975).

140. F. N. Rhines and R. J. Wray, "Investigation of the Intermediate Temperature Ductility Minimum," Trans. ASM, Vol. 54, 1961, pp. 117-128.

141. V. K. Sikka, R. W. Swindeman, and C. R. Brinkman, "Elevated Temperature Tensile Ductility Minima in Types 304 and 316 Stainless Steel," accepted for publication in the Fourth International Conference on Fracture, to be held at Waterloo, Canada, June 19-24, 1977.

142. F. Garofalo, R. W. Whitmore, W. F. Domis, and F. von Gemmingen, "Creep and Creep-Rupture Relationships in an Austenitic Stainless Steel," Trans. AIME, Vol. 221, 1969, pp. 310-319.

143. F. Garofalo, "Ductility in Creep," in Ductility, American Society for Metals, Metals Park, Ohio, 1967, pp. 108-109.

VITA

Marvin Keith Booker was born in Beckley, West Virginia, on May 21, 1953. He attended elementary schools in Georgia and Tennessee, and was graduated from Madison (Tennessee) High School in June, 1971. The following fall he entered Vanderbilt University, and in May, 1974, he received a Bachelor of Arts (Magna cum Laude) degree in Physics and Mathematics. He is a member of Phi Beta Kappa. He has been employed in the Metals and Ceramics Division of Oak Ridge National Laboratory since May, 1974.

He entered the Graduate School at The University of Tennessee in September, 1974, and received the Master of Science degree with a major in Metallurgical Engineering in June, 1977.

He is married to the former Barbra L. Perry.